Universität Hamburg

DER FORSCHUNG | DER LEHRE | DER BILDUNG

Characterisation and establishment of the chPLA2R1 mouse model and the identification of pathomechanisms

Dissertation for the attainment of
The academic title
Doctor rerum naturalium

Presented by

Annabel Schnarre

Department of Biology
University of Hamburg

Hamburg, 2025

1) Gutachter: Prof. Dr. Wolfgang Streit
2) Gutachter: Priv.-Doz. Dr. Gunther Zahner
Verteidigt am 05.06.2026

„Die Forschung ist immer auf dem Wege, nie am Ziel“

- Adolf Pichler

The presented work was conducted from September 2021 until May 2025 in the III. Department of Medicine in the University Medical Center Hamburg-Eppendorf under the supervision of PD Dr. Gunther Zahner.

Eidestattliche Erklärung

Hiermit versichere ich an Eides statt, die vorliegende Dissertationsschrift selbst verfasst und keine anderen als die angegebenen Hilfsmittel und Quellen benutzt zu haben. Sofern im Zuge der Erstellung der vorliegenden Dissertationsschrift generative Künstliche Intelligenz (gKI) basierte elektronische Hilfsmittel verwendet wurden, versichere ich, dass meine eigene Leistung im Vordergrund stand und dass eine vollständige Dokumentation aller verwendeten Hilfsmittel gemäß der Guten wissenschaftlichen Praxis vorliegt. Ich trage die Verantwortung für eventuell durch die gKI generierte fehlerhafte oder verzerrte Inhalte, fehlerhafte Referenzen, Verstöße gegen das Datenschutz- und Urheberrecht oder Plagiate.

Hamburg, den

_____
Annabel Schnarre

I hereby declare and affirm that this doctoral dissertation is my own work and that I have not used any aids and sources other than those indicated. If electronic resources based on generative artificial intelligence (gAI) were used in the course of writing this dissertation, I confirm that my own work was the main and value-adding contribution and that complete documentation of all resources used is available in accordance with good scientific practice. I am responsible for any erroneous or distorted content, incorrect references, violations of data protection and copyright law or plagiarism that may have been generated by the gAI.

Hamburg, den

_____
Annabel Schnarre

Ich versichere, dass dieses gebundene Exemplar der Dissertation und das in elektronischer Form eingereichte Dissertationsexemplar (über den Docata-Upload) und das bei der MIN Fakultät zur Archivierung eingereichte gedruckte gebundene Exemplar der Dissertationsschrift identisch sind.

Hamburg, den

_____
Annabel Schnarre

I, the undersigned, declare that this bound copy of the dissertation and the dissertation submitted in electronic form (via the Docata upload) and the printed bound copy of the dissertation submitted to the faculty (responsible Academic Office or the Doctoral Office Physics) for archiving are identical.

Hamburg, den

_____
Annabel Schnarre

Table of contents

I. Acknowledgments

Firstly, I would like to thank **PD. Dr. Gunther Zahner**, who welcomed me into his lab and research group. Thank you for being an exceptionally supportive and trustworthy mentor. I deeply appreciate your openness to discuss all my questions and your hands-on support in the lab. Your continuous support and belief in my abilities have had a profound impact on my development as a researcher. I am truly grateful for your guidance and the opportunities you have given me.

A special thanks goes to **Prof. Dr. Wolfgang Streit**, who kindly agreed to be my first reviewer. Thank you for your trust, your time, and the opportunity to have you involved in this work.

I would also like to thank **PD Dr. Nicola Tomas** for his valuable support and advice during the course of this work. His input has been an important contribution to the completion of this thesis.

My sincere thanks also go to my colleagues who supported me throughout the years in the lab: **Silke Dehde, Ming Huang, Jana Abt, Larissa Seifert, Renke Lucas**, and **Sarah Köllner**. Thank you all for your support in the lab and for the great group outings that made the working days brighter.
A heartfelt thank-you goes to **Ming** for your tremendous support throughout the entire single-nucleus RNA-Seq process - from glomisolation all the way to the computational analysis. I also want to thank **Jana** for being both my lab partner and coffee-break companion - without you, the lab would have felt a lot emptier.

Finally, I would like to thank my family and my husband for being by my side throughout this journey and for your unwavering support, encouragement, and patience. I hope you are all proud.

II. Index of figures

III. Index of Tables

IV. List of abbreviations

abbreviation	
%	percent
°C	degree Celsius
µg	microgram(s)
µm	micrometer(s)
µm2	square micrometers
AA	arachidonic acid
APCs	antigen presenting cells
art.EC	arteriolar endothelial cells
ATAC-Seq	assay for Transposase-Accessible Chromatin using Sequencing
BSA	bovine serum albumin
BUN	blood urea nitrogen
C1	complement component 1
C2	complement component 2
C2b4b	Classical/lectin C3 convertase
C2b4b3b	C5 convertase
C3	complement component 3
C3bBb	alternative C3 convertase
C4	complement component 4
chPLA2R1	chimeric PLA2R1
CNT	connecting tubule
cPLA2α	cytosolic phospholipase A2
CTLD	C-type lectin-like domains
CysR	cysteine-rich domain
DCT	distal convoluted tubule
DEGs	differentially expressed genes
eaMN	experimental active membranous nephropathy
ELISA	Enzyme linked Immunosorbent assay
Epha6	Ephrin Type-A Receptor
ERK 1/2	extracellular signal-regulated kinase 1/2
ESRD	end stage renal disease
EXT1/EXT2	Exostosin 1/Exostosin 2
FACS	fluorescence-activated cell sorting
FNII	fibronectin-like type II
FP	foot processes
FSGS	focal segmental sclerosis
Fx1A	insoluble sub-fraction from rat proximal tubule brush borders termed fraction 1A
GBM	glomerular basement membrane
GEC	glomerular endothelial cell
Glom. EC	glomerular endothelial cells
H_3PO_4	phosphoric acid
hIgG	human immunoglobulin class G
HLA II	human leukocyte antigen class II genes

hPLA2R1	human PLA2R1
HRP	horse raddish peroxidase
IC-A	intercalating cells type A
IC-B	intercalating cells type B
IgG	immunoglobulin class G
IntDen	integrated density
JGA	juxta glomerular apparatus
KO	knock out
M	Molar
MAC	membrane attack complex
MAPK	Mitogen-activated protein
MASP	mannose associated serin proteases
MBL	mannan binding lectin
MerTK	receptor tyrosine kinase Mer
mg	milligram(s)
MGE	mouse glomerular extract
mIgG	murine immunoglobulin class G
min	minute(s)
ml	milliliter(s)
mM	milli Molar
MN	Membranous nephropathy
mPLA2R1	murine PLA2R1
Nck	non-catalytic region of tyrosine kinase protein
NELL1	neural epidermal growth factor-like 1 protein
ng	nanogram(s)
OD	optical density
p53	tumor suppresor protein
PC	principal cells
PEC	parietal epithelial cells
PI3K	phosphoinositid-3-kinase
PLA2R1	phospholipase A2 receptor 1
prMN	primary MN
Prolif	proliferating cells
PT	proximal tubules
ROS	reactive oxygen species
RT	room temperature
SD	slit diaphragm
Sema3B	semaphorin-3B
snRNA Seq	single nucleus RNA sequencing
sPLA2	soluble phospholipase A2
sPLA2	soluble phospholipase A2
STAT	signal transducers and activators of transcription
TAL	thick ascending limb
THSD7A	thrombospondin type 1 domain-containing 7A
TMB	3,3′,5,5′-Tetramethylbenzidine
vas. sm	vascular smooth muscle cells

V. Summary

Membranous nephropathy (MN) is the most common cause of nephrotic syndrome in adults, with a very heterogeneous patient outcome. Primary MN is a rather slowly progressive and chronic disease that is defined by the accumulation of immune deposits at the glomerular basement membrane. These immune deposits are formed through autoantibodies targeting surface proteins of podocytes like phospholipase A 2 receptor 1 (PLA2R1) or thrombospondin type 1 domain-containing 7A (THSD7A). Binding of these autoantibodies will subsequently lead to the binding of complement factors and ultimately result in podocyte damage. However, the exact pathomechanism of how the antibodies damage the podocytes remained largely unknown and the role of the complement system in disease initiation and progression is discussed controversially. To dissect the detailed pathomechanisms and the role of the complement system, a suitable animal model is essential. Since PLA2R1 is not expressed on podocytes in mice, transgenic mouse lines had to be generated. Previously two such mouse models were established, both with some major limitations. One model is based on a mouse line that expresses murine PLA2R1 in poddocytes. These mice exhibit a normal phenotype and will only get sick after passive transfer of the anti-PLA2R1 antibodies. The other model is based on a mouse line expressing human PLA2R1 on the podocytes. These mice will develop autoantibodies from birth on, thus exhibiting a very rapid and exerbating phenotype. Both mouse lines can not resemble the rather slow development of MN. In an effort to generate a mouse model with an active and inducible diease onset, we sought to develop a chimeric mouse strain. We hypothesised that the first three human head domains are immunogenic enough to provoke a robust disease onset, while the backbone of murine C-type lectin-like domains (CTLD) 2 to 8 will maintain the tolerance towards the chimeric protein, preventing the spontaneous formation of autoantibodies.

In vivo characterisation of the chimeric PLA2R1 mice, showed that the knock-in of chimeric PLA2R1 does not interfere with a healthy podocyte morphology and behavior. Upon immunisation with hPLA2R1 the mice develop an antigen-specific and immune-mediated disease. Additionally, the mice showed the typical clinical pattern in morphology regarding mIgG and complement deposition. To better understand the role of the complement system in disease progression, we generated a mouse line expressing the chPLA2R1 with a simultaneous, global knock-out of complement component 3 (C3). After immunisation, these showed an attenuated course of disease. Onset of proteinuria was delayed and less severe, accompanied by a longer overall survival. These experiments showed that the complement system plays a role in the pathogenesis of this model of experimental PLA2R1 associated MN. However, the mice still got sick, indicating that also complement independent mechanisms play a role in disease initiation and progression. To gain insight into potential pathomechanisms, single nucleus RNA sequencing analysis revealed ephrin type-A receptor (Epha6) and receptor tyrosine kinase Mer (MerTK) as relevant genes for disease progression. Based on the snRNA-Seq results pathway analysis showed

predicted activation of pathways involving actin-cytoskeleton remodeling and receptor tyrosine kinase signaling in diseased mice.

VI. Zusammenfassung

Die Membranöse Nephropathie (MN) ist die häufigste Ursache für ein nephrotisches Syndrom bei Erwachsenen, wobei der klinische Verlauf sehr heterogen ist. Die primäre MN ist eine chronisch verlaufende, langsam progrediente Erkrankung, die durch die Ablagerung von Immunkomplexen an der glomerulären Basalmembran gekennzeichnet ist. Diese Immunablagerungen entstehen durch Autoantikörper, die gegen Podozyten-spezifische Oberflächenproteine wie Phospholipase A2 Rezeptor 1 (PLA2R1) oder Thrombospondin Typ 1 enthaltende Domäne 7A (THSD7A) gerichtet sind. Die Bindung der Autoantikörper an sie Antigene führt zur Aktivierung des Komplementsystems und resultiert in einer Schädigung der Podozyten. Der genaue Pathomechanismus, über den die Autoantikörper die Podozyten schädigen, ist bislang jedoch weitgehend ungeklärt. Darüber hinaus wird die Rolle des Komplementsystems bei der Entstehung und dem Fortschreiten der Erkrankung kontrovers diskutiert. Zur Untersuchung dieser Mechanismen ist ein geeignetes Tiermodell unerlässlich. Eine Herausforderung besteht darin, dass PLA2R1 auf Podozyten von Mäusen nicht exprimiert wird, was die Entwicklung entsprechender Mausmodelle erheblich erschwert. Dennoch konnten bislang zwei Mausmodelle etabliert werden, die jedoch einige wesentliche Einschränkungen aufweisen: Das erste Modell basiert auf einer Mauslinie, die murines PLA2R1 in Podozyten exprimiert. Diese Mäuse zeigen einen normalen Phänotyp und die Erkrankung kann erst durch den passiven Transfer von Anti-PLA2R1-Antikörper ausgelöst werden. Das andere Modell basiert auf einer Mauslinie, die humanes PLA2R1 in den Podozyten exprimiert. Diese Mäuse produzieren bereits sehr früh Antikörper gegen das humane PLA2R1 und zeigen somit einen sehr schnellen und aggressiven Verlauf. Beide Mauslininen können den typischen, eher langsam fortschreitenden Verlauf der humanen MN nicht adäquat abbilden. Mit dem Ziel, ein Mausmodell mit einem aktiven und induzierbaren Krankheitsbeginn zu entwickeln, wurde ein chimärer Mausstamm konzipiert. Wir stellten die Hypothese auf, dass die ersten drei humanen Kopfdomänen ausreichend immunogen sind, um einen robuste Immunantwort zu induzieren, während das Rückgrat der murinen C-Typ Lectin-ähnliche Domänen (CTLD) 2 bis 8 die Toleranz gegenüber dem chimären Protein aufrechterhält und die Bildung von Autoantikörpern verhindert.

Die In-vivo-Charakterisierung der chimären PLA2R1-Mäuse zeigte, dass der Knock-in von chimärem PLA2R1 die normale Morphologie und das Verhalten der Podozyten nicht beeinträchtigt. Nach Immunisierung mit hPLA2R1 entwickeln die Mäuse eine antigenspezifische und immunvermittelte Erkrankung. Desweiteren zeigten die Mäuse auch die typischen Merkmale des klinischen Erscheinungsbildes in Bezug auf die Morphologie, sowie murines Immunoglobulin G (mIgG) und Komplementablagerung. Um die Rolle des Komplementsystems im Krankheitsverlauf besser zu verstehen,

wurde eine Mauslinie erzeugt, die chPLA2R1 exprimiert und gleichzeitig einen globalen Komplementkomponente 3 (C3) Knock-out aufweist. Nach der Immunisierung zeigten diese Mäuse einen milderen Krankheitsverlauf. Der Beginn der Proteinurie war verzögert und weniger schwerwiegend, außerdem war die Überlebensrate der C3-defizienten Mäuse im Vergleich zu Kontrollmäusen erhöht. Diese Ergebnisse deuten darauf hin, dass das Komplementsystem eine wesentliche Rolle in der Pathogenese dieses experimentellen Modells der PLA2R1-assoziierten MN spielt. Dennoch entwickelten auch die C3-defizienten Mäuse eine Erkrankung, was darauf hinweist, dass zusätzlich komplementunabhängige Mechanismen zur Initiierung und zum Fortschreiten der Erkrankung beitragen. Um erste Einblicke in mögliche Pathomechanismen zu gewinnen, wurde eine Einzelkern-RNA-Sequenzierungsanalyse (snRNA-seq) durchgeführt. Diese Analyse identifizierte den Ephrin Typ-A Rezeptor (Epha6) und die Rezeptor-Tyrosinkinase Mer (MerTK) als potenziell relevante Gene für den Krankheitsverlauf. Basierend auf den snRNA-Seq Ergebnisse konnten mittels weiterführender Analysen Signalwege identifiziert werden, die in den Erkrankten Mäusen vermehrt aktiviert wurden. Diese Signalwege sind mit der mit der Umgestaltung des Aktin-Zytoskeletts und der Rezeptor-Tyrosinkinase vermittelten Signalübertragung assoziiert.

1. Introduction

1.1 Membranous Nephropathy

The kidneys are the central organs for filtration and detoxification. Their main function is to excrete metabolic waste products and toxins from the blood while retaining vital nutrients. Beyond these functions, they maintain the body's water, electrolyte, and acid-base balance, regulate blood pressure, and exhibit important endocrine functions. The functional units of the kidneys called nephrons, consisting of a glomerulus and a tubular system. Glomeruli are spherical structures containing a capillary tuft tightened by mesangial cells and enclosed by the Bowman capsule. They are the primary site of the filtration process enabled by a specialized structure, the filtration barrier, which is composed of fenestrated endothelium, the glomerular basement membrane (GBM) and podocytes, specialized endothelial cells enwrapping the outer glomerular capillaries with their foot processes (FP), exhibiting an interdigitating pattern with FPs of neighbouring podocytes. FPs are attached to the GBM forming the slit diaphragm, a highly specific cell-cell connection, allowing the selective passage of water and small molecules while retaining larger proteins and cells (1). Morphological integrity, particularly of the podocytes, is crucial for a functional filtration barrier (2). In case of podocyte injury high amounts of proteins can escape through the filtration barrier into the urine, resulting in a condition known as proteinuria. A nephrotic syndrome is reached when proteinuria exceeds 3.5 g a day and is accompanied by peripheral edema, hypoalbuminemia and hyperlipidemia (3).

Membranous nephropathy (MN) is amongst the most common causes of nephrotic syndrome in adults. It accounts for approximately 20 to 30% of the nephrotic syndromes in white and non-diabetic adults (4-6). Currently, MN is classified into primary or idiopathic and secondary forms, with only 20% of cases having a directly identifiable cause. The term 'secondary' reflects its occurrence as a complication of another primary disease. Malignancies, infections, medication or other diseases like systemic lupus erythematosus and hepatitis B are common causes for the secondary form of MN (7, 8). In these cases, the MN is resolved when the first issue is successfully treated. In the remaining 80% of patients, an underling cause could not be identified, which is why this form was classified as idiopathic or primary MN (prMN) (6, 9). This changed when in 2009 Beck *et al*. found autoantibodies against phospholipase A2 receptor 1 (PLA2R1) as the major cause of idiopathic MN (10). Since then, prMN was known to be an autoimmune mediated disease directed to intrinsic antigens on podocytes (6).

Histologically prMN is characterised by the thickening of the GBM and granular deposition of immunoglobulin class G (IgG) and complement components along the capillary walls, which can be seen in light microscopy and immunofluorescence staining. In electron microscopy two other key features of MN are visible: 1) the

formation of electron dense deposits in the subepithelial space and within the GBM and 2) podocyte effacement (11).

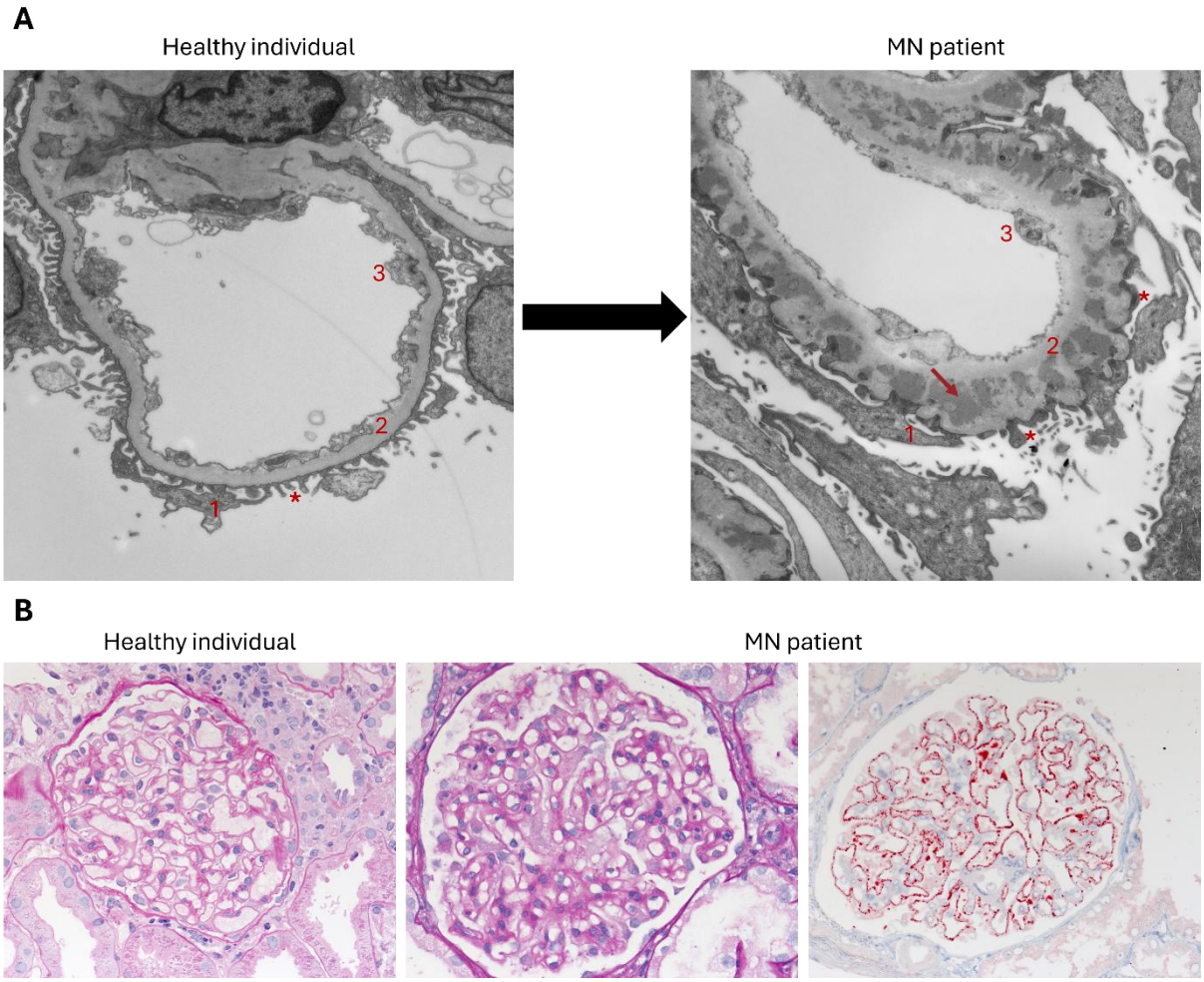

Figure 1: Histological features of membranous nephropathy. *A) Electron microscopic image of a healthy (left) and diseased (right) glomerular filtration barrier. The filtration barrier is composed of 1: podocytes, 2: the glomerular basement membrane (GBM) and 3: endothelium. In MN the glomerular basement membrane is broadened, the foot processes of the podocytes (asterisk) are effaced and electron dense deposits are found in the subepithelial space (red arrow). B) PAS staining of healthy control (right) and patients with MN (left and middle). In the PAS from the MN patient (middle) the thickening of the GBM is visible. Immunohistochemical staining (right) of for IgG in renal biopsy specimens from MN patients show an increased and granular deposition of IgG along the capillary wall. All images were kindly provided by Prof. Dr. Thorsten Wiech, Institute of Pathology, UKE.*

1.2 Ethiology and clinical features

Although prMN can affect people of all ages, regions and ethnic groups, there are clear trends as to which groups are more likely to develop the disease. As prMN is a common cause for nephrotic syndrome in adults, it is very rare in children. The median age of diagnosis is between fifty and sixty. Furthermore, there is a two to one prevalence of male patients (6, 12).

Clinically about 80% of patients with prMN develop a nephrotic syndrome at the date of diagnosis, whereas the other 20% initially have subnephrotic proteinuria. However, around 60% of the subnephrotic patients will gain nephrotic syndrome within one consecutive year, if they develop an antibody-titer against PLA2R1 (7). Particularly, the early phase of disease often has an indolent course, with the immune complexes

building up slowly and progressively damaging the podocytes, which is why the symptoms like proteinuria usually appear slowly and can be unrecognized for month (6). Clinical course and outcome are very hard to predict, since there is a huge heterogeneity between the patients. Approximately one third of the patients undergo spontaneous remission within the first two years. The relapse rate among patients in remission is between 25% and 30% (6, 13). The numbers of patients that will develop progressive kidney failure and ultimately end stage renal disease (ESRD) vary, dependent on treatment and previous clinical course. A ten year follow up from two different clinical trials showed that 35 to 40% of the patients will develop ESRD when they are treated conservatively, whereas only eight to ten percent of patients treated with immunosuppressive agents developed ESRD (6). One study found that in absence of remission one quarter of the patients will progress to ESRD within eight years and another 50% after ten to 15 years of disease (14).

1.3 Antigens in prMN

Since the discovery of PLA2R1 as the major autoantigen in 70-80% of patients in 2009 (10), efforts have been made to identify other autoantigens. The second autoantigen discovered was thrombospondin type 1 domain-containing 7A (THSD7A), which is present in approximately three percent of patients (15). In recent years, more minor autoantigens have been identified, including neural epidermal growth factor-like 1 protein (NELL1), Exostosin 1/Exostosin 2 (EXT1/EXT2), and semaphorin-3B (Sema3B) (6).

1.3.1 PLA2R1

PLA2R1 is a type I transmembrane glycoprotein and a member of the C-type lectin superfamily. It consists of an N-terminal cysteine-rich domain (CysR), a fibronectin-like type II (FNII) domain and a repeat of eight C-type lectin-like domains (CTLD), a transmembrane domain, a short intracellular domain and has a molecular mass of 180 kDa [1] (**Figure 2**A). PLA2R1 is expressed in several tissues like lung, kidney, pancreas and alveolar type II pneumocytes (16). The biological functions are complex and not fully discovered yet, but as indicated in the name, it is the receptor for several soluble phospholipase A2 (sPLA2) isoforms. Binding of sPLA2 to PLA2R1 has various pleiotropic effects, depending on cell type and sPLA2 isoform. One of the most studied sPLA2 isoform is group 1B sPLA2 (sPLA2 IB). In various rat and murine cultured cells binding of sPLA2 IB to PLA2R1 resulted in the activation of the mitogen-activated protein kinase (MAPK) signaling pathway leading to various effects like cell proliferation and migration, hormone release and chemokine production (16). In WI38 cells, a cultured lung cell line, PLA2R1 regulated cellular senescence by the production of reactive oxygen species and the concordant activation of DNA damage pathway p53 (17). On the contrary, in podocytes and neurons the binding of sPLA2 IB to PLA2R1 can induce apoptosis (17, 18). Moreover, PLA2R1 can bind collagen I and IV, suggesting a role in cell adhesion and migration (19). Despite these biological functions, it is the major autoantigen in membranous nephropathy.

1.3.2 PLA2R1 autoantibodies

Autoantibodies from patients are mainly from the IgG4 subtype, nonetheless a minor proportion of PLA2R1 specific autoantibodies are also from other IgG subtypes (20). Most autoantibodies are directed to an epitope that is located in the CysR domain (Figure 2A) Additionally, patients also developed autoantibodies against regions in CTLD1, CTLD7 and CTLD8, although the titers are lower compared to CysR (21-25). In 2022 Fresquet *et al*. revealed the structure of PLA2R1, showing that these immunogenic domains, containing different epitopes, are in close proximity to each other. Further, they are all located on the surface making them accessible for antibodies (26) (**Figure 2**B).

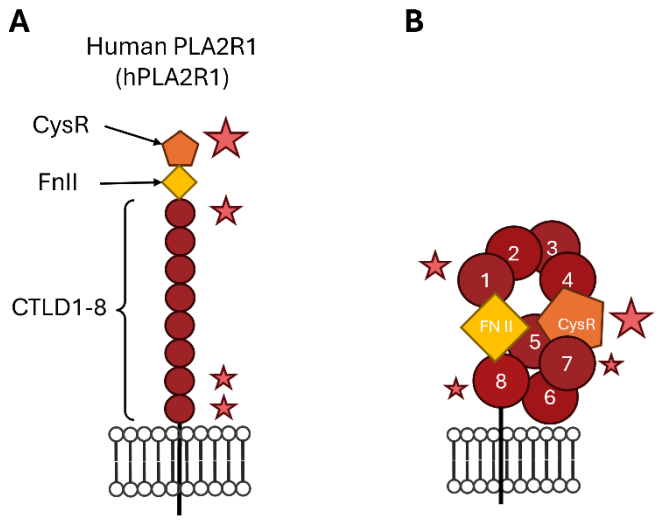

Figure 2: Structure of PLA2R1 A) *Schematic structure of the extra cellular domains of PLA2R1. It consists of an N-terminal cysteine-rich domain (CysR), a fibronectin-like type II (FNII) domain and a tandem repeat of 8 C-type lectin-like domains (CTLD1-8), a transmembrane domain and a short intracellular domain.* ***B)*** *Arrangement of PLA2R1 domains according to Fresquet et al. (26). The immune dominant domains (CysR, CTDL1, CTLD7, CTLD8) are in close proximity, accessible and exposed. Light red stars indicate autoantibody binding sites. Size correlates with immunogenic potential.*

1.4 Pathology and pathomechanisms

The events that trigger the production of autoimmune antibodies are still unknown (27-29). There are several hypotheses for how and why autoantibodies against podocyte proteins are generated. Various mechanisms can lead to the generation of autoreactive B Cells, such as loss of central or peripheral tolerance, genetic factors altering either the antigen or the affinity of the human leukocyte antigen class II genes (HLA II) towards the antigen, antigen presentation in other tissues or molecular mimicry. Additionally, there is a link between air pollution and incidence of PLA2R1 associated MN. A study from China proposed a potential pathomechanism involving the lung as a kind of disease origin. Air pollution, particularly the exposure to fine particulate matter < 2.5 µm can lead to oxidative stress in the airways and lungs, causing the cells to produce pro-inflammatory cytokines resulting in the stimulation of antigen-presenting cells (30). Since PLA2R1 is expressed on alveolae macrophages, it can be endocytosed and being presented to antigen presenting cells (APCs) in this pro-inflammatory context, triggering the maturation of the APCs. Activated APCs will

stimulate and activate T-cells ultimately leading to the activation of B-cells. Of note, this will only be possible if there are some self-reacting lymphocytes that escaped the central tolerance. These B-cells will transform into plasma cells constantly producing and secreting autoantibodies against PLA2R1 (30). Although the proposed mechanism is intriguing, it is not confirmed so far. Furthermore, this theroy can probably not explain all cases of prMN. Another unresolved issue is how the autoantibodies can pass through the GBM and why the disease is limited to the kidney. Further the underlying pathomechanisms, how the IgG deposition causes podocyte damage, remain largely illusive (20, 28).

1.4.1 Role of the complement system

Most patient biopsies show complement deposition, implying complement associated damage as one possible pathological pathway (11).

There are three ways to activate the complement system: 1) classical pathway, 2) lectin pathway and 3) alternative pathway. All pathways lead to formation of a C3 convertase and the subsequent downstream pathway (**Figure 3**). Consequently, the pathways differ in how the C3 convertase is formed. The classical pathway is activated when C1q binds to antigen-antibody complex on a cell surface leading to the formation of the C1-complex. This complex undergoes conformational changes resulting in autoproteolysis of the C1s proenzyme. C1s cleaves C4 and C2 into C4a + C4b and C2a + C2b. C4a and C2a are released as peptides and C4b bind to C2b, resulting in the formation of the classical/lectin C3 convertase C4b2b. In contrast, the lectin pathway is antibody independent and based on pattern recognition molecules like the mannan binding lectin (MBL). When MBL recognises mannose residues it binds to associated serin proteases (MASP) leading to the subsequent cleavage of C4 and C2 and formation of C4b2b. Finally, the alternative pathway is driven by slow spontaneous hydrolysis of C3 and is consecutively active. Factor B binds to hydrolyzed C3b and the resulting complex is cleaved by factor D. Thereby forming C3 convertase of the alternative pathway C3bBb. All C3 convertases cleave C3 into C3a and C3b, where C3b will also bind to the classical convertase leading to the formation of the C5 convertase (C4b2b3b). This convertase will cleave C5 into C5b and C5a. C5b recruits C6, C7, C8 and C9 leading to the formation of the final membrane attack complex (MAC) C5b-9, resulting in pore formation in the target cell membrane (31).

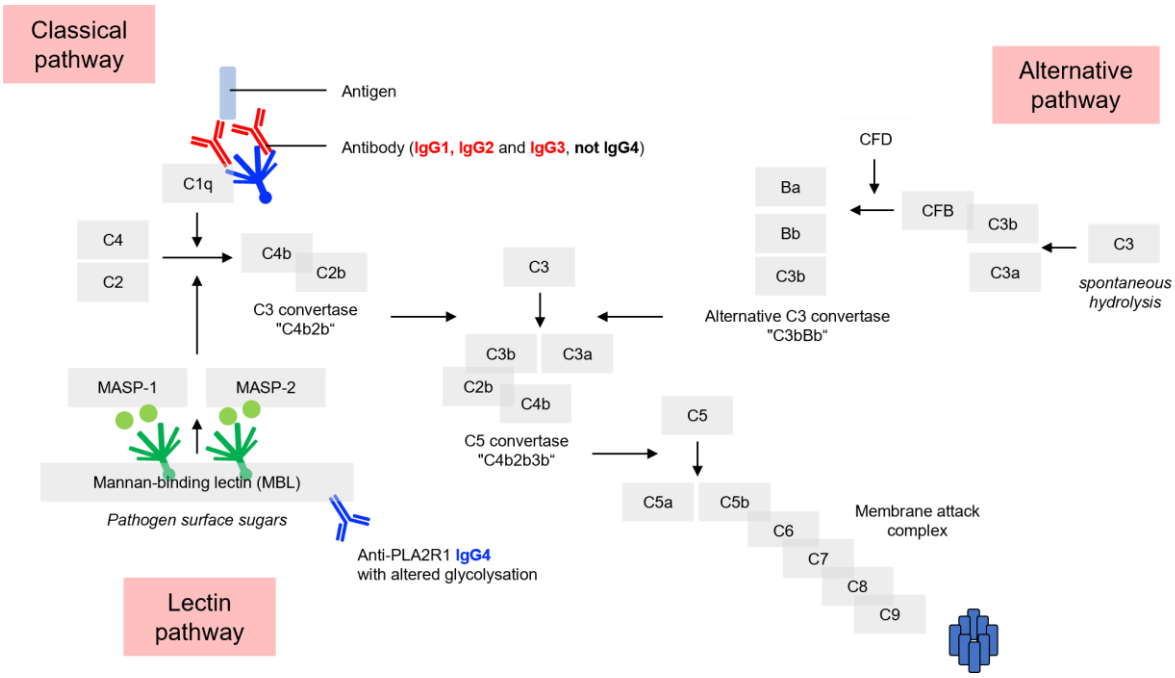

***Figure 3: Overview on the complement system**. The three activation pathways of the complement system: classical, lectin, and alternative. All pathways lead to the formation of a C3 convertase, the subsequent formation of the C5 convertase ultimately leading to the formation of the membrane attack complex. This figure was kindly provided by PD Dr. Nicola Tomas and slightly modified (32).*

In the context of MN, it is reasonable to assume that the antigen-antibody complexes activate the complement system and damage the podocytes by the insertion of the MAC into the membrane. However, the impact of the complement system in disease initiation and which pathway may be involved is controversially discussed due to the main subclass of anti-PLA2R1 antibodies, which is IgG4. This subclass has the least binding capacity to C1q and therefore, only limited ability to activate the classical pathway. (20, 29).

In context of autoantibodies in prMN the activation of the classical pathway is most likely. While earlier studies reported mostly negative C1q staining in patient biopsies, Seiftert et al. demonstrated C1q deposition in the majority of MN patients, indicating a potential involvement of the classical pathway (20). Moreover, they found THSD7A and PLA2R1 specific autoantibodies from the IgG1, 2 or 3 subclass, in all patients. Contrary to IgG4, IgG1, 2 and 3 are able to bind C1q and activate the classical pathway. They hypothesize, that the small amount of other IgG subclasses is sufficient for complement activation (20). Another study found that under-glycosylation of PLA2R1 specific IgG4 promotes the activation of the lectin pathway. They showed that prMN patients have an altered glycosylation pattern, the activation of the lectin pathway in the disease (33). Yet, only a subset of patients showed MBL deposition and prMN can also occur in genetically-MBL deficient patients (20, 34). However, Seifert *et al*. demonstrated in a THSD7A associated MN mouse model that a systemic knockout of C3 attenuates the disease course but can not prevent the onset of disease, indicating that there are also complement independent pathomechanisms (20).

1.4.2 Complement independent mechanism

Since the physiological function of PLA2R1, especially in podocytes, remains largely unknown it is difficult to study potential complement independent mechanism of the disease (35). Additionally, the lack of robust animal models hampered the investigation of its physiological functions *in vivo* (36).

As already mentioned, the binding of sPLA2 to PLA2R1 has pleiotropic effects including activation of MAPK signaling pathway, thus influencing proliferation, migration and hormone release (16-18). In the glomerulus, PLA2R1 can promote apoptosis via ERK1/2-cPLA2α-AA-p53 signaling pathway (18). In 2017 a study demonstrated the interaction of PLA2R1 with annexin A2-S100A10 complex. The authors speculate that, PLA2R1 may be a major component in actin cytoskeleton reorganization and tight junction assembly (36). Moreover, PLA2R1 can bind collagen I and IV, suggesting a role in cell adhesion (19). All these functions and interactions might be impaired by the binding of antibodies to PLA2R1, which may contribute to glomerular damage. This theory is supported by a study from 2014, demonstrating that PLA2R1 antibodies can interfere with the attachment of the podocytes to GBM by disturbing the interaction between PLA2R1and Collagen IV (37). However, all these theories remain speculative until there is experimental evidence (35).

1.5 Mouse models

To study the pathomechanisms of the disease and testing potential therapeutic targets animal models are essential.

The first model to study the mechanisms behind MN was the active Heymann nephritis model in rats. These rats were immunized with Fx1A, an extract of rat kidneys and Freund's adjuvants (FA) (38). FA is a water-in-oil emulsion containing heat-inactivated *mycobacterium tuberculosis*, designed to enhance the immune response. The rats developed antibodies against Fx1A, which was later identified as megalin (39, 40). Megalin is expressed in the tubule brush border and the podocytes in rats. After discovering megalin as the antigen-target in the Heyman nephritis model, additionally a passive model was established to study the mechanisms of the disease. Both active and passive Heymann nephritis rat models showed all histopathological and clinical aspects of the MN patients, making it a good model to study the pathomechanisms. The most relevant insights from these models were the in-situ formation of subepithelial immune complexes at the site of the antigen and the activation of complement system (39-42). Although the Heymann nephritis showed similar symptoms and clinical features as MN in patients, this model has some limitations. The most relevant limitation is that megalin is not expressed In human podocytes (43) and therefore it is not a target in human MN. Another restiction in the usability of this rat model is the lack of genetically-engeneered rat strains (44). Mouse models are desirable for many reasons like the broad availability of genetically engeneered strains and convienient manipulation. Over decades a suitable MN mouse models are lacking (44). This began to change when in 2009 PLA2R1 was discovered as the major autoantigen in MN (10)

followed by THSD7A in 2014 (15). Unfortunately, in contrast to THSD7A mice do not express PLA2R1 in their podocytes. Thus, THSD7A-associated mouse models could be established in wildtype mice (20, 45, 46). To study PLA2R1-dependent pathomechnisms transgenic mouse straines need to be established.

1.5.1 Passive model

The first mouse strain expressing a murine PLA2R1 in the podocytes was published 2019 by our group (47) (**Figure** 4A). The knockin of the murine PLA2R1 did not lead to any phenotype during the first four month of age. Only the passive transfer of rabbit-anti ,ouse PLA2R1 antibodies lead to the development of an MN-like phenotype. Three days after passive transfer the mice depeloped profund proteinuria that was stable over the observation period of one week. Furthermore, the mice showed IgG deposition along the capillary walls and complement deposition. Additionally, electron microscopy showed electrone dense deposits near the slitdiaphragm.

This passive model showed the pathogenicity of the anti mouse PLA2R1 antibodies. The major disadvantage is that the mice do not develop autoantibodies upon immunisation with the mPLA2R1. In conclusion, this model is not ideal for studying the disease's pathomechanisms, as its initiation and progression differ significantly from those observed in patients. Furthermore, it is not suitable for inverigations of B-cell or plasmacell therapeutics.

1.5.2 Spontaneous model

The second strain that our group published is a mouse expressing the human PLA2R in their podocytes (49) (Figure 4A). Starting with the age of five to six weeks mice develop proteinuria, with an exacerbating cause of disease. Latest by the age of twelve weeks all mice were severely sick and had to be sacrificed. All mice developed PLA2R1 specific antibodies. Furthermore, IgG deposition and relocation of PLA2R1 towards the capillary walls was detected in all mice. Electron micorscopy revealed the deposition of electron dense deposits in the subepithelial space as well as severe podocyte effacement.

This spontaneous model has the advantage that the antibodies are produced by the mice themself and therefore it is suitale to evaulate antigenspecific treatment like chimeric autoantibody receptor T cells or the clearance of the autoantibodies through endogenous degradation systems. The major disadvantage of this model is its rapid and aggressive development and progression, preventing extended observations of the mice. Consequently, the model fails to accurately replicate the slower disease progression observed in patients. Additionally, the early onset of MN in these young mice does not reflect the situation in the patients.

1.5.3 Chimeric mouse model

In order to create an inducible mouse model mimicking the rather slow development of MN, we sought to create a chimeric mouse strain. We hypothesised that the first three human head domains are immunogenic enough to provoke a robust disease onset,

while the backbone of murine CTLD2 to 8 will maintain the tolerance towards the chimeric protein, preventing the formation of autoantibodies (Figure 4A). Hence, after immunisation with recombinant human PLA2R1 the mice develop antibodies against the human head domains leading to the development of a membranous nephropathy like phenotype (48).

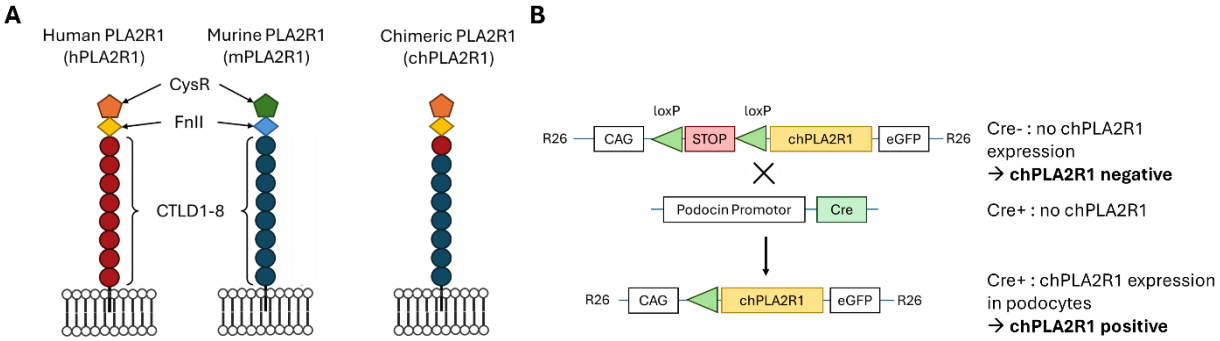

Figure 4: Schematic structure of the different PLA2R1 constructs and breeding scheme. A*) Schematic structure of human (hPLA2R1), murine (mPLA2R1) and chimeric (chPLA2R1) PLA2R.* ***B****) Schematic depiction of the chPLA2R1 full-length knock-in into the Rosa 26 (R26) gene locus. After breeding with podocin Cre positive mice, their littermates express chPLA2R1 specifically in podocytes.*

1.6 Aim of this work

The objectives of this thesis are first of all to establish the chimeric mouse model and examine the suitability of the proposed MN-like phenotype in response to active immunisation. Based on that the chimeric PLA2R1 mouse model is characterised, with respect to its disease progression, time course, and antibody titer development. The second goal is the assessment of the role of the complement system in both disease initiation and progression. The final objective is to perform in-depth analysis to identify potential molecular pathways activated during disease progression, which lead to podocyte damage. A detailed investigation of these pathways will provide insights into the mechanisms driving the disease.

2. Material and Methods

2.1 Material

2.1.1 Equipment

Table 1: List of equipment

Equipment	Model	Manufacturer
Centrifuges	ThermoScientific Multifuge X pro Series Centrifuge 5415D	Eppendorf, Hamburg, Germany
Confocal Microscope	LSM 800 with airyscan	Carl Zeiss AG, Oberkochen
Light Microscope	Axio Scope. A1	Carl Zeiss AG, Oberkochen
Microscope	Leica S6E	Leica Microsysteme Vertrieb, Wetzlar, Germany
Electrophoresis chamber	Mini Protean Tetra System for SDS PAGE	Mini Protean Tetra System for SDS PAGE
ELISA Reader	Tecan sunrise	Tecan, Switzerland
Gel Documentation	Amersham Imager 600	GE Healthcare, Chicago, IL, USA
Photometer	NanoDrop ND1000	PeqLab, Erlangen, Germany
Pipettes	Pipetman [0.2 - 2 µl, 2 – 20 µl, 10 - 100 µl, 20 -200 µl, 100 – 1000 µl] Accu-Jet	Gilson, Middleton, WI, USA Brand, Wertheim, Germany
Multichannel pipette	Transferpette	Brand, Wertheim, Germany
Multi-stepper		Eppendorf, Hamburg, Germany
Power supplies	Electrophoresis Power Supply 601	Amersham Bioscience, Freiburg, Germany
Rocker	GFL 3013	Omnilab Laborzentrum, Bremen, Germany
Steam cooker	FS3000	Braun GmbH, Kronberg im Taunus, Germany
Thermocycler	S1000 ThermalCycler	Biometra GmbH, Göttingen, Germany
Tissue Lyser	GentleMACS	Miltenyi Biotec B.V. & Co. KG, Bergisch-Gladbach, Germany
Vortexer		
Western Blot system	Trans-Blot Turbo Transfer System	BioRad Laboratories, Inc. Hercules, USA

Scales	Navigator Research	Ohaus, Switzerland Sartorius, Göttingen, Germany

2.1.2 Consumables

Table 2: List of consumables

Material	Manufacturer
96 Well plates High-bind, flat	Sarstedt, Nümbrecht, Germany
Disposable serological pipettes (5 ml/10 ml/25 ml)	Sarstedt, Nümbrecht , Germany
Injekt-F 1 ml Syringe	B. Braun SE, Germany
Mini-PROTEAN TGX Gels 10-well, 12-well, 15-well, 4-15 %	BioRad Laboratories, Inc. USA
Omnifix 1 ml Syringe	B. Braun SE, Germany
Petri dishes (10 cm)	Greiner-Bio-One, Frickenhausen, Germany
Zellculturschale TC 10	Sarstedt, Nümbrecht , Germany
Pipette tips	Sarstedt, Nümbrecht , Germany
Pipette tips, filtered	Starlab International Inc., Germany
Reaction tube 1.5 ml/ 2 ml	Sarstedt, Nümbrecht , Germany
Reaction tube – low bind 1.5 ml/ 2 ml	Eppendorf, Hamburg, Germany
Reaction tube 15 ml / 50 ml	Sarstedt, Nümbrecht , Germany
Low- retention filter tips 1250 µl	Sarstedt, Nümbrecht , Germany
Reaction tube 15 ml low bind	Sarstedt, Nümbrecht , Germany
Sealing Tape optically clear	Sarstedt, Nümbrecht , Germany
Cell Strainers	PluriSelect Life Science, Germany

2.1.3 Enzymes and Buffers

Table 3: List of enzymes and buffers

Enzyme/ Buffer	Manufacturer
GoTaq® G2 DNA polymerase	Promega, Madison, WI, USA
5x green GoTaq® Flexi Buffer	Promega, Madison, WI, USA
MgCl2 (25 mM)	Promega, Madison, WI, USA
Phusion® High-Fidelity DNA Polymerase	Thermo Scientific, Dreieich, Germany
5x Phusion® HF Buffer	Thermo Scientific, Dreieich, Germany
Collagenase V	Sigma/ Merck KGaA, Darmstadt, Germany
DNAse	Roche Diagnostics GmbH, Mannheim, Germany
RNasinPlus	Promega, USA
SUPERase·IN	Invitrogen, USA

2.1.4 Kits

Table 4: List of kits

Kit	Manufacturer
ChromiumNextGEMSingleCell3-GeneExpression v3.1(DualIndex) RevF	10X Genomics, USA
Nuclei Isolation Kit: NucleiPURE (NUC201)	Merck, Germany

2.1.5 Antibodies

Table 5: List of antibodies

Antibody	Conjugate	Dilution	Manufacturer
Donkey anti-mouse IgG	HRP	1:10000	Jackson Laboratories, USA
Goat anti-mouse IgG1		1:5000	Rockland Immunochemicals, USA
Goat anti-mouse IgG2a		1:5000	Rockland Immunochemicals, USA
Goat anti-mouse IgG2b		1:5000	Rockland Immunochemicals, USA
Goat anti-mouse IgG3		1:5000	Rockland Immunochemicals, USA
Goat anti-mouse albumin		100µg per 100 µl	Sigma-Aldrich, USA
Detection Ab, Goat anti mouse Albumin	HRP	1:40000	Bethly Laboratories, USA
Guinneapig anti-nephrin		1:200	Acris Antibodies, Germany
Rabbit anti Laminin		1:500	Sigma-Aldrich, USA
Rabbit anti C3		1:500	Abcam, UK
Goat anti C1q		1:400	Complement Technology, Inc., USA
Goat anti C2		1:400	Complement Technology, Inc., USA
Goat anti CfB		1:50	Complement Technology, Inc., USA
Goat anti CfH		1:00	Complement Technology, Inc., USA
Rabbit anti C4b		1:500	Hycult Biotech, Netherlands
Rabbit anti C5b-9		1:500	Abcam, UK
Rabbit anti PLA2R1-K1115		1:800	UKE, Germany
Rabbit anti DACH1		1:200	Sigma-Aldrich, USA
Guinneapig anti synaptopodin		1:200	Synaptic Systems (SYSY) GmbH, Germany

rabbit anti-Epha6		1:50	Proteintech, USA	
rabbit anti-MerTK		1:50	R&D Systems, USA	
rabbit anti-phosphoMerTK (Tyr749, Tyr753, Tyr754)		1:100	Invitrogen, USA	
donkey anti-mouse IgG H+L	Cy2	1:100	Jackson Laboratories	ImmunoResearch
donkey anti-rabbit IgG	AF488		Jackson Laboratories	ImmunoResearch
donkey anti-rabbit IgG	Cy3		Jackson Laboratories	ImmunoResearch
donkey anti-goat	AF488		Jackson Laboratories	ImmunoResearch
donkey anti guinneapig	Cy3		Jackson Laboratories	ImmunoResearch
donkey anti guinneapig	Cy5		Jackson Laboratories	ImmunoResearch
donkey anti guinneapig	Cy2		Jackson Laboratories	ImmunoResearch

2.1.6 Staining substances

Table 6: List of further staining substances

Chemical	Conjugate	Dilution	Manufacturer
WGA	rhodamine	1:400	Vector-Laboratories, USA
Draq5		1:1000	Cell Signaling Technology, Inc., Netherlands
Hoechst		1:1000	Sigma-Aldrich, USA

2.1.7 Buffers and Solutions

All chemicals were bought from Carl Roth GmbH (Karlsruhe, Germany), Sigma-Aldrich Chemie GmbH (Steinheim, Germany), Merck KGaA (Darmstadt, Germany) or Roche Diagnostics GmbH (Penzberg, Germany) if not clearly stated otherwise.

Table 7: Buffer and solution contents

Buffer/Solution		
Agarose gel		In TAE Buffer
Agarose	1.0 % (w/v)	
DPBS -CaCl -MgCl		Gibco, Life Technologies, USA
DPBS +CaCl +MgCl		Gibco, Life Technologies, USA
Procaine Hydrochloride	1.0 % (w/V)	Sigma, in DPBS
TMB solution		Aviva Systems Biology Corporation, USA
H_3PO_4 solution 37%		Sigma-Aldrich, USA

Histowash	10 X	50 mM Tris (pH 7.6), NaCl, 0.05 % Tween-20 in A.dest
Picrinic acid		Hengeler Analytik, Germany
NaOH		Hengeler Analytik, Germany

2.1.8 Chemicals

Table 8: List of chemicals

Chemical	**Manufacturer**
Tween20 -10%	Merck, Germany
TritonX100	Merck, Germany
DTT	Biomol GmbH, Germany
DEPC	Carl Roth GmbH + Co. KG, Germany
BSA	Carl Roth GmbH + Co. KG, Germany
UltraPureBSA	Invitrogen, USA
Trypanblue	Gibco, Life Technologies, USA

2.1.9 Software and Databases

Table 9: List of used software and databases

Software/Database	**Application**	**Developer**
Graphpad Prism 8.3	Data presentation and statistical analysis	GraphPad Software, Inc., USA
NCBI	Literature research	NIH, USA
GoogleScholar	Literature research	Google, USA
ImageJ	Image processing program	ImageJ, USA
R and Rstudio V 4.4.0	Analysis and presentation of snRNA seq data	Posit, USA
Seurat V 4.0.0	Analysis and presentation of snRNA seq data	Satija Lab, USA
SoupX package	Removal of ambient RNA	M.D. Young and S. Behjati, UK
fgsea package	Pathway analysis	Bioconductor, USA

2.2 Methods

2.2.1 Animal Experiments

Chimeric PLA2R mice were bred in the animal facility of the University Medical Center Hamburg-Eppendorf. Animals had access to water and standard animal chow ad libidum. All animal experiments were performed according to national and institutional animal care and ethical guidelines. Experiments were approved by the Veterinarian Agency of Hamburg and the local animal care committee (registration numbers 020/19 and 027/23)

2.2.2 Experimental autoimmune PLA2R11-membranous nephropathy (PLA2R1 EAMN)

Mice were immunised with recombinant human PLA2R1 (rec. hPLA2R1) and received a total of two immunizations three weeks apart. For first immunization one µg of rec. hPLA2R1 was mixed with the same volume of TiterMax Gold and injected subcutaneously. For the boost one µg of rec. hPLA2R1 was mixed with one quarter of TiterMax Gold. Control mice received subcutaneous injections of equal amount of adjuvants in PBS. Mice were at the age of 12 - 15 weeks when immunised. Serum was taken five weeks after first immunisation and during organ extraction. Urine was collected before immunization and then weekly, starting at three weeks after immunisation. Urinary and serum albumin was quantified using Albumin ELISA. Urine albumin values were standardised against urinary creatinine (measured in Jaffé Kinetic). Other blood parameters like cholesterol, triglycerides and blood urea nitrogen (BUN) were measured by standard procedures using COBAS system (Roche). Mice were sacrificed after a predefined observation period for blood, urine and kidneys.

Criteria to determine whether mice needed to be sacrificed before the observation period was over included, amongst others, development of visible ascites, respiratory distress due to fluid accumulation and a weight gain of <20% within one week.

2.2.3 Enzyme linked Immunosorbent assay ELISA

All ELISA experiments were performed in 96-well polystyrene high binding plates (Sarstedt). In this study, different ELISA setups were used, that are described in the following sections.

2.2.3.1 Human PLA2R1

Titer ELISA was used to determine and compare the titer of animals with the same immunization in different cohorts.

Plates were coated with a recombinant PLA2R1 protein, containing all domains from CysR to CTLD8, with a streptavidin tag (hPLA2R1 CysR-CTLD8 strep). Therefore, the plate was coated with 75 ng/well hPLA2R1 CysR-CTLD8 strep in carbonate-bicarbonate coating buffer (C3041, Sigma) over night at 4°C. After coating, wells were washed three times with 300 µl washing buffer (Tris-buffered saline with Tween-20 T9039, Sigma) and free binding sites were blocked with 100 µl postcoat buffer (Tris-

buffered saline with 1% BSA T6789, Sigma) for 30 minutes at room temperature. Wells were washed again three times with 300 µl washing buffer. Subsequently, 100 µl of 1:100 diluted mouse serum (in postcoat buffer with 0.05% Tween20) was added to the wells in duplicates and incubated for one hour at room temperature. To determine the titer against hPLA2R, a mixture of high titer sera derived from wildtype (WT) mice that were immunised with hPLA2R1 was used as a reference (diluted in postcoat buffer with 0.05% Tween20, ranging from 3000 RU to 4). After washing, 100 µl of HRP-conjugated anti-mIgG secondary antibody (1:10000, Jackson ImmunoResearch) was added for one hour at room temperature. Wells were then washed again before the TMB ELISA peroxidase substrate solution (Avia Systems Biology) was applied for 2 minutes at room temperature followed by 100 µl of 1 mol/L H_3PO_4 solution to stop the substrate reaction. The OD at 450 nm was measured using an ELISA reader (Tecan, Margellan). Antibody titers against hPLA2R1, relative units (RUs) were calculated according to the standard curve. For reactivity with the hPLA2R1 the OD at 450 nm was determined and compared to the blank condition.

2.2.3.2 PLA2R1 Domain ELISA

Domain ELISA was used to the reactivity of mouse sera with different parts of hPLA2R1.

Plates were coated with 100 ng of either purified and strep-tagged CysR-FnII, CTLD1-2, CTLD2-6 or CTLD7-8 in 100 µl carbonate-bicarbonate coating buffer (C3041, Sigma) over night at 4 °C. After coating, wells were washed three times with 300µl washing buffer (Tris-buffered saline with Tween20 T9039, Sigma) and free binding sites were blocked with 100 µl postcoat buffer (Tris-buffered saline with 1% BSA T6789, Sigma) for 30 minutes at room temperature. Wells were washed again three times with 300 µl of washing buffer. Subsequently, 100 µl of 1:500 diluted mouse serum (in postcoat buffer with 0.05% Tween20) was added to the wells in duplicates and incubated for one hour at room temperature. After washing, 100 µl of HRP-conjugated anti-mIgG secondary antibody (1:10000, Jackson ImmunoResearch) was added for one hour at room temperature. Wells were then washed again before the TMB ELISA peroxidase substrate solution (Avia Systems Biology) was applied for 2 minutes at room temperature followed by 100 µl of 1 mol/L H_3PO_4-solution to stop the substrate reaction. The OD at 450 nm was measured using an ELISA reader (Tecan, Margellan). The OD at 450 nm was determined and compared to the blank condition.

2.2.3.3 mPLA2R1

Domain ELISA was used to measure the potential cross reactivity of the mouse sera to mPLA2R1.

Plates were coated with 100 ng mPLA2R1 CTLD2-CTLD8 strep fragment in 100 µl carbonate-bicarbonate coating buffer (C3041, Sigma) over night at 4°C. After coating, wells were washed three times with 300µl washing buffer (Tris-buffered saline with Tween-20 T9039, Sigma) and free binding sites were blocked with 100 µl postcoat buffer (Tris-buffered saline with 1% BSA T6789, Sigma) for 30 minutes at room

temperature. Wells were washed again three times with 300 µl of washing buffer. Subsequently, 100 µl of 1:100 diluted mouse serum (in postcoat buffer with 0.05% Tween20) was added to the wells in duplicates and incubated for one hour at room temperature. To determine the titer against mPLA2R1, a mixture of high titer sera derived from WT mice that were immunised with mPLA2R1 was used as a reference (diluted in postcoat buffer with 0.05% Tween20, ranging from 2000 RU to 5). After washing, 100 µl of HRP-conjugated anti-mIgG secondary antibody (1:10000, Jackson ImmunoResearch) was added for one hour at room temperature. Wells were then washed again before the TMB ELISA peroxidase substrate solution (Avia Systems Biology) was applied for 2 minutes at room temperature followed by 100 µl of 1 mol/L H_3PO_4-solution to stop the substrate reaction. The OD at 450 nm was measured using an ELISA reader (Tecan, Margellan). Antibody titers against mPLA2R1, relative units (RUs) were calculated according to the standard curve. For reactivity with the hPLA2R1 the OD at 450 nm was determined and compared to the blank condition.

2.2.3.4 mIgG Subclass ELISA

mIgG Subclass ELISA was used to determine the composition of the subclasses of the anti-PLA2R1 antibodies.

Plates were coated with chimPLA2R1 (CysR domain to CTLD8 domain) in a concentration of 100 ng per 100 µl in carbonate-bicarbonate coating buffer (C3041, Sigma-Aldrich, Taufkirchen, Germany) over night at 4°C. After coating, wells were washed three times with 300µl washing buffer (Tris-buffered saline with Tween-20 T9039, Sigma) and free binding sites were blocked with 100 µl postcoat buffer (Tris-buffered saline with 1% BSA T6789, Sigma) for 30 minutes at room temperature. Wells were washed again three times with 300 µl of washing buffer. Subsequently, 100 µl of diluted mouse serum (1:50 in diluent buffer with 0.05% Tween20) was added to the wells in duplicates and incubated for one hour at room temperature. After washing, 100 µl of the antibodies against the different subclasses were added (IgG1, IgG2a, IgG2b, IgG3, all goat, 1:5000, Rockland 610-101-040, 610-101-041, 610-101-043, 610-101-043) and incubated for 1 hour, followed by 3 washing steps. Afterwards, 100 µl HRP-conjugated anti-mIgG secondary antibody (1:10000, Jackson ImmunoResearch) was added for one hour at room temperature. Wells were then washed again before the TMB ELISA peroxidase substrate solution (Avia Systems Biology) was applied for 2 minutes at room temperature followed by 100 µl of 1 mol/l H3PO4-solution to stop the substrate reaction. The OD at 450 nm was measured using an ELISA reader (EL808, Bio-Tek instruments). For reactivity with the different subclasses, the OD at 450 nm was determined and compared to the blank condition.

2.2.3.5 Albumin ELISA

Albumin concentrations in urine and serum was measured with this ELISA to monitor the disease progression. In combination with the creatinine concentration in the urine, proteinuria was calculated.

Plates were coated with 100 ng/well goat anti mouse albumin IgG (A90134A, Bethly) in coating buffer (C3041, Sigma) over night at 4 °C. On the next day plates were blocked with 100 µl/well postcoat (T6789, Sigma) for at least 30 min at RT. To analyze the concentration of the Albumin, an albumin reference (diluted in postcoat buffer with 0.05% Tween20, ranging from 15, 31, 62, 125, 250, 500 and 1000 relative units [RU]) was applied as a standard curve. Serum samples were diluted 1:30000 and Urine samples were diluted according the their urine-stix value (neg: 1:100; 0.5-1: 1:1000; 1.5: 1:10000; 2:1:30000; 2.5: 1:50000; 3: 1:100000; 3.5: 1:200000; 4: 1:1000000) in dilution buffer (postcoat buffer with 10% Tween20, E108, Sigma) and incubated in doublets for 1h at RT. The detection antibody (anti mouse albumin IgG-HRP) was diluted 1:40000 and incubated for 1h at RT. The ELISA was developed for 3 min in the dark with 100 µl TMB (OOA01684, Aviva/Biozol) before being stopped with 100 µl 1 M H_3PO_4

In between each step, the plates were washed three times with 300 µl washing buffer. The OD was measured with the Tecan Reader (Margellan) to calculate the serum titers.

2.2.4 Creatinine Assay

Creatinine Assays were performed in 96 polysterene plates (Sarstedt). 10 µl Urine and 10 µl Standard solution (ranging from 0.5, 0.4, 0.3, 0.2, 0.1, 0.05 mg/ml creatinine in 0.9% NaCl) were pipetted in doublets into the plate. Then 50 µl of picric acid solution (Hengeler analytik) was added and measured immediately at the Tecan Reader. After 5 minutes a second measurement was performed. The concentration of creatinine was calculated in excel using linear regression.

To obtain the albumin to creatinine Ratio the albumin value was divided by the corresponding creatinine value and multiplied by 10^6.

2.2.6 Measurement of Serum parameters

120 µl serum was analysed for cholesterol, triglycerides, urea and creatinine in COBAS system.

2.2.7 Immunofluorescence

Paraffin sections (2 µm) of formalin fixed, paraffin embedded mouse kidneys were deparaffinised and rehydrated to water. Dependent on the desired antigen, antigen retrieval was obtained by either boiling the sections in DAKO Target retrieval buffer S1699 pH6 for 30 min or protease XXIV digestion (5 µg/ml, Sigma-Aldrich) for 15 min at 37°C. Unspecific binding was blocked using blocking buffer (5% horse serum (Vector Laboratories) and 0.05% Triton X-100 (Sigma-Aldrich) in PBS) for at least 30 min at RT on a vertical shaker. Primary antibodies were diluted in blocking buffer and incubated over night at 4°C. Staining was visualised with affinity purified, fluorochrome conjugated secondary antibodies (Jackson ImmunoResearch Laboratories or Invitrogen, 1:100) in blocking buffer for 1 h at RT. Nuclei were stained with DRAQ5 (1:1000; Cell Signaling 40482) or HOECHST (1:1000; Sigma-Aldrich). Sections were

mounted with Fluoromount-G (Invitrogen). Stainings were evaluated with a confocal LSM800 with Airyscan using ZEN blue software (all Zeiss).

For immunofluorescent staining in mice, the following primary antibodies were used: nephrin (guinea pig, 1:200; Acris Antibodies BP5030), laminin (rabbit, 1:400; Sigma-Aldrich L9393), WGA-rhodamin (1:400; Vector-Laboratories), PLA2R1 (rabbit, 1:800; UKE), C3 (rabbit, 1:500, abcam), Epha6 (1:50, proteintech), MerTK (1:50, R&D Systems), phosphor-MerTK (1:100, Invitrogen), and murine IgG (donkey anti-mouse IgG H+L -Cy2, 1:100; Jackson ImmunoResearch Laboratories).

2.2.8 DACH1 staining

Paraffin sections (2 µm) of formalin fixed, paraffin embedded mouse kidneys were deparaffinised and rehydrated to water. Antigen retrieval was obtained by boiling the sections in DAKO Target retrieval buffer S2367 pH9 for 15 min. After cooling for 30 min the slides were washed with Histowah solution (50 mM Tris -pH 7.6, 150mM NaCl and 0.05% Tween20). Unspecific binding was blocked using blocking buffer (5% horse serum (Vector Laboratories) and 0.05% Triton X-100 (Sigma-Aldrich) in PBS) for at least 30 min at RT on a vertical shaker. Primary antibodies against DACH1 (rabbit, Sigma) and Synaptopodin (guinnea pig, SYSY) were diluted 1:200 in blocking buffer and incubated over night at 4°C. Staining was visualised with affinity purified, fluorochrome conjugated secondary antibodies (Jackson ImmunoResearch Laboratories or Invitrogen, 1:100) in blocking buffer for 1h at RT. Nuclei were stained with DRAQ5 (1:1000; Cell Signaling 40482). Sections were mounted with Fluoromount-G (Invitrogen). Stainings were evaluated with a confocal LSM800 with Airyscan using ZEN blue software (all Zeiss). Per mouse section ten randomly chosen glomeruli were acquired.

2.2.9 DACH1 quantification with ImageJ

DACH1 was stained and evaluated as described above; additionally, a scalebar was inserted with the ZEN blue software. To count the podocytes and measure the area of the glomeruli ImageJ was used. To assess the number of the Podocytes in one glomerulum, all DACH1 and DRAQ5 double positive nuclei were counted using the counting tool. Furthermore, the area of the glomeruli was measured with the free-hand tool. To determine the correct scale the function “set scale” in ImageJ was used. The length of the scalebar was measured using the line tool. The length of three scalebars was measured and the mean was used to set the correct scale. The podocyte density per μm^2 was calculated by dividing the Area by the podocyte number multiplied by 1000000.

2.2.10 mIgG subclass quantification with ImageJ

Mouse IgG subclasses were stained and evaluated as described above. As signal intensities of the different mIgG sublcasses varied, laser intensities were adjusted to avoid signal saturation and subsequently allow signal quantification (mIgG1: 0.05%, mIgG2a and mIgG2b: 0.1%, mIgG3: 0.15%). To quantify signal intensities, the images were processed using ImageJ. Glomeruli were encircled using the free hand selection

tool. Pictures were then converted into 8-bit, a threshold was set for each sublcass to reduce background fluorescence and integrated fluorescence intensity (IntDen) was measured. Finally, mIgG1, mIgG2a and mIgG2b values were multiplied by 3, 1.5 and 1.5, respectively, to correct for the different laser intensities and enable comparison of the different mIgG subclasses. Per mouse section a minimum of ten randomly chosen glomeruli were acquired.

2.2.11 Glomeruli isolation via differential adhesion method

PBS perfused kidneys from hPLA2R1-positive mice were unpacked, minced into small pieces, put into two 2 ml reaction cups and digested in 1.5 ml collagenase solution (1.2 mg/ml collagenase 1A, 100 U/ml DNAseI, 2.5 mg/ml BSA in HBSS and DMEM/F12) at 37°C at 1300 rpm agitation. Digested kidneys of one mouse were pooled in a 15 ml falcon (prerinsed with HBSS + 0.5% BSA). Reaction cups were washed two times with HBSS + 0.5% BSA, the falcon was filled to a volume of 11 ml and centrifuged at 290 g for 1 min. Supernatant was discarded and the pellet was resuspended in 5 ml HBSS. Collagenase-digested tissue was gently pressed through a 100 µm cell strainer followed by a wash with 10 ml HBSS. Subsequently, prefiltered gloms run through another filter step. The suspension was gently pressed through a 85 µm cell strainer followed by a 10 ml wash with HBSS. This solution was put on a 40 µm cell strainer to collect the glomeruli on top of the filter. After all the liquid passed through, the cell strainer was held top-down over a 10 cm TC dish (prerinsed with HBSS) and the remaining tissue was washed of the strainer with ~40 ml HBSS with a needle attached to a syringe. The glomeruli and remaining tubule fragments have different adhesion times, so the whole washing step should not take longer than two to three minutes. During this time most of the tubule attach to the bottom of the dish while most glomeruli are still floating. The liquid from the dish was transferred on a new 40 µm cell strainer using a 10 ml serological pipette and the procedure was repeated. Then the liquid from the second dish was transferred into a 50 ml conical centrifugation tubes (pre rinsed with HBSS + 0.5% BSA) and centrifuged at 290 g for 5 min. The supernatant was removed carefully, and the glomeruli pellet was resuspended in 1.3 ml PBS and transferred to a 1.5 ml low bind Reaction cup. Glomeruli were counted and spun down at 290 g for 4 min. Supernatant was removed and the pellet was carefully covered with 700 µl RNA later (Invitrogen)and stored at 4°C overnight. On the next day the glomeruli in RNA later were transferred to -80 °C. The entire procedure was performed at 4 °C with the exception of the collagenase digestion at 37 °C.

2.2.12 Isolation of single nuclei

The same amount of ice cold PBS was added to the glomeruli stored in RNA later and mixed carefully. Glomeruli were centrifuged at 500 g for 5 min and as much supernatant as possible was carefully removed. Glomeruli were resuspended in 50 µl lysis buffer (Nuclei PURE Lysisbuffer, 1%Triton X-100, 1mM DTT, RNAsePlus [20 U/ml], SupernaseIN [40 U/ml]) and transferred into a douncer. The suspension was dounced 30 times and transferred back into the original reaction cup. The douncer was washed with 300 µl lysis buffer that was also transferred to the reaction cup. All five minutes

the suspension was mechanically dissociated by pipetting 20 times. The status of the dissociation was checked every ten minutes. Lysis was stopped when most glomeruli released the nuclei, which was the case after 30 to 40 min. The nuclei suspension was strained through a 30 µm strainer into a 15 ml low bind conical centrifugation tubes and centrifuged at 120 g for four min. The supernatant was carefully removed, and the pellet resuspended in 50 to 100 µl PBS + 0.1% BSA, dependent on the size of the pellet. Nuclei numbers were counted with Trypan blue staining using the automated cell counter (BioRad). The nuclei concentration was adjusted to approximately one million nuclei/ml. Immediately after isolation the nuclei were prepared for Chip loading. The whole experiment was performed on ice.

Two mice, with similar proteinuria, were pooled after douncing and treated as one sample.

2.2.13 Chipload, Library construction and Sequencing

Chiploading and library construction was performed in UKE Single cell core facility. For the chipload the Chromium Next GEM 3' single cell Reagent Kit 3.1 Dual Index Rev E (10X genomics) was used.

The libraries were send for sequencing to BGI in Poland.

2.2.14 Analysation of single nuclei sequencing data

The sequencing results were aligned to the *mus musculus* (mm)10 reference genome by Cellranger V7.0.0 by Ning Song and Dr. Zeba Sultana. Further processing and analysis was done with Seurat V4.4.0. For quality control each dataset was cleaned from mitochondrial RNA with the SoupX package (49). Therefore, all datasets were converted into a seuratobject and processed as indicated in the SoupX vignette. The SoupX cleaned datasets were merged and for further cleaning, the percentage of ribosomal and mitochondrial genes was assessed with the PercentageFeatureSet(). All cells with a higher percentage than three percent ribosomal genes, one percent mitochondrial genes, less than 200 and more than 7500 counts were excluded. Then the dataset was processed for integration by running NormalizeData(), FindVariableFeatures(), ScaleData() and RunPCA(). All functions were run with the default seetings. After the first cleaning of the datasets all four samples were integrated into one dataset using CCA integration from Seurat. The integrated object was further processed as indicated in the Seurat Vignette with ScaleData(),RunPCA (npcs = 40), RunUMAP(), FindNeighbors(), FindClusters(). Unless otherwise specified all functions were run with default settings. Clusters were identified using common marker genes. Based on the expression of these markers manual doublet removal was performed. After manual doublet removal the dataset was integrated again, with another round of manual doublet removal and cell cluster annotation. To ensure a very clean dataset for differential gene expression analysis, the podocyte cluster of was subsetted and integrated again, followed by another round of doublet removal. Further the expression of chPLA2R1 was classified as chPLA2R1-positive if their expression values exceeded zero and chPLA2R1-negative when the expression equals zero. The function

FindMarkers (ident.1 =model, ident.2 =control, test.use = “wilcox”) was used to find differentially expressed genes (DEGs) between the model groups and control groups of each timepoint. Based on the DEG list pathway analysis were performed with the fgsea package (50). Pathway analysis was performed with different background genesets from Hallmark, Canonical pathways, Wiki pathways, Reactome and Gene ontology (whole gene ontology sets and the subsets: biological process, cellular component and molecular function). The different gene sets were downloaded from the mouse molecular signatures database (MSigDB) collections from UC San Diego and the BROAD institute (https://www.gsea-msigdb.org/gsea/msigdb/mouse/collections.jsp).

2.2.15 Validation and Integrated density quantification with ImageJ

For single nucleus RNA sequencing (snRNA Seq) validation analysis the mice that went into the experiments were analysed. For higher animal number three additional mice per group from other experiments matching the criteria (hPLA2R1 immunised, organ extraction at week 9, proteinuria ranging between 8 and 50 g/g) were also analysed.

Epha6, MerTK and phosphor-MerTK were stained as described above. Optimal laser intensity was chosen individually for each stained target. To quantify signal intensities, the images were processed using ImageJ. Glomeruli were encircled using the free hand selection tool. Pictures were then converted into 8-bit, a threshold was set for each target to reduce background fluorescence and integrated fluorescence intensity (IntDen) was measured. Per mouse section ten randomly chosen glomeruli were acquired and analysed.

2.2.16 Graphs and statistical analysis

All graphs from the result sections 3.1 to 3.4 were made with GraphPad Prism 8. Furthermore, all statistical analysis were performed in GraphPad Prism 8 either with a Mann-Whitney Test when comparing two groups, Log-rank Mantel-Cox test for survival analysis or a mixed effect analysis when comparing three groups. All graphs and plots in the results section 3.4 were made in R Studio.

3. Results

3.1 Generation and characterisation of a mouse strain expressing a chimeric PLA2R1 in podocytes

Our group previously generated two mouse strains: One expressing the human PLA2R1 and the other expressing the murine PLA2R1 specifically in podocytes. The murine PLA2R1 expression was well tolerated, and the mice did not develop auto-antibodies against the murine PLA2R1. Unfortunately, efforts to actively immunise mice with the murine protein to provoke a reproducible the onset of a disease remained unsuccessful. To prove the pathogenicity of the PLA2R1 antibodies, antibodies against the mPLA2R1 were passively transferred into the mice. Three days after transferring these antibodies the mice developed a MN phenotype. In contrast, the mice expressing human PLA2R1 rapidly formed antibodies against hPLA2R1 and got a severe MN phenotype, requiring to terminate the experiments at an age of six to eight weeks after birth. Consequently, due to the spontaneous course of disease, active immunisation in this model is not possible.

Therefore, we hypothesised that combining the advantage of the highly immunogenic human head domains (25) and a tolerable murine backbone will lead to a so called chimeric PLA2R1 (chPLA2R1) consisting of the three most immunogenic N-terminal human head domains (CysR, FnII and CTLD1) and the seven other C-terminal murine domains (CTLD2-8). The large murine backbone will maintain the tolerance towards the chimeric protein. And the human head domain will be sufficient for the antibodies to bind and initiate the disease after immuisation with the human PLA2R1. Thus, enabling the establishment of a PLA2R1 associated experimental active MN model (PLA2R1-eaMN) with a more prolonged course of disease in adult mice.

To generate these mice we used a Cre-based transgenic knock-in approach in which the chPLA2R1 transgene was inserted into the mouse Rosa26 locus. Cross breeding of these chPLA2R1 mice with podocyte-specific Cre recombinase positive ones allowing the removal of the floxed stop-cassette, enabling chPLA2R1 expression exclusively in podocytes. These animals are further named as chPLA2R1-positive mice. In contrast, mice not cross bred with this Cre recombinase positive mouse line cannot express chPLA2R1 respectively, they are further referred as chPLA2R1-negative (see Introduction **Figure 4**B). Western blot analysis of multiple organs confirmed the exclusive expression of chPLA2R1 in the kidneys (**Figure 5**)

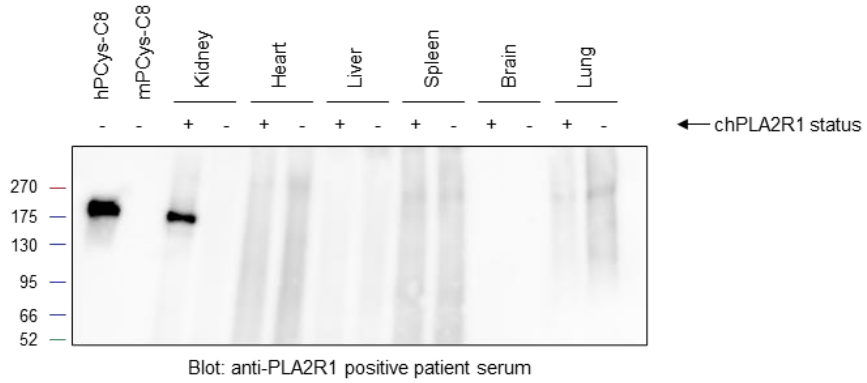

***Figure 5: Evaluation of transgene expression in different organs**. Western blot analysis (non-reducing conditions) of multiple tissues from chPLA2R1-positive (+) and -negative (-) mice at 25 weeks of age. Serum from a patient with PLA2R1-associated MN was used as the primary antibody (1:100) followed by detection with a secondary anti-human IgG4 antibody.*

Firstly, we were interested in the principle behavior of chPLA2R1 mice. To address this, chPLA2R1-positive and -negative mice were observed for a total of 25 weeks under untouched conditions. During this time both chPLA2R1 mouse-lines did not show any MN phenotype and also no abnormalities in behavior. The proteinuria was measured weekly and until the end of the observation period there was no proteinuria in chPLA2R1-postive and -negative mice detectable (**Figure 6**A). In addition, there were no differences in body weight or serum parameters such as albumin and blood urea nitrogen between chPLA2R1-positive mice and chPLA2R1-negative littermates (**Figure 6**B-F). Both groups did not show development of antibodies against chPLA2R1 during the time course of the experiment. These observations clearly implicate no spontaneous disease formation.

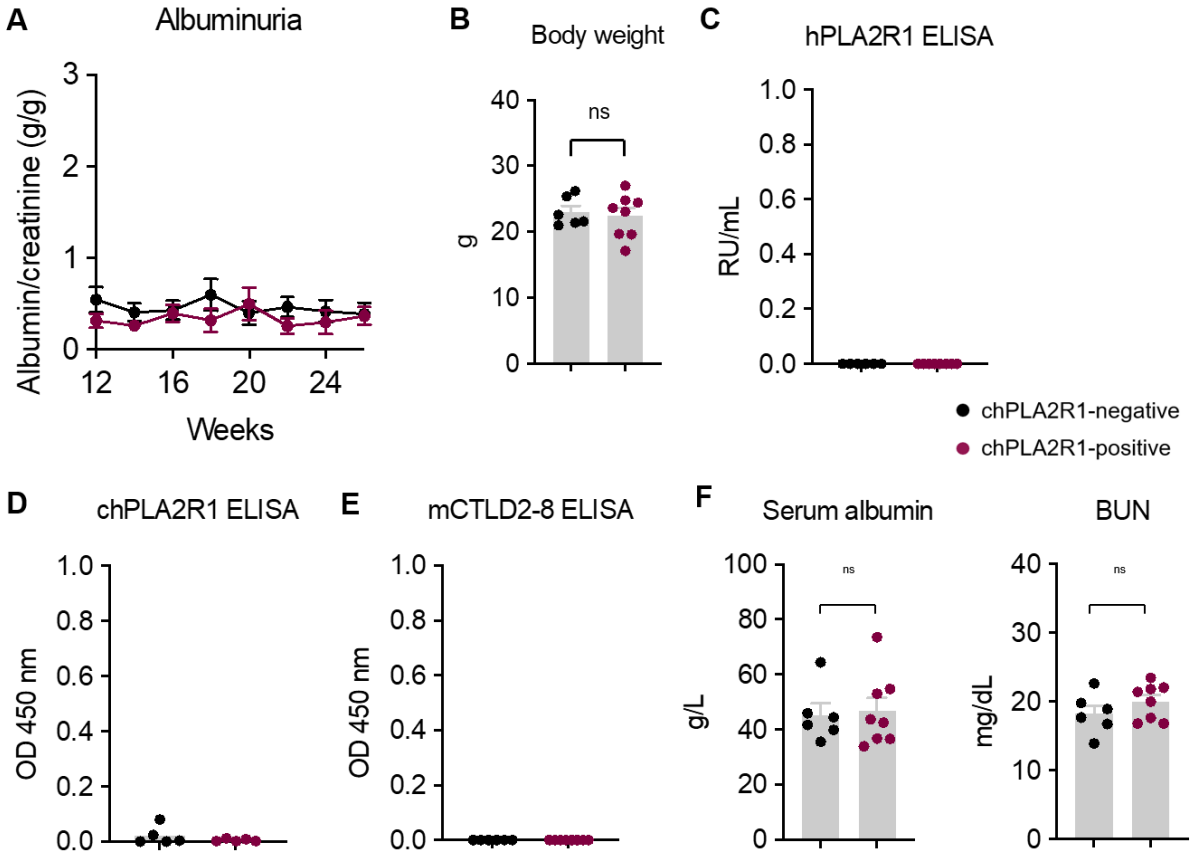

***Figure 6: Characterisation of mice expressing chPLA2R1 in podocytes**. **A)** Albuminuria measured by the albumin to creatinine ratios in chPLA2R1 positive (n = 8) and negative (n = 6) mice. **B)** Body weight in chPLA2R1-positive (n=8) and -negative (n = 6) mice 25 weeks after birth. Not significant (ns, Mann-Whitney test). Serum Titers against **C)** human PLA2R, **D)** chimeric PLA2R and **E)** murine PLA2R in chPLA2R1-positive (n = 8) and -negative (n = 6) mice 25 weeks after birth. **F)** Serum albumin (left) and blood urea nitrogen (right, BUN) levels in chPLA2R1-positive (n = 8) and -negative (n = 6) mice 25 weeks after birth. Not significant (ns, Mann-Whitney test)*

In the next step, we evaluated the histological morphology and phenotype of the chPLA2R1 mice. Immunofluorescence staining of chPLA2R1 (**Figure 7**A) confirmed a strong intracellular, cytoplasmatic expression of chPLA2R1 and very low presence at the membrane. Nephrin expression appeared normal in chPLA2R1-positive mice indicating no major impact on the slit diaphragm. In accordance, the ultrastructural analysis by electron microscopy did not show any alterations of the GBM (**Figure 7**B). Additionally, PAS staining revealed an inconspicuous histological morphology of the glomeruli and tubular interstitial tissue (**Figure 7**C) in 25 weeks old chPLA2R1-positive and -negative mice. Furthermore, staining against mIgG (**Figure 7**D) in chPLA2R1-positive mice was negative, which is consistent with the absence of anti-PLA2R1 antibodies in the serum. As expected, in PLA2R1-negative mice neither chPLA2R nor mIgG could be detected. Finally, in line with all previous results there was no alterations of the podocyte number per area (**Figure 7**E) in the 25 week old chPLA2R1-positive mice when compared to their chPLA2R1-negative littermates. Taken together, all these analyses showed no histological or clinical phenotype of MN in chPLA2R1 expressing mice.

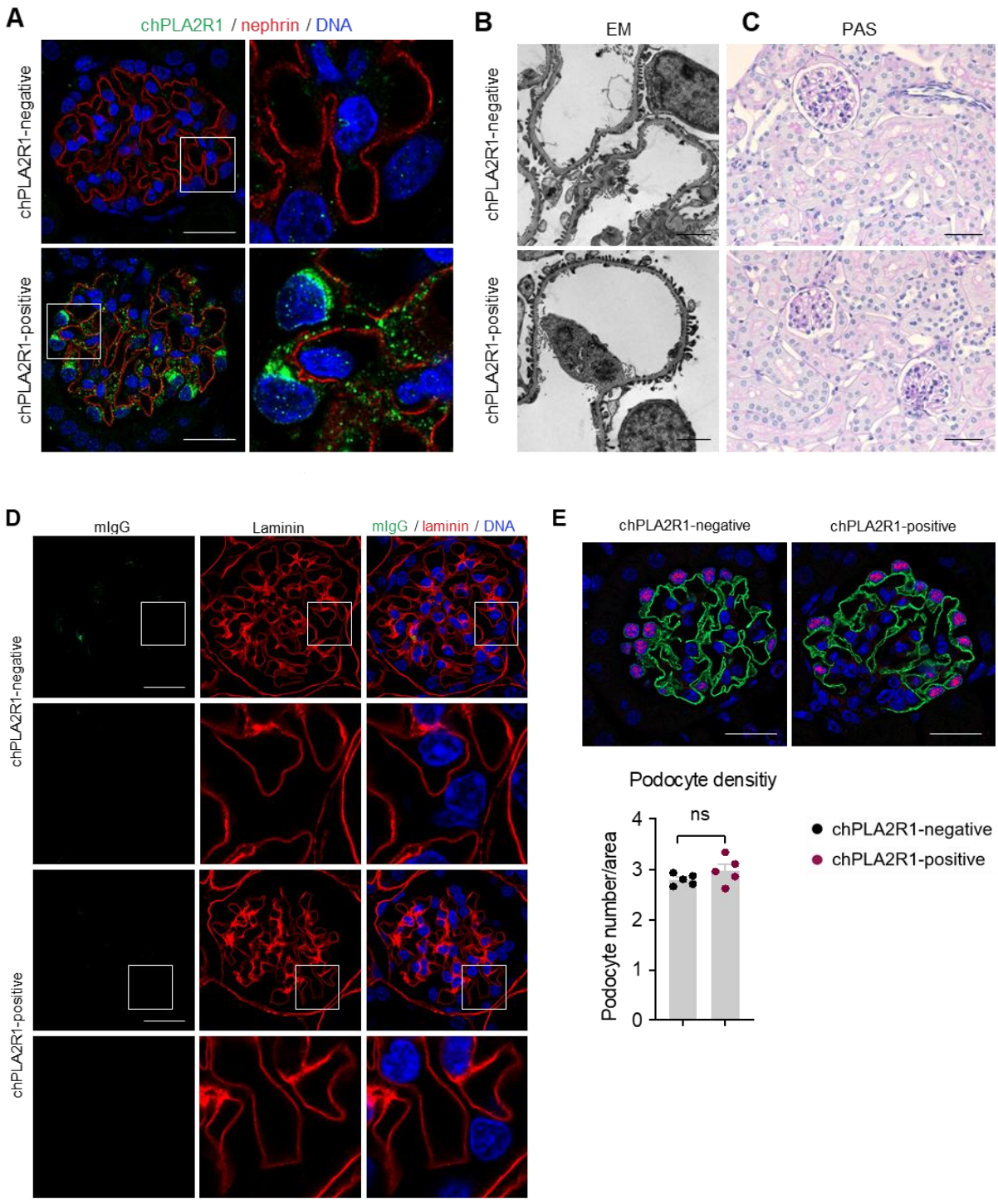

Figure 7: Microscopic analysis of the kidneys in chPLA2R1 expressing mice ***A****) Representative immunofluorescence staining for chPLA2R (green) and co-staining with nephrin (red) in chPLA2R1-positive and -negative mice 25 weeks after birth (n = 3 per group). Bar = 20 µm.* ***B****) Electron microscopic (EM) analysis of the glomerular filtration barrier in chPLA2R1-positive and -negative mice 25 weeks after birth (n = 3 per group). Bar = 2 µm.* ***C****) Representative image of periodic-acid-shiff (PAS) staining in chPLA2R1-positive and -negative mice 25 weeks after birth (n = 3 per group). Bar = 50 µm* ***D****) Representative immunofluorescence staining for murine IgG (green) in co-staining with laminin (red) in chPLA2R1-positive and -negative mice 25 weeks after birth (n = 3 per group). Bar = 20 µm. Panels in second and last row indicate fife times enlargements of the boxed areas in the images above.* ***E****) Representative immunofluorescence staining for DACH1 (red) in co-localisation with synaptopodin (green). Nuclei are blue. Quantification of DACH1-positive nuclei in 25 weeks old chPLA2R1-positive and -negative mice (n = 5 analysed per group). Bar = 20 µm. Not significant (ns, Mann-Whitney test).*

3.2 Establishment of an experimental PLA2R1 associated model of membranous nephropathy

3.2.1 Characterisation of hPLA2R1-immunised chPLA2R1-positive mice

After successfully characterising chPLA2R1-positive mice, we now aimed to induce PLA2R1-eaMN by active immunisation of 12-weeks old male mice that received two administrations with the complete ectodomain of hPLA2R1 (further referred as hPLA2R immunised, n = 21) or sodium chloride (further referred as control, n = 6), both in combination with the adjuvants TiterMaxGold, at an interval of three weeks. To evaluate a potential MN phenotype, the mice were monitored for overall 12 weeks after first immunisation (**Figure 8**A). Three weeks after immunisation the hPLA2R1-immunised mice started to slightly increase their albuminuria compared to their baseline values (**Figure 8**B). Six weeks after first immunisation the albuminuria strongly increased. Throughout the observation period, several mice developed severe proteinuria requiring to terminate the experiment earlier than 12 weeks to avoid the formation of ascites and pleural effusion (**Figure 8**C). Titers against hPLA2R1 could already be detected five weeks after first immunisation (**Figure 8**D). The highest titers were measured around eight weeks, before they decreased again. Most animals showed a substantial reactivity against hCysR-FnII, hCTLD1-2 and hCTDL7-8, whereas there was almost no reactivity against hCTLD2-6. Furthermore, there are no antibodies against the murine backbone (mCTLD2-8) of the chPLA2R1 detectable (**Figure 8**F), demonstrating that the antibodies are only directed against the immunogenic parts of the recombinant human PLA2R. Of note, the control animals did not developed detectable titers against any of the tested constructs. Western blot analysis clearly showed an anti-hPLA2R antibody/PLA2R1-antigen binding exclusively under non-reducing conditions as well as no mPLA2R1 detection at all (**Figure 8**G). Moreover, these antibodies also recognised chPLA2R1 (**Figure 8**E). Circulating immune complexes consisting of anti-hPLA2R1 and hPLA2R1, which was used for immunisation, could not be detected (**Figure 8**H). The analysis of serum parameters showed a significant decrease of serum albumin in hPLA2R1-immunised mice compared to the controls (**Figure 8**I), which is in line with the profound increase of albuminuria. Cholesterol (**Figure 8**J) and triglyceride (**Figure 8**K) concentrations were significantly decreased in hPLA2R1-immunised mice, demonstrating the development of a nephrotic syndrome. Increased blood urea nitrogen which indicates affected kidney functions, most likely due to severe albuminuria was only detectable in two hPLA2R1-immunised animals (**Figure 8**L). In summary, these experiments show that the immunisation of the chPLA2R1 mice, with hPLA2R1, cause the development of anti-hPLA2R1 antibodies and lead to nephrotic syndrome.

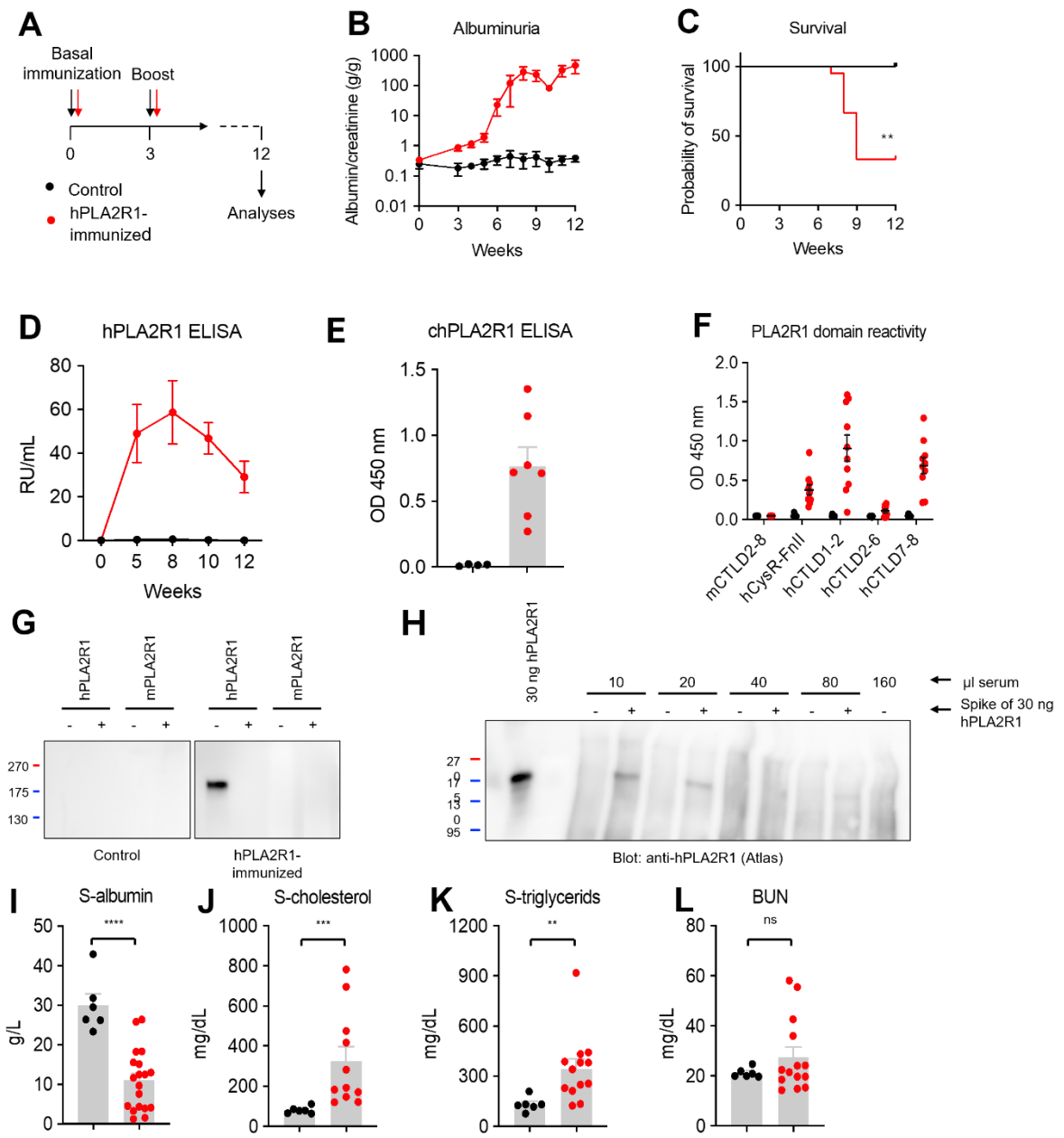

***Figure 8: Characterisation of hPLA2R1-immunised chPLA2R1 mice**. **A**) Experimental setup. Mice were immunised with TiterMax Gold adjuvant with NaCl (further referred as control, n = 6) or hPLA2R1 (further referred as hPLA2R1-immunised, n = 21) in three independent experiments. **B**) Albuminuria as measured by the albumin-to-creatinine ratio in control (n = 6) and hPLA2R1-immunised (n = 21) mice. **C**) Survival analysis (control n = 6, hPLA2R1-immunised n = 21). Log-rank Mantel-Cox test, **P < 0.01. D) Anti-hPLA2R1 antibody titers measured by ELISA in controls (n = 6) and hPLA2R1-immunised mice (n = 21). **E**) Anti-chPLA2R1 antibody levels in controls (n = 4) and hPLA2R1-immunised mice (n = 7) as measured by ELISA at the end of the observation period. **F**) Domain reactivity of anti-hPLA2R1 antibodies of control mice (n = 6) hPLA2R1-immunised mice (n = 21) at the end of observation time. **G**) Western blot analysis of sera from a control mouse and an hPLA2R1-immunised mouse on recombinant hPLA2R1 and murine PLA2R1 (mPLA2R1) under non-reducing (-) and reducing (+) conditions (representative blots from 3 investigated animals per group). **H**) In an attempt to detect a potential circulating soluble form of hPLA2R1 in the serum of hPLA2R1-immunised chPLA2R1-positive mice, immunoprecipitation assays using a monoclonal anti-hPLA2R1 antibody were performed using serum 12 weeks after the first immunisation. Different amounts of mouse sera (derived from hPLA2R1-immunisedchPLA2R1-positive mice) were used, always without and with a "spike" of 30 ng of hPLA2R1. hPLA2R1 was detected in the spiked conditions, but not the conditions without a spike, indicating that no (or only very minor) amounts of the hPLA2R1 used for immunisation enter the blood to potentially form hPLA2R1/anti-hPLA2R1 immune complexes. Immunoprecipitates were electrophoresed under reducing conditions, blotted, and detected with a commercial anti-PLA2R1 antibody (Atlas). **I**) Serum (S-) albumin levels in control (n = 6) and hPLA2R1-immunised mice (n = 19) at the end of the observation period. ****P < 0.0001 (Mann-Whitney test). **J**) Serum (S-) cholesterol and **K**) Serum (S-) triglyceride levels in control (n = 6) and hPLA2R1-immunised mice (n = 19) at the end of the observation period. ***P < 0.001, **P < 0.01 (Mann-Whitney*

*test). **L**) Blood urea nitrogen levels in control (n = 6) and hPLA2R1-immunised mice (n = 19) at the end of the observation period. Not significant (ns, Mann-Whitney test). CTLD = c-type lectin domain; ELISA = enzyme linked immunosorbent assay; FnII = fibronectin type II domain*

Following up on these results we analysed the histomorphological changes in immunised chPLA2R1-positive mice compared to control mice 12 weeks after immunization. Light microscopic evaluation of periodic acid-schiff stained kidneys showed a slight thickening of the GBM in hPLA2R1-immunised mice as well as the formation of numerous non-argyrophilic pinholes and spikes in Jones methenamine silver staining (**Figure 9**A). Both findings are typical signs of MN in light microscopy. These changes did not occur in the control mice. Ultrastructural analyses using electron microscopy revealed extensive foot process effacement, subepithelial electron-dense deposits and a broadening of the GBM exclusively in hPLA2R1 immunised mice (**Figure 9**B). In line with this the number of podocytes per area was also significantly decreased (**Figure 9**C).

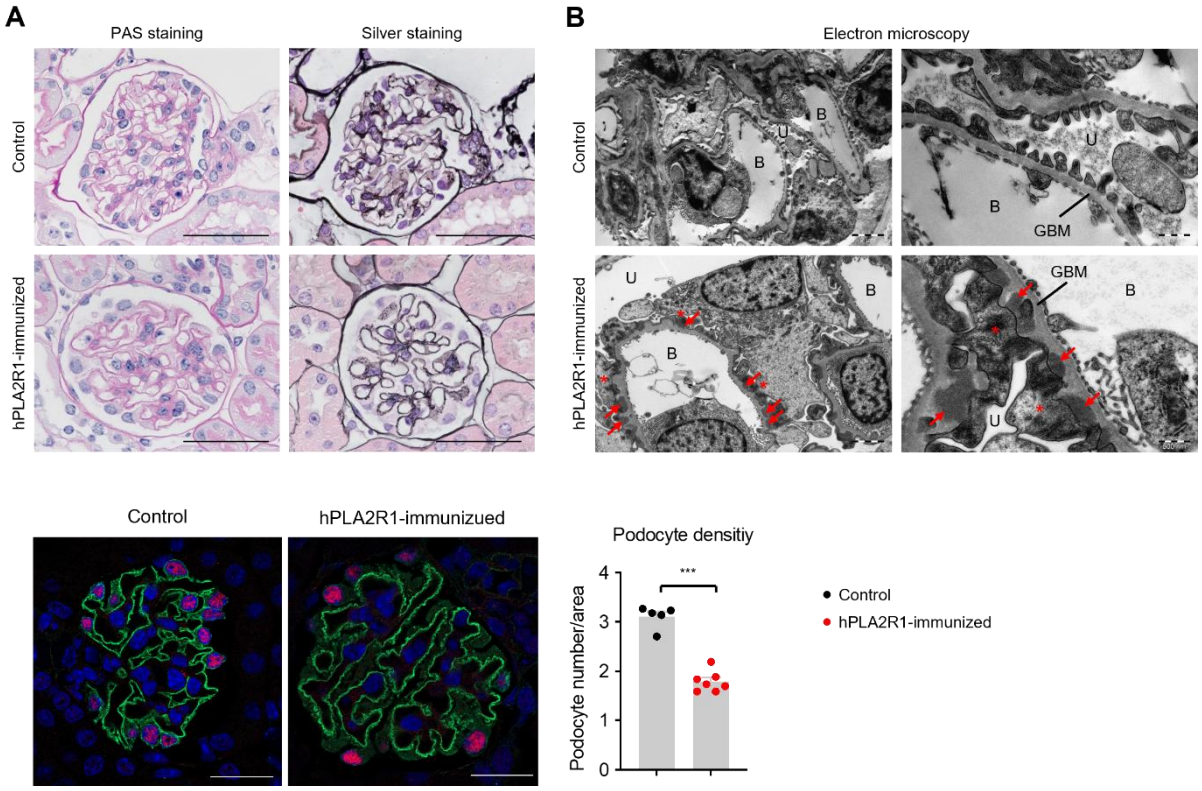

***Figure 9: Light and electrone microscopic changes and Podocyte density in chPLA2R1 positive mice after immunisation with hPLA2R1**. A) Representative images of Periodic acid-Schiff (APS) staining (left) and Jones methenamine silver staining (right) in control (n = 2) and hPLA2R1-immunised(n = 5). The red arrows mark spikes. Bar = 50 µm. B) Electron microscopic analysis of the glomerular filtration barrier in control and hPLA2R1-immunised mice (n = 3 analysed per group). The red arrows mark subeptelial electron-dense deposits. The asterisks mark effaced podocyte foot processes. Bars = 2 µm (left) and 500 nm (right). B, blood side; GBM, glomerular basement membrane; U, urinary side. C) Representative immunofluorescence staining for DACH1 (red) in co-localisation with synaptopodin (green). Nuclei are blue. Quantification of DACH1-positive nuclei in hPLA2R1-immunised (n = 7) and control (n = 5). Bar = 20 µm. ***P < 0.001 (Mann-Whitney test).*

Immunofluorescence staining of murine IgG showed a distinct granular deposition along the GBM in hPLA2R1-immunised chPLA2R-positive mice, but no IgG deposition in control mice (**Figure 10**A). The IgG deposition was localised at the subepithelial site of the GBM, as indicated by its relation to laminin. In control mice chPLA2R1 showed

a granular, cytoplasmic pattern, whereas in hPLA2R1-immunised mice it was highly accumulated at the basolateral membrane of the podocytes (**Figure 10**B). In addition, the relocation towards the podocyte membrane, chPLA2R1 strongly co-localised with the mIgG, suggesting a specificity for the glomerular mIgG towards chPLA2R1 (**Figure 10**C). To examine the specificity of glomerular mIgG in more detail, antibodies from frozen kidney sections of control and hPLA2R1-immunised mice were eluted and tested for reactivity against recombinant hPLA2R1 as well as mouse glomerular extracts (MGE) derived from hPLA2R1-positive/*Rag2*$^{-/-}$ mice using western blot analyses (**Figure 10**D). Mouse glomerular extracts from hPLA2R1-positive/*Rag2*$^{-/-}$ mice were used as a source of endogenously expressed hPLA2R1. The eluted mIgG from hPLA2R1-immunised mice recognised a protein of 180 kD in both mouse glomerular extract and recombinant hPLA2R1 samples. On the opposite there was no PLA2R1 protein detected in the elution of frozen kidney sections from control mice. These results demonstrate that glomerular mIgG of hPLA2R1-immunised mice is specific for hPLA2R1. To further characterise the specific anti-hPLA2R1-IgG, subclass analysis via immunofluorescence staining and ELISAs were performed. Staining for the different mIgG subclasses revealed that mIgG1 is the predominant subclass followed by mIgG2a, 2b and 3 (**Figure 10**F, G). In control mice the staining for mIgG were negative (**Figure 10**E). Corresponding to that, the most dominant subclass of anti-hPLA2R1mIgG circulating in the serum of hPLA2R1-immunised mice was again mIgG1, followed by mIgG2a, 2b and 3 (**Figure 10**H). These findings reflect the situation in the patient with PLA2R1-asscociated MN. There, the predominant IgG subclass, in the serum and in the kidney, is human IgG4 (hIgG4). mIgG1 is often considered to be the equivalent of hIgG4, because they exhibit similar features. Both IgG subtypes are described as unable to bind C1q and therefore cannot activate the complement system via the classical pathway. Taken together, these results demonstrate that chPLA2R1 positive mice develop the typical histomorphological signs of MN after immunisation with hPLA2R1.

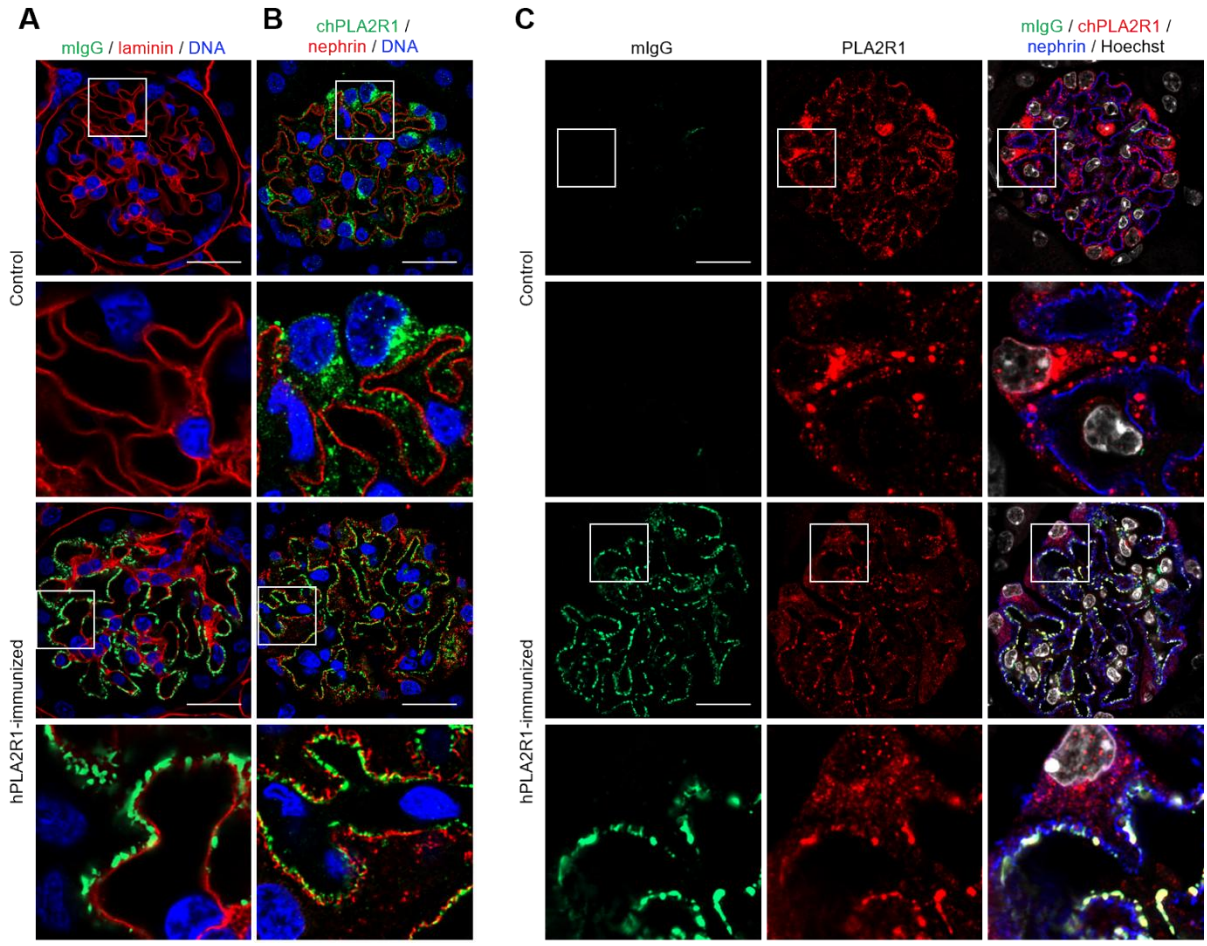
A
mIgG / laminin / DNA
B
chPLA2R1 /
nephrin / DNA
C
mIgG
PLA2R1
mIgG / chPLA2R1 /
nephrin / Hoechst
Control
hPLA2R1-immunized

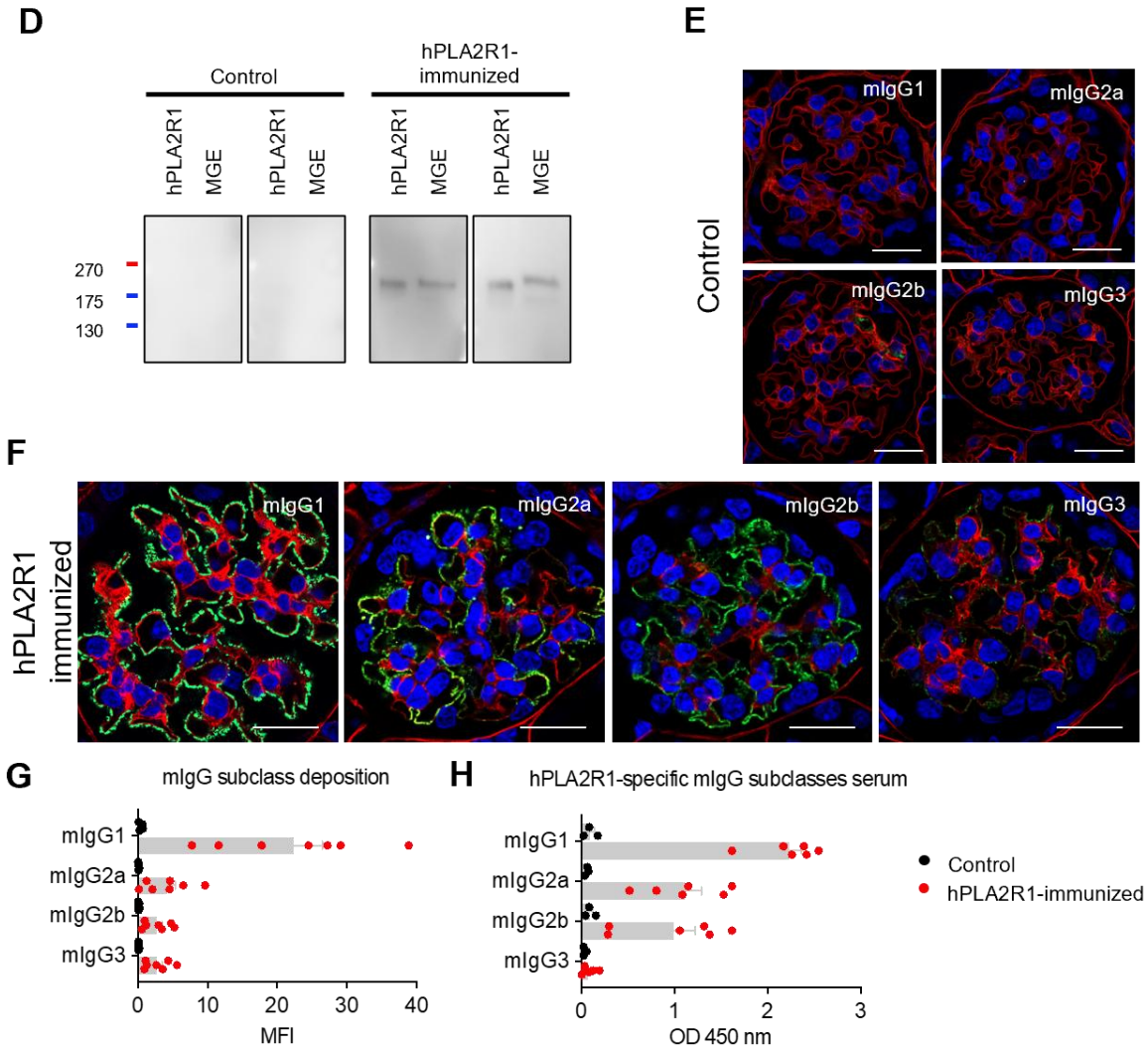

Figure 10: Immunofluorescence analysis of chPLA2R1, mIgG and mIgG subclass expression in hPLA2R1-immunised mice. ***A****) Immunofluorescence staining for mouse IgG (mIgG, green) in co-localisation with laminin (red) in control and hPLA2R1-immunised mice (n = 4 analysed per group.) The lower panels represent enlargements of the boxed areas in the upper panels. Bar = 20 µm.* ***B****) Immunofluorescence staining for chPLA2R1 (green) in co-localisation with nephrin (red) in control and hPLA2R1-immunised mice (n = 4 analysed per group). The lower panels represent enlargements of the boxed areas in the upper panels. Bar = 20 µm.* ***C****) Immunofluorescence staining for mIgG (green) in co-localisation with chPLA2R1 (red) and nephrin (blue) in control and hPLA2R1-immunised mice (n = 4 analysed per group). The lower panels represent enlargements of the boxed areas in the upper panels. Bar = 20 µm.* ***D****) Western blot analysis of antibodies eluted from frozen kidney sections of experimental mice (n = 3 analysed per group) on recombinant hPLA2R1 and mouse glomerular extracts (MGE) derived from mice expressing hPLA2R1.* ***E****) Representative immunofluorescence staining for mIgG1, mIgG2a, mIgG2b and mIgG3 in controls (n = 5). Scale bars indicate 20 µm.* ***F****) Representative immunofluorescence staining for mIgG1, mIgG2a, mIgG2b, and mIgG3 hPLA2R1-immunised mice (n = 7). Bar = 20 µm.* ***G****) Quantitative analysis (mean fluorescence intensity, MFI) of glomerular mIgG subclass deposition in controls (n = 5) and hPLA2R1-immunised mice (n = 7).* ***H****) mIgG subclass-specific anti-hPLA2R1 antibody levels as measured by ELISA in controls (n = 3) and hPLA2R1-immunised mice (n = 6)*

3.2.2 Complement deposition in hPLA2R1-immunised chPLA2R1-positive mice

Although, hIgG4 as well as mIgG1 is considered to be unable to activate the complement system, patients with PLA2R1 associated MN typically show complement deposition along the capillary walls. In regard to this the mice were analysed for complement activation, by immunofluorescence staining for different complement

components. C1q was used as a marker for the classical pathway, C4d as a marker of the classical or lectin pathway, complement factor B (CFB) as the main activator of the alternative pathway, the central complement factor C3 and the terminal complement factor C5. All these components were stained negative in control mice and positive in hPLA2R1-immunised mice, demonstrating substantial complement system activation and deposition in glomeruli after immunisation with hPLA2R1 (**Figure 11**A). Furthermore, C1q strongly co-localised with mIgG and chPLA2R1 indicating that all three components are deposited in the glomerular immune complexes (Figure 11B, C). In conclusion, all these results show, despite a dominant mIgG1 response, a significant deposition of complement factors in the glomeruli of hPLA2R1-immunised chPLA2R1-positive mice. Furthermore, all previous results demonstrated the successful development of an experimental and inducible model of PLA2R1 associated membranous nephropathy in mice, exhibiting essential characteristics of the MN.

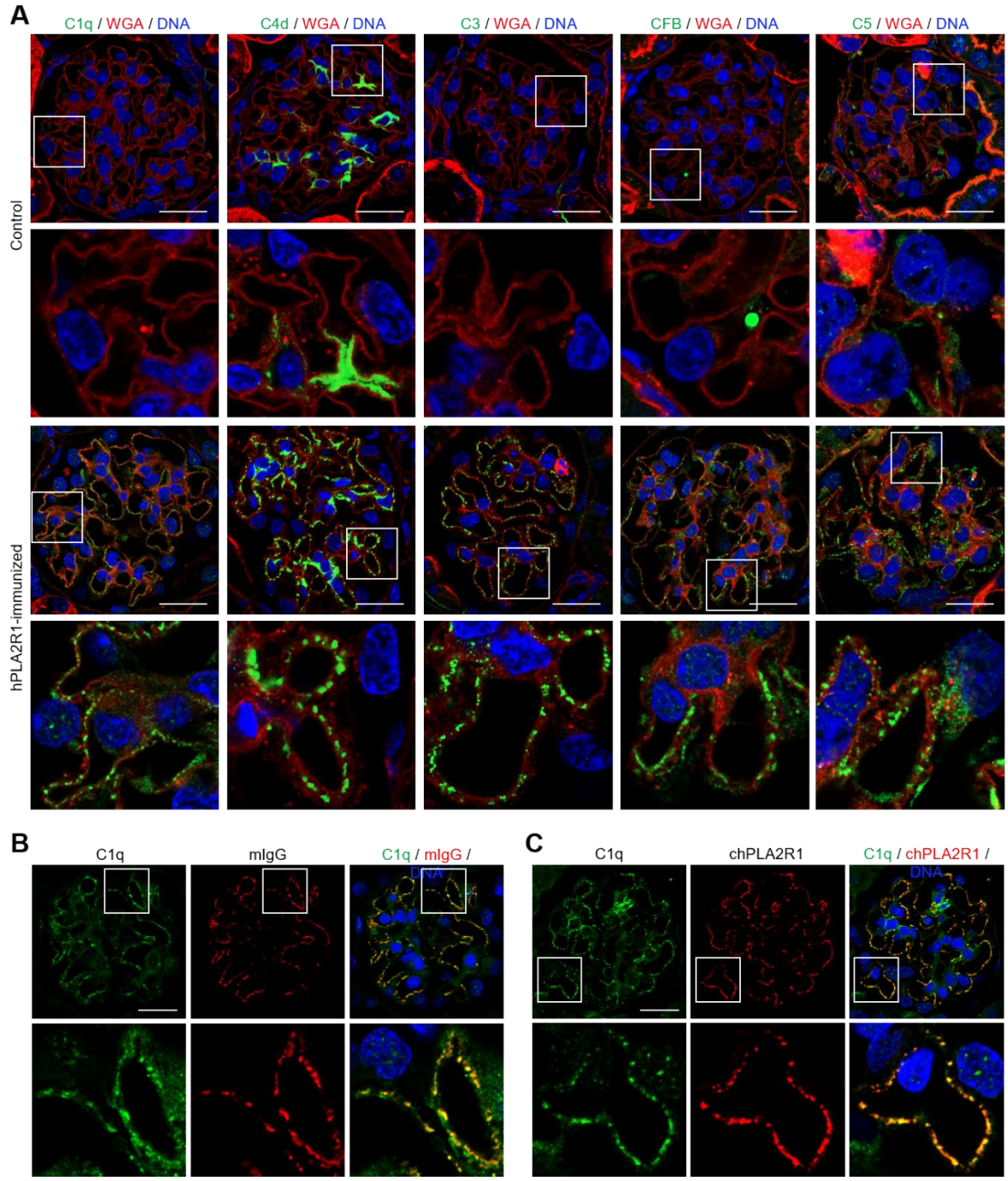

Figure 11: Complement deposition in hPLA2R1-immunised chPLA2R1-positive mice. ***A****) Immunofluorescence staining for complement C1q, C4d, C3, complement factor B (CFB) and C5 (all in green) in co-localisation with wheat germ agglutinin (WGA, red) in control and hPLA2R1-immunised mice (n = 4 analysed per group.) The lower panels represent enlargements of the boxed areas in the upper panels. Bar = 20 µm.* ***B****) Immunofluorescence staining for complement C1q (green) in co-localisation with mIgG (red). The lower panels represent enlargements of the boxed areas in the upper panels. Bar = 20 µm.* ***C****) Immunofluorescence staining for complement C1q (green) in co-localisation with chPLA2R1 (red). The lower panels represent enlargements of the boxed areas in the upper panels. Bar = 20 µm.*

3.3 Generation and characterisation of chPLA2R1-positive, C3-knockout mice

Based on the finding of substantial complement deposition in PLA2R1-eaMN, the pathogenic role of the complement system was further investigated. For this purpose

the chPLA2R1-positive mice were crossed with mice lacking the central complement component C3 ($C3^{-/-}$), resulting in the generation of chPLA2R1-positve/$C3^{-/-}$ and chPLA2R1-positve/$C3^{WT}$ littermates. The previous established hPLA2R1 immunisation protocol (**Figure 8**A) was applied in chPLA2R1-positve/$C3^{-/-}$ (n = 28) and chPLA2R1-positve/$C3^{WT}$ (n = 25). As control groups mice from both genetic lines were treated with sodium chloride plus adjuvant (further referred as control, n = 13). To evaluate the disease progression in both immunised mouse lines the mice were monitored for 12 weeks after first immunisation (**Figure 12**A). Starting at week four both chPLA2R1-positve/$C3^{-/-}$ and chPLA2R1-positve/$C3^{WT}$ mice had slightly increased albuminuria compared to the controls (**Figure 12**B). Until week eight both models have a comparable increase in proteinuria, nonetheless chPLA2R1-positve/$C3^{-/-}$ mice always had lower levels than chPLA2R1-positve/$C3^{WT}$. From week nine on chPLA2R1-positve/$C3^{WT}$ mice had significantly increased proteinuria compared to chPLA2R1-positve/$C3^{-/-}$ mice. In chPLA2R1-positve/$C3^{WT}$ mice the level of proteinuria did not increase further after week nine. Whereas proteinuria in chPLA2R1-positve/$C3^{-/-}$ mice slightly increased in week eleven again. Further, significantly more mice in the chPLA2R1-positve/$C3^{WT}$ group developed severe proteinuria compared to chPLA2R1-positve/$C3^{-/-}$ mice, requiring to sacrifice the mice earlier (**Figure 12**C). The titers against hPLA2R1 were similar in both immunised groups (**Figure 12**D). Of note, control mice developed neither proteinuria nor titers against PLA2R1. The serum analysis showed that chPLA2R1-positve/$C3^{-/-}$ mice had higher serum albumin and lower cholesterol levels than chPLA2R1-positve/$C3^{WT}$ mice (**Figure 12**E). The levels of serum albumin and cholesterol in the chPLA2R1-positve/$C3^{-/-}$ group were comparable to the control group. The lower proteinuria, higher serum albumin and cholesterol levels and the longer survival indicate that chPLA2R1-positve/$C3^{-/-}$ mice had an attenuated course of disease. The ultrastructural analyses showed that foot process effacement and numbers of electron dense deposits were much more severe in chPLA2R1-positve/$C3^{WT}$ mice than in chPLA2R1-positve/$C3^{-/-}$ mice (**Figure 12**F), supporting the previous impression of a milder course of disease. None of these ultrastructural changes occurred in the control mice. All chPLA2R1-positve/$C3^{-/-}$ as well as chPLA2R1-positve/$C3^{WT}$ mice immunised with hPAL2R1 showed mIgG deposition along the capillary walls, whereas in control mice mIgG was absent (**Figure 12**G).

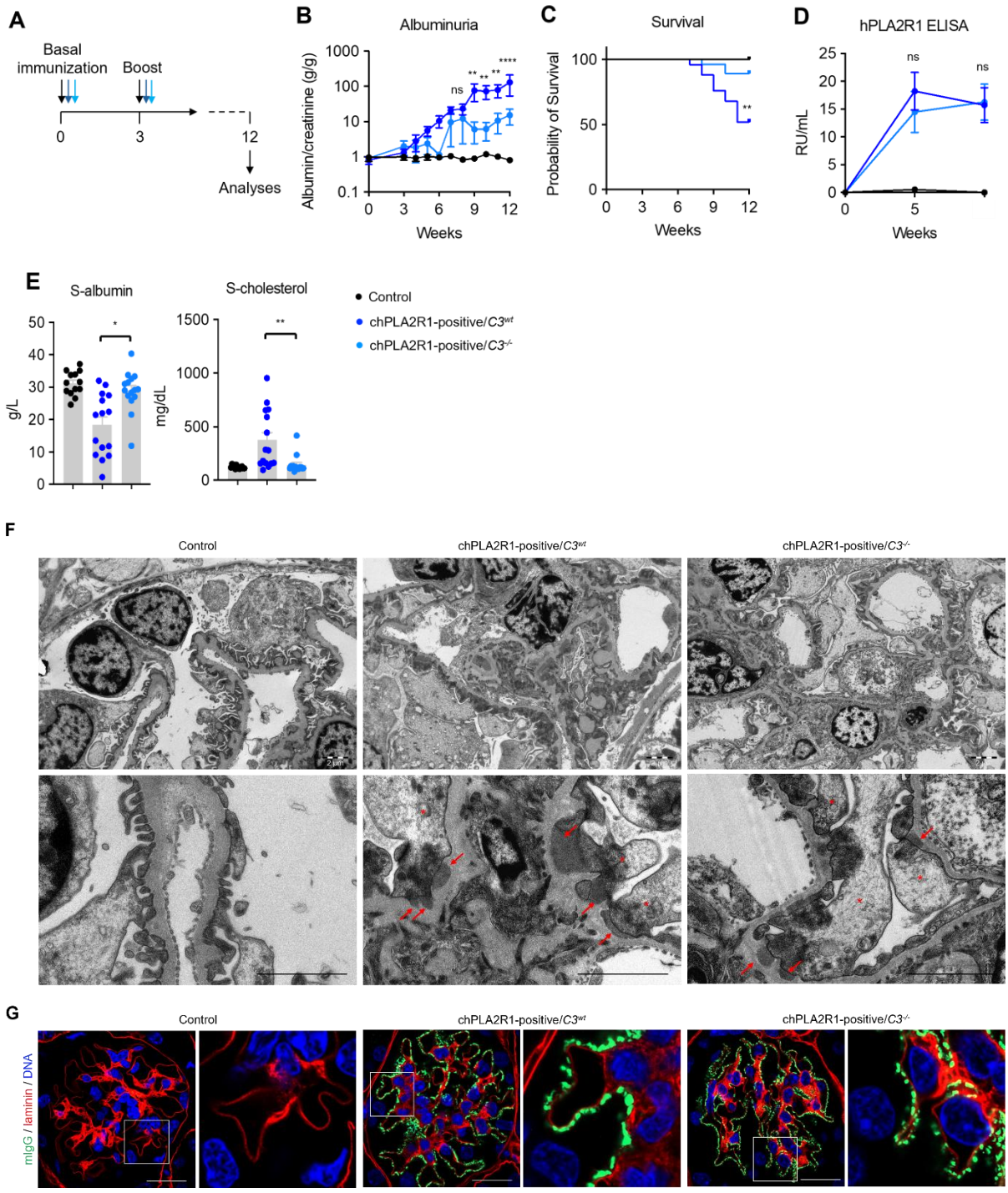

Figure 12: Complement deficient mice had an attenuated course of membranous nephropathy. A) *Experimental setup. chPLA2R1-positve/C3$^{-/-}$ and chPLA2R1-positve/C3^{WT} mice were immunised with TiterMax Gold adjuvant with hPLA2R1 (chPLA2R1-positve/C3$^{-/-}$ n = 28, chPLA2R1-positve/C3^{WT} n = 25) or NaCl (mice from both genetic backgrounds, further referred as control, n = 13) in three independent experiments.* ***B)*** *Albuminuria as measured by the albumin-to-creatinine ratio in control (n = 13) and hPLA2R1-immunised chPLA2R1-positve/C3$^{-/-}$ (n = 28) and chPLA2R1-positve/C3^{WT} (n = 25) mice. Mixed-effect-analysis* ***C)*** *Survival analysis (control n =13 and hPLA2R1-immunised chPLA2R1-positve/C3$^{-/-}$ n = 28 and chPLA2R1-positve/C3^{WT} n = 25). Log-rank Mantel-Cox test, **P < 0.01.* ***D)*** *Anti-hPLA2R1 antibody titers measured by ELISA in control (n = 13) and hPLA2R1-immunised chPLA2R1-positve/C3$^{-/-}$ (n = 28) and chPLA2R1-positve/C3^{WT} (n = 25) mice. Not significant (ns, 2-way analysis of variance).* ***E)*** *Serum (S-) albumin (left) and Serum (S-) cholesterol (right) levels in control (n = 13) and hPLA2R1-immunisedchPLA2R1-positve/C3$^{-/-}$ (n = 15) and chPLA2R1-positve/C3^{WT} (n = 16) mice at the end of the observation period. *P < 0.5, **P < 0.1 (Mann-Whitney test).* ***F)*** *Electron microscopic analysis of the glomerular filtration barrier in control and hPLA2R1-immunised chPLA2R1-positve/C3$^{-/-}$ and chPLA2R1-positve/C3^{WT} mice (n = 3 analysed per group). The red arrows mark subepitelial electron-dense deposits. The asterisks mark effaced podocyte foot processes. Bars = 2 µm.* ***G)*** *Immunofluorescence staining for mIgG (green) co-stained with laminin (red) in control*

and hPLA2R1-immunised chPLA2R1-positve/C3$^{-/-}$ and chPLA2R1-positve/C3^{WT} mice. Right panels represent enlargements of the boxed areas in the left panels. Bar = 20 µm.

Next, we analysed the deposition of complement components in all groups. Positive staining for C1q and C4d were observed in immunised chPLA2R1-positive/C3$^{-/-}$ and chPLA2R1-positve/C3^{WT} mice, indicating complement system activation in both groups (**Figure 13**). Staining for C3, CFB and C5 were only positive in the group of the immunised chPLA2R1-positve/C3^{WT} mice. Negative staining for C3 in chPLA2R1-positve/C3$^{-/-}$ confirmed the successful C3 knockout. Of note, over all staining in fact demonstrated an initial activation of the complement cascade but due to the absence of the downstream components the complement systems was not effective anymore.

In conclusion, these experiments demonstrated that the complement system plays a role in the pathogenesis in this model of experimental PLA2R1 associated MN. However, further complement independent mechanisms are also existing during progression of this disease.

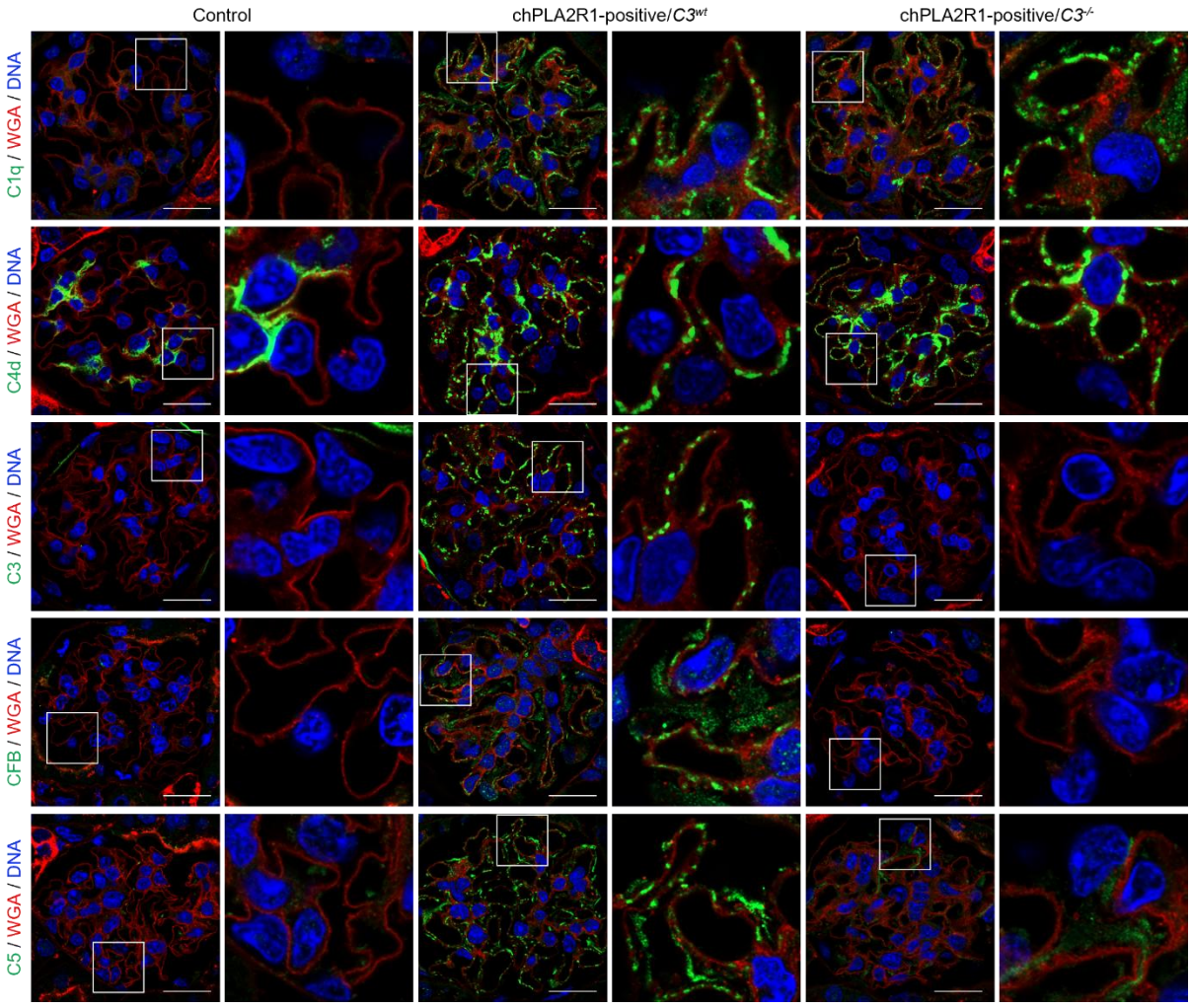

Figure 13: Complement deposition in hPLA2R1-immunised chPLA2R1-positve/C3-/- and chPLA2R1-positve/C3WT mice. *Immunofluorescence staining for complement C1q, C4d, C3, complement factor B (CFB), and C5 (all green) in co-localisation with wheat germ agglutinin (WGA, red) in controls and hPLA2R1-immunised*

chPLA2R1-positve/C3$^{-/-}$ and chPLA2R1-positve/C3^{WT} (n = 3 analysed per group). Bar = 20 µm. Images on the right represent enlargements of the boxed areas in the images on the left.

3.4 Deep characterisation of molecular mechanisms

3.4.1 Time course evaluation in the experimental PLA2R1-associated MN mouse model

After establishing PLA2R1-eaMN including the complement system´s role in the pathogenesis, the next aim was to investigate potential molecular disease mechanisms in chPLA2R1-positve mice using single nucleus RNA sequencing (snRNA seq).

The first step was the identification of an early and late disease time point. The early time point is defined as the initiation phase, where immune complexes start to build up and PLA2R1 is initially fixed at the podocyte membrane by the antibodies without any or very low proteinuria. The late time point is defined as a stage with manifested disease, though proteinuria as well as podocyte-impairment is mild. In order to obtain a very detailed time course of the disease, chPLA2R1-positive mice were immunised according to the previously established hPLA2R1 immunisation protocol and mice were sacrificed weekly starting at week two until week ten after immunisation (**Figure 14**A). Four weeks after immunisation the immunised mice started to slightly increase their albuminuria compared to their baseline values (**Figure 14**B). In week five, most animals have an albumin-to-creatinine ration lower than three g/g. From week seven on the proteinuria continuously increased. Noteworthy, the mice showed a very heterogeneous proteinuria (**Figure 14**C) and could be divided into three subgroups: one subgroup with less proteinuria (less than 5 g/g), moderate (5 - 50 g/g) and severe (more than 50 g/g) proteinuria. In week eight and nine, a substantial number of animals with moderate proteinuria are available. Immunised mice develop titers against PLA2R1 as early as four weeks after immunisation (**Figure 14**D). Titer levels varied along the time course and were present during the whole observation period.

chPLA2R1 expression and localisation as well as mIgG deposition were evaluated in immunofluorescence staining. Simultaneously these staining were evaluated for the glomerular integrity by co-staining with nephrin and laminin. The staining for mIgG showed that almost all mice in week five already had a thin IgG deposition (**Figure 14**E). In contrast, all sick mice that developed proteinuria after nine weeks had profound IgG deposition. In accordance with this the staining for chPLA2R1 revealed, that the mice in week five either had an incomplete or complete shift of the chPLA2R1 from the cytoplasma to the membrane, as indicated by its relation to nephrin (**Figure 14**F). In comparison with that, proteinuric mice in week nine showed a full shift of chPLA2R1 to the basolateral membrane, as indicated by its relation to nephrin. Additionally, mice of both time points showed no alterations neither in laminin nor nephrin appearance, indicating an intact glomerular structure. Furthermore, there was no significant podocyte loss in the proteinuric mice nine weeks after immunisation compared to the controls, supporting that there is no severe glomerular damage (**Figure 14**G).

Based on these results and in combination with the development of the proteinuria we decided for week five as the early disease time point, with a proteinuria less than three g/g, incomplete shift of PLA2R1 to the membrane and thin IgG deposition. As late disease time point, we decided for week nine with a proteinuria ranging between eight to 50 g/g together with complete shift of PLA2R1 to the membrane and profound IgG deposition.

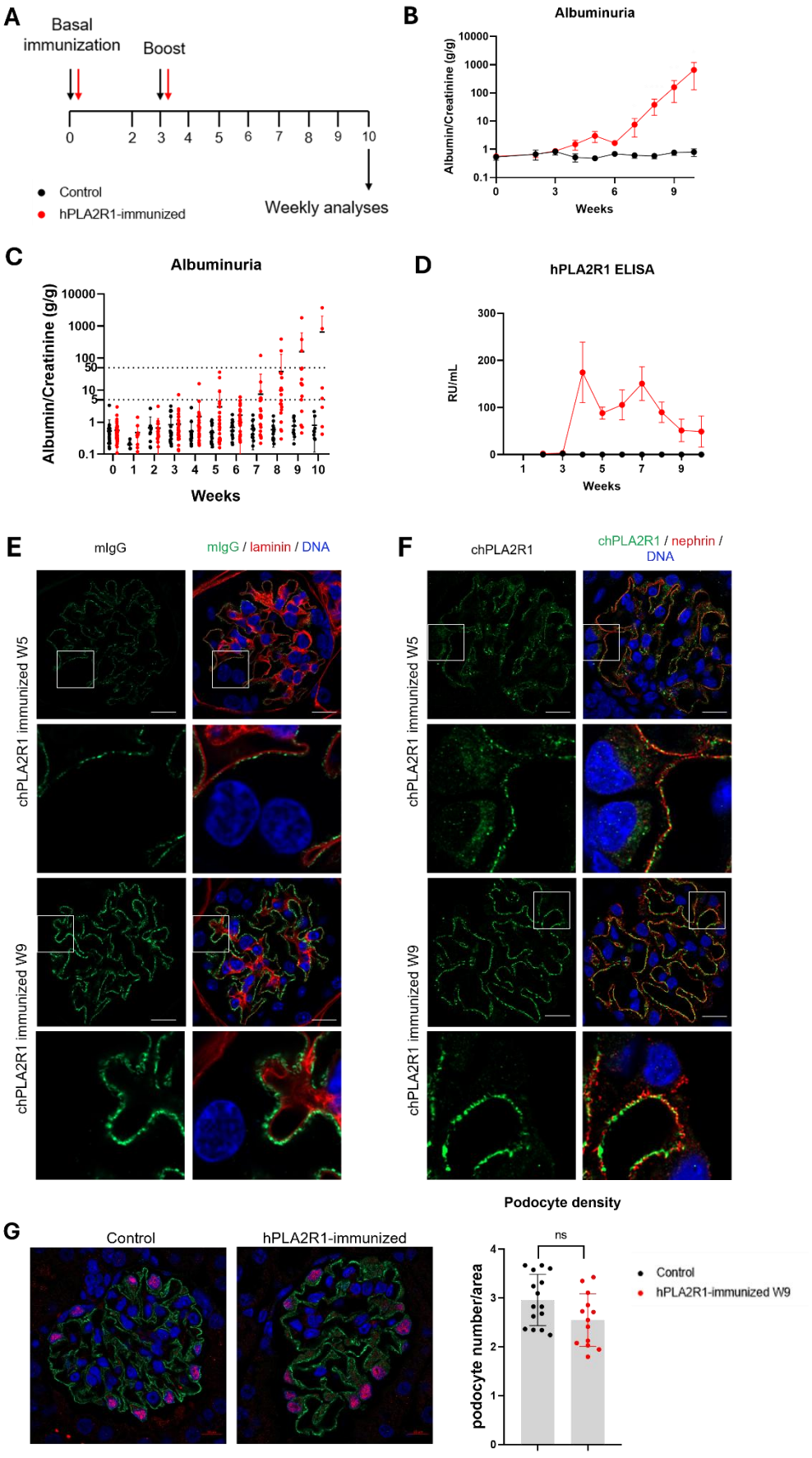

Figure 14: Detailed time course of MN. A*) Experimental setup. chPLA2R1-positive mice were immunised with hPLA2R1 (further referred as control) or sodium chloride (further referred as hPLA2R1-immunised) from six*

independent experiments. Animal numbers vary between different time points, each time point has at least n = 8. ***B****) Albuminuria as measured by the albumin-to-creatinine ratio in control and hPLA2R1-immunised chPLA2R1-positve mice. Animal numbers vary between different time points, each time point has at least n = 8. Mann-Whitney-test, ****P< 0.0001, **P< 0.01, *P< 0.05.* ***C****) Individual albuminuria values, as measured by the albumin-to-creatinine ratio in control and hPLA2R1-immunised chPLA2R1-positive mice. Additional lower dashed line indicates values of 5 g/g, additional upper dashed line indicates values of 50 g/g. Animal numbers vary between different time points, each time point has at least n = 8.* ***D****) Anti-hPLA2R1 antibody titers measured by ELISA in control and hPLA2R1-immunised chPLA2R1-positve mice. Animal numbers vary between different time points, each time point has at least n=8.* ***E****) Immunofluorescence staining for mouse IgG (mIgG, green) in co-localisation with laminin (red) in hPLA2R1-immunised mice five and nine weeks after immunisation (n = 8 analysed per group.) The lower panels represent enlargements of the boxed areas in the upper panels. Bar = 20 µm.* ***F****) Immunofluorescence staining for chimeric PLA2R1 (chPLA2R1, green) in co-localisation with nephrin (red) in hPLA2R1-immunised mice five and nine weeks after immunisation (n = 8 analysed per group.) The lower panels represent enlargements of the boxed areas in the upper panels. Bar = 20 µm.* ***G****) Representative immunofluorescence staining for DACH1 (red) in co-localisation with synaptopodin (green). Nuclei are blue. Quantification of DACH1-positive nuclei in control (n = 15) and hPLA2R1-immunised (n = 15). Bar = 20 µm. Not significant (ns, Mann-Whitney test).*

3.4.2 Single nucleus RNA sequencing analysis of PLA2R1-eaMN

After defining an early and late disease time point, which will be further referred as week 5 (w5) and week 9 (w9), the next aim was to identify the molecular changes at both time points. Therefore, single nucleus transcriptome (snRNA-seq) analysis derived from isolated glomeruli of control and hPLA2R1-immunised chPLA2R-positive mice were evaluated.

In order to obtain the best possible quality of the data, multiple rounds of cleaning the dataset from ambient RNA was necessary. Then, all groups were merged and integrated into one large dataset. After integration manual doublet removal, based on marker gene expression, was performed. Due to the cleaning process, the contamination of mitochondrial (percent.mt) and ribosomal RNA (percent.rb) drastically decreased (**Figure 15**A). After cleaning the lower and upper quantiles of the total counts of transcripts per cell (nCount) ranging between 2100 to 4800, the number of genes per cell (nFeature) ranging from 1300 to 2000 and the content of mitochondrial RNA ranging between zero and 0.1% in each dataset. The ribosomal RNA content ranging between 0.5 to 1.6% in control week 5 (c5), control W9 (c9) and model W9 (m9) group (**Figure 15**B). Whereas, in model W5 (m5) the third quantile of ribosomal content reaches up to 2.3. Looking at the overall contribution of the different groups to the total cell numbers in the final dataset, approximately 60% of the cells were from the week nine groups (c9 and m9) and 40% from the week 5 (c5 and m5) (**Figure 15**C).

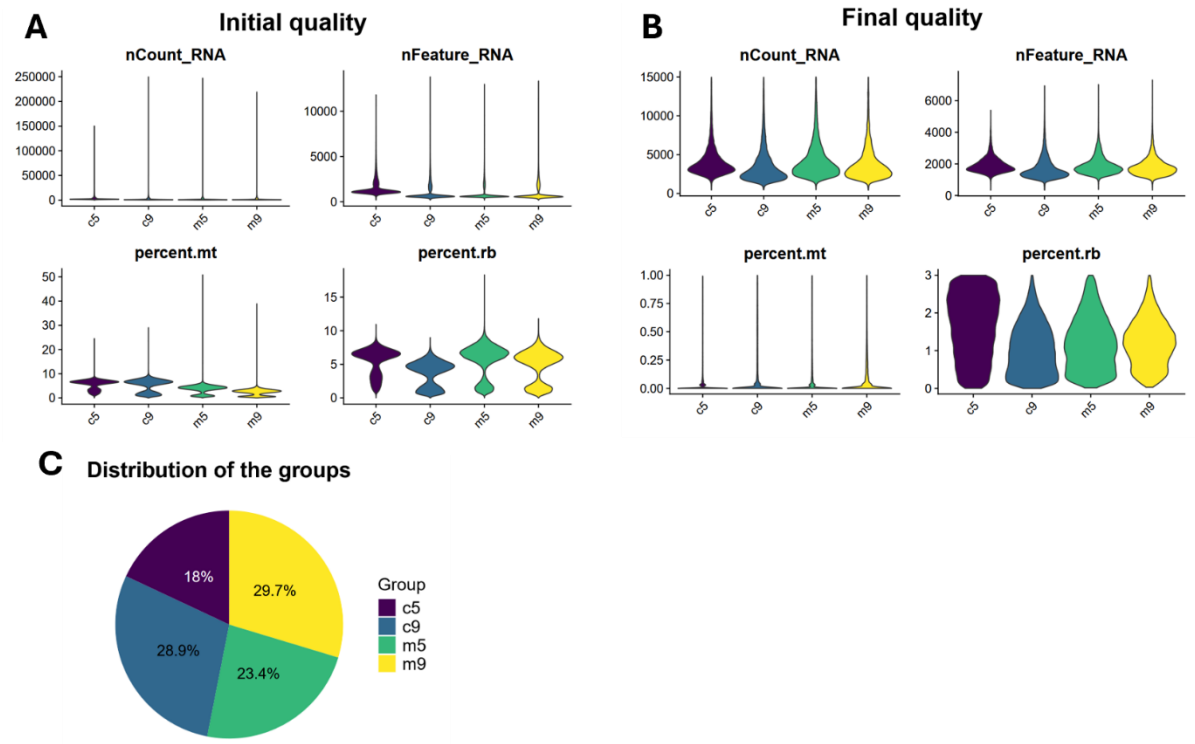

Figure 15: Quality of snRNA-seq dataset. A) *Violin plot showing the raw data of total counts of transcripts per cell (nCount_RNA), number of genes per cell (nFeature_RNA), percentage of mitochondrial (percent.mt) and ribosomal RNA (percent.rb) from all groups. The analysed groups were control week 5 (c5), control model 5 (m5), control week 9 (c9) and model week 9 (m9).* ***B)*** *Violin plot showing the final total counts of transcripts per cell (nCount_RNA), number of genes per cell (nFeature_RNA), percentage of mitochondrial (percent.mt) and ribosomal RNA (percent.rb) from all groups.* ***C)*** *Pie chart representing the proportional distribution of the groups across the dataset.*

The final dataset included a total of 62,228 cells representing glomerular and tubular cell types. The uniform manifold approximation and projection (UMAP) analysis identified 16 distinct clusters each identified based on specific marker gene expression (**Figure 16**A, C). As expected, the three predominant cell types were mesangial cells (Mesangium; 24%), glomerular endothelial cells (Glom. EC; 24.3%), and podocytes (17.6%) (**Figure 16**B), reflecting the glomerular origin of the isolated cells. Besides the glomerular cell types, different cell types from the tubular system were detected as well as immune cells. Next, the distribution of groups across different cell types was analysed, as shifts in distribution may reflect changes in biological processes. While variation was observed among cell types, a notable observation was that in proliferating cells, the m9 group was predominant, representing nearly half of the population indicating an increase in this celltype after nine weeks of disease. In contrast, the distribution of groups within the podocyte population was largely similar, although this does not exclude biological changes occurring in these cells.

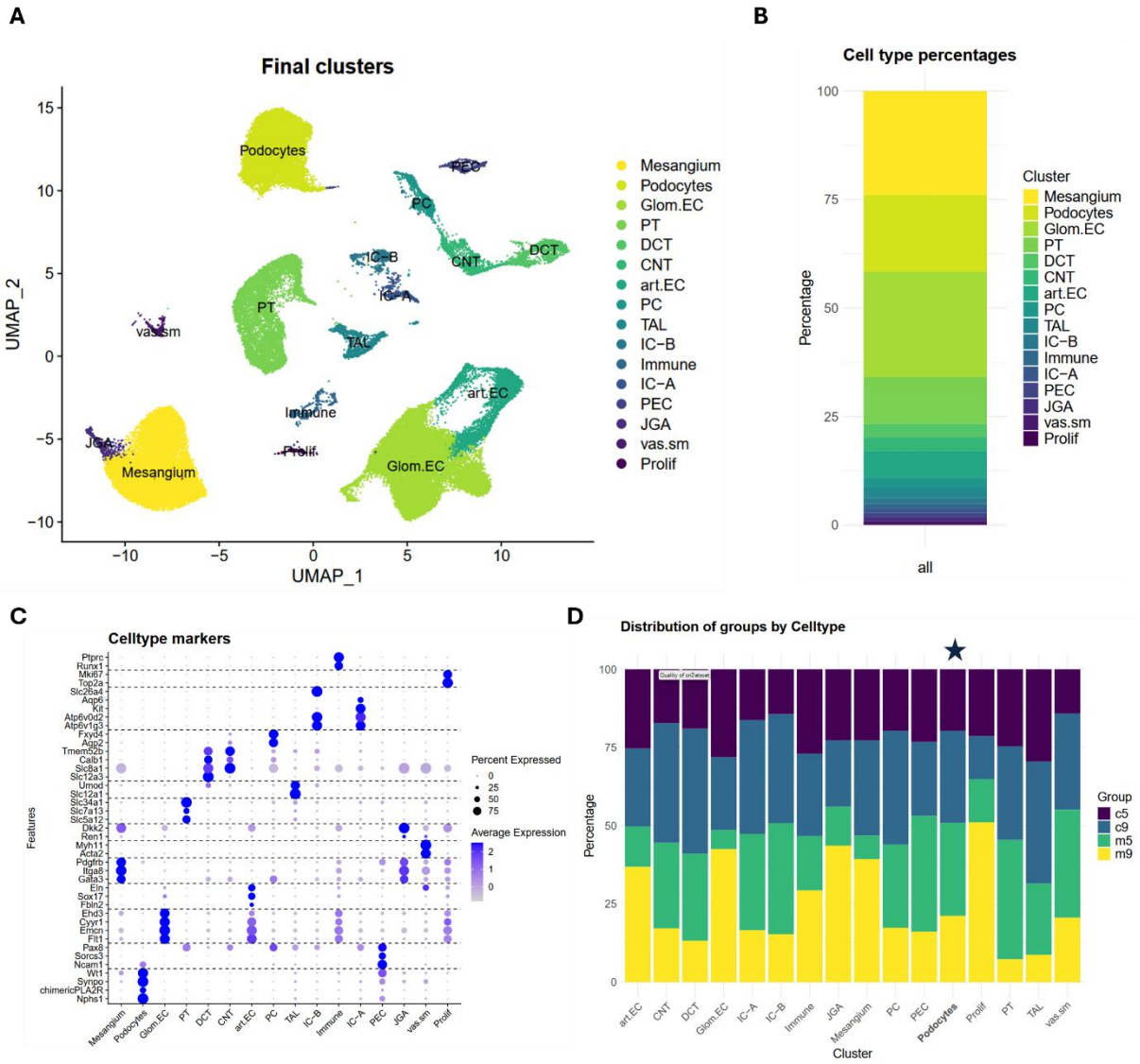

Figure 16: UMAP and cell type distribution of the final dataset. A) *Final cell clusters in UMAP. Identified cell clusters are Podocytes = podocytes, Mesangium = mesangial cells, Glom.EC = glomerular endothelial cells, PT = proximal tubules, DCT = distal convoluted tubule, CNT = connecting tubule, art.EC = arteriolar endothelial cells, PC = principle cells, TAL = thick ascending limb, IC-B = intercalating cells type B, Immune = immune cells, IC-A = intercalating cells type A, PEC = parietal epithelial cells, JGA = juxta glomerular apparatus, vas.sm = vascular smooth muscle cells, Prolif = proliferating cells.* ***B)*** *Bar chart representing the proportional distribution of the cell types across the dataset.* ***C)*** *Dot plot showing the markers used for identification of the different cell types.* ***D)*** *Bar chart representing the distribution of the different groups across the different cell types. Asterisk indicates the podocytes.*

Since prMN primarily affects podocytes, the analysis focused on changes in this cell type. Specifically, the focus will be on chPLA2R1-positive podocytes, as only these cells can be targeted by the disease-causing anti-PLA2R1 antibodies. The chPLA2R1-positive podocyte population was obtained through a two-step approach: first, the podocyte cluster was subsetted, re-integrated, and refined, resulting in a total of 8,510 cells. Podocytes were classified as chPLA2R1-positive if their expression values exceeded zero, identifying 52% (4,391 cells) as positive (**Figure 17**A-C). Looking at the contribution of the groups within the chPLA2R1-positive podocyte population, approximately 60 percent of the cells were from the week nine groups (c9 and m9) and 40% from the week 5 (c5 and m5).

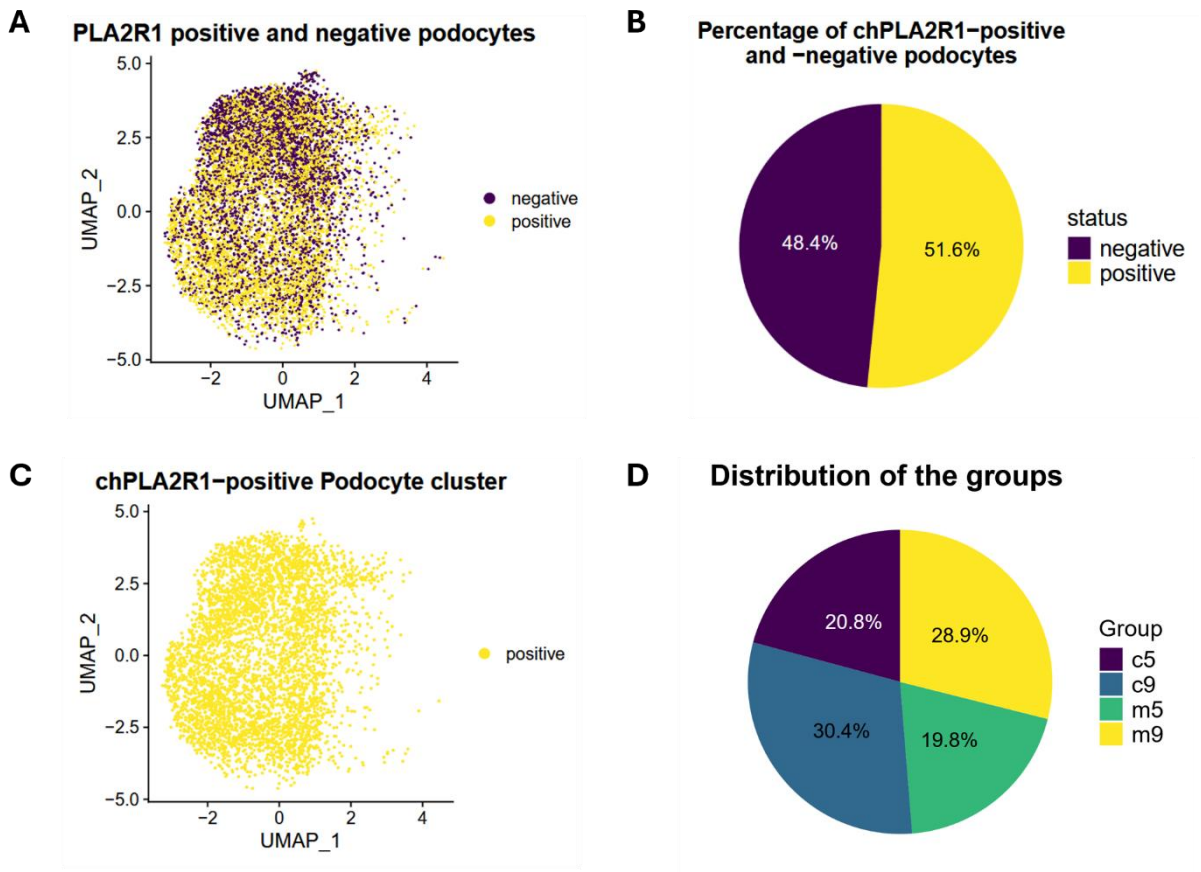

Figure 17: chPLA2R1 expression in podocyte subcluster. A*) UMAP of the subsetted, reintegrated and cleaned podocyte subclusters showing chPLA2R1 expression in podocytes. Podocytes with expression values greater zero were considered as chPLA2R1-positive (yellow) and podocytes with expression value equals zero were considered as chPLA2R1-negative (purple).* ***B)*** *Pie chart illustrating the percentage of chPLA2R1-positive and negative podocytes across the whole podocyte population.* ***C)*** *UMAP of the chPLA2R1-positive subpopulation.* ***D)*** *Pie chart representing the proportional distribution of the groups across the chPLA2R1-positive podocytes.*

To identify the changes and potential signaling cascades initiated after the binding of the anti-PlA2R1 antibodies to the podocytes, differential gene expression (DGE) analysis was performed on these chPLA2R1-positive podocytes. This was followed by fast gene set enrichment analysis (fgsea) to identify potentially regulated pathways.

In the m5 group, genes primarily involved in actin cytoskeletal organisation were upregulated compared to c5 group. Consequently, pathways that are associated with the regulation of actin cytoskeleton are up regulated. On the other hand, genes and accordingly pathways that are associated with metabolism and ion transport across the membrane are downregulated (**Figure 18**A-C). Similarly, genes related to cytoskeletal regulation, general signal transduction and gene regulation are up regulated in w9 when compared to c9 group. In line with this fgsea revealed an up regulation of pathways such as axon guidance and development as well as transmembrane receptor protein tyrosine kinase signaling. On the other hand, genes associated with metabolic processes and energy conversion were down regulated, reflected in the down regulation of pathways such as oxidative phosphorylation, aerobic respiration and ATP synthesis (**Figure 18**D-F). When comparing the top 50 differentially expressed genes, that are present in both groups, there is some overlap between the most up and down regulated genes in both time points indicating that

some changes starting in early phase will manifest and persist until the disease is fully established (**Figure 18**G).

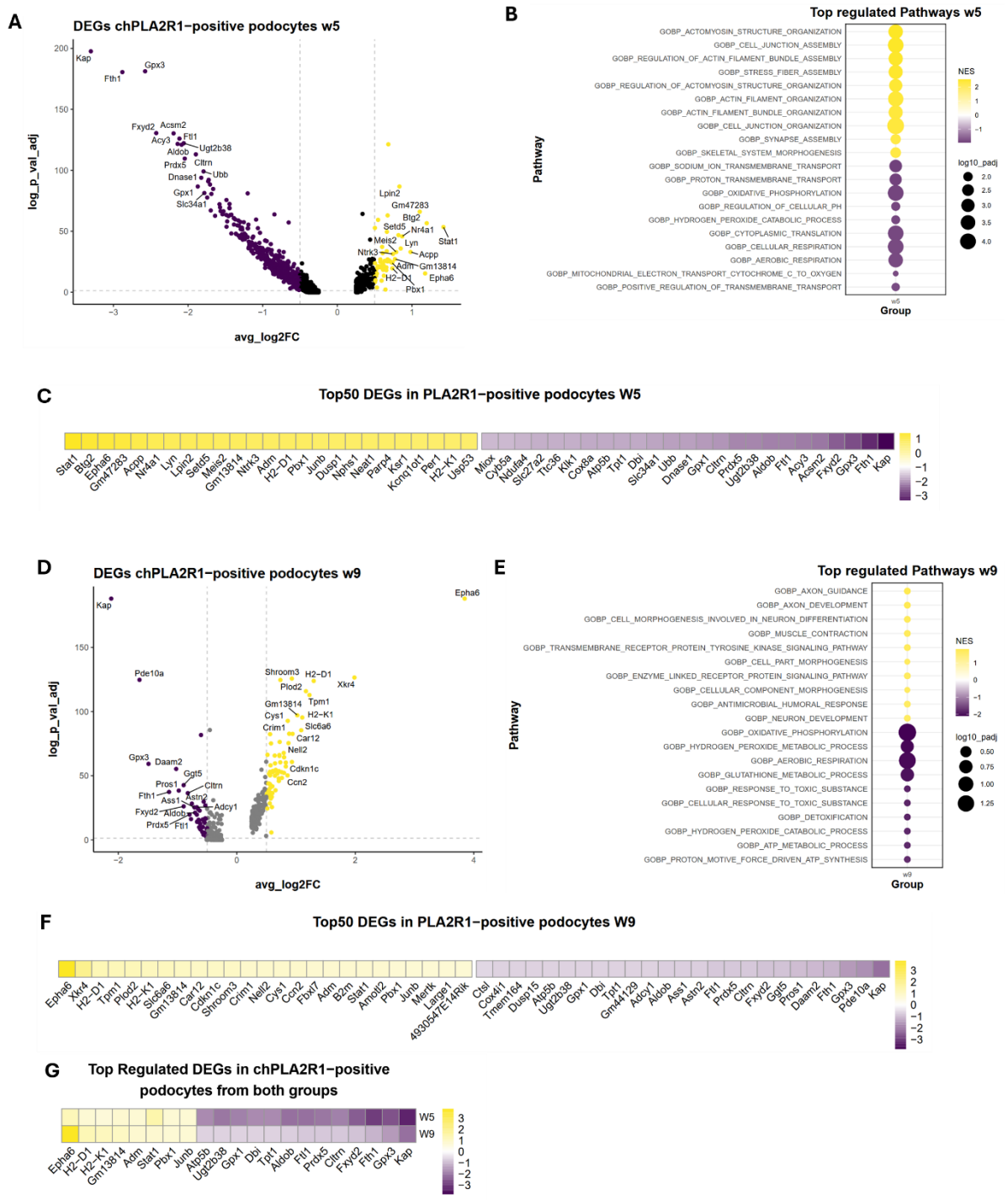

Figure 18: chPLA2R1-positive podocytes and DEG analysis of the different time points. A) *Vulcan plot depicting the up and down regulated DEGs in chPLA2R1-positive podocytes from the early timepoint (w5). Up regulated genes (yellow): average log2FC (avg_log2FC) ≥ 05 and log p-adjusted value (log_p_val_adj) ≤ 0.05. Down regulated genes (purple): avg_log2FC ≤ -0.5 and log_p_val_adj ≤ 0.05. not regulated genes (grey): all genes between avg_log2FC > -0.5 and < 0.5 and or log_p_val_adj >0.05.* ***B)*** *Dot plot illustrating the top 10 up (yellow) and down (purple) regulated pathways based on fast gene set enrichment analysis (fgsea) of the DEGs from chPLA2R1-positive podocytes of the early timepoint. Reference gene set and pathway list from gene ontology subset: biological process. Dot color correlates with the normalised enrichment score (NES) and dot size with the negative log10 p-adjusted value (-log10_padj).* ***C)*** *Heatmap of top 25 up (yellow) and 25 down (purple) regulated genes of chPLA2R1-positive podocytes of the early timepoint (w5). Small break in the middle of the heatmap indicates the switchover from up to down regulated genes.* ***D)*** *Vulcan plot depicting the up and down regulated DEGs in chPLA2R1-positive*

podocytes from the late timepoint (w9). ***E)*** *Dot plot illustrating the top 10 up (yellow) and down (purple) regulated pathways based on fast gene set enrichment analysis (fgsea) of the DEGs from chPLA2R1-positive podocytes of the late timepoint (w9).* ***F)*** *Heatmap of top 25 up (yellow) and 25 down (purple) regulated genes of chPLA2R1-positive podocytes of the late timepoint (w9). Small break in the middle of the heatmap indicates the switchover from up to down regulated genes.* ***G)*** *Heatmap of top 25 up and down regulated DEGs present in both early (w5) and late (w9) timepoint.*

3.4.3 Validation of snRNA-seq results

Further investigation and validation of the DEGs at the level of protein expression was only performed in the w9 group as it appears more promising for a first approach for pathogenic pathways since the disease is already established at this time.

As an initial validation approach, immunofluorescence analysis was performed for Epha6 and MerTK. These proteins were chosen because they are upregulated in both the chPLA2R1-eaMN and THSD7A-eaMN models, indicating their potential relevance across different MN models (unpublished data, not shown here). Furthermore, Epha6 is the most upregulated gene in both MN models, and MerTK is also among the top 25 differentially expressed genes (DEGs). The quantitative analysis of the immunofluorescence images showed a significant increase in Epha6 ($p = 0.036$) and MerTK ($p = 0.021$) signal in hPLA2R1-immunised mice compared to control mice (**Figure 19**A-D). Furthermore, the active form of MerTK, phosho-MerTK (p-MerTK) also had a significantly ($p = 0.015$) increased signal in hPLA2R1-immunised mice, suggesting enhanced MerTK signaling (**Figure 19**E, F). Taken together, the snRNA sequencing results demonstrated upregulation of the Epha6 and MerTK genes, and the immunofluorescence analysis confirmed that this up regulation corresponded to higher protein expression. Furthermore, the increased levels of p-MerTK indicate enhanced MerTK signaling in diseased mice at the later time point.

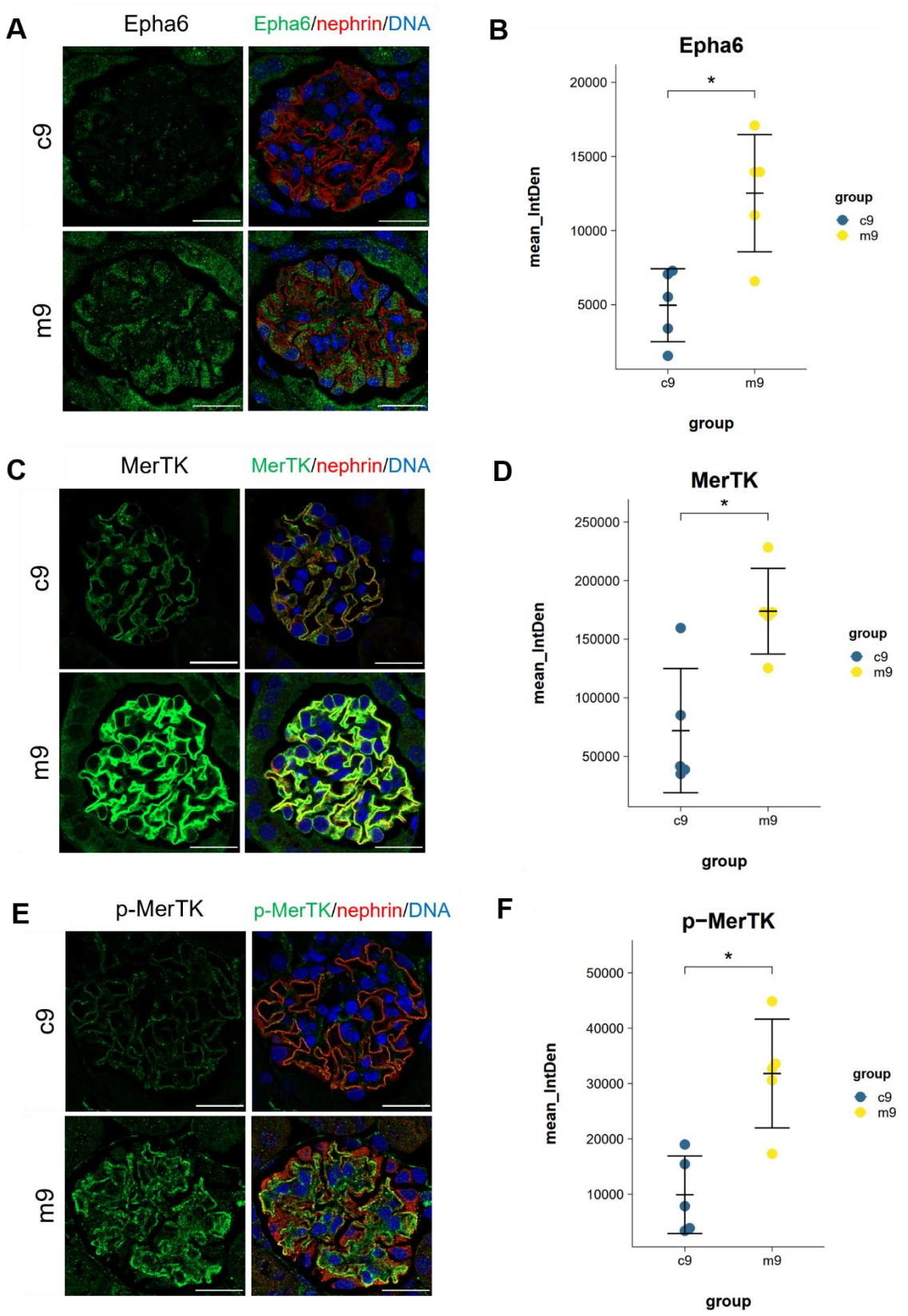

Figure 19: Immunofluorescence staining and quantitative expression analysis of Epha6, MerTK and p-MerTK.
A) *Immunofluorescence staining of Epha6 (green) in co-staining with nephrin (red) in control and hPLA2R1-immunised mice (n = 5 analysed per group). Bar = 20 µm* ***B)*** *Evaluation of integrated density (IntDen) from Epha6 signal in immunofluorescence images. 10 pictures per animal were analysed, n = 5. * P < 0.05 (Man-Whitney Test).* ***C)*** *Immunofluorescence staining of MerTK (green) in co-staining with nephrin (red) in control and hPLA2R1-immunised mice (n = 5 analysed per group). Bar = 20 µm.* ***D)*** *Evaluation of integrated density (IntDen) of MerTK signal in immunofluorescence images. 10 pictures per animal were analysed, n = 5. *P < 0.05 (Man-Whitney Test).*

E) *Immunofluorescence staining of pohspho-MerTK (p-MerTK, green) in co-staining with nephrin (red) in control and hPLA2R1-immunised mice. (n = 5 analysed per group). Bar = 20 µm.* ***F)*** *Evaluation of integrated density (IntDen) of p-MerTK signal in immunofluorescence images. 10 pictures per animal were analysed, n = 5. *P < 0.05 (Man-Whitney Test)*

4. Discussion

Membranous nephropathy is an antibody mediated autoimmune disease affecting the glomeruli. Autoantibodies in patients target podocyte antigens like PLA2R1 and THSD7A, thereby damaging the glomerular filtration barrier through unknown mechanisms. Consequently, specific treatment approaches are currently not applicable and patients are treated, dependent on their status either with supportive treatment, general immunosuppression or rituximab – none of this are very specific (8). Furthermore, there are very limited mouse models for PLA21-associated MN, resembling the course of disease to investigate possible pathomechanisms. Such mouse models are crucial to investigate the pathomechanisms and potential therapies. Therefore, one of the main objectives of this work was to establish and characterise the chPLA2R1-positive mouse model in which PLA2R1 associated MN can be induced and progresses similarly to patients.

4.1 Generation and characterisation of a mouse strain expressing a chimeric PLA2R1 in podocytes

The generation of the transgenic mouse line, expressing a chPLA2R1 consisting of the three N-terminal human domains (CysR, FnII, CTLD1) and the seven C-terminal murine domains (CTLD2-8) exclusively in the podocytes (chPLA2R1-positive mice) was successful. This is consistent with results from the spontaneous model, where hPLA2R1 expression was also restricted to podocytes - an expected outcome given the use of the same knock-in system (51). In contrast to the spontaneous model the absence of chPLA2R1 in the thymus did not result in autoantibody formation, likely because mPLA2R1 is expressed there, as shown in figure S3 in Tomas et. al 2023 (51). Since the majority of chPLA2R1 is murine and only the three N-terminal domain is human, immune tolerance towards chPLA2R1 was maintained. Notably, the knock-in of the chPLA2R1 did not affect the glomerular structure or podocyte morphology, being a foreign protein in podocytes (Figure 6). This is similary to the passive mouse model, where the knock-in of the mPLA2R1 also did not cause any morphological changes in the podocytes. Furthermore, chPLA2R1 exhibited a localization pattern comparable to that of hPLA2R1 in human podocytes (10) and mPLA2R1 in our passive model (47).

4.2 Establishment of an experimental PLA2R1 associated model of membranous nephropathy

Following immunization with hPLA2R1 the mice produced antibodies against hPLA2R1, developed proteinuria, and exhibited hypoalbuminemia as well as hyperlipidemia, which are hallmark symptoms of MN. Anti-hPLA2R1 antibodies recognised CysR-FN-II, CTLD1, and CTLD7-8 of hPLA2R1, while CTLD2-6 of hPLA2R1 and CTLD2-8 of mPLA2R1 were not recognised. The domain recognition profile against hPLA2R1 strongly resembled the recognition profile of anti-PLA2R1 autoantibodies from patients with MN (21, 22, 24, 25). This suggests that these

epitope-containing domains possess particular immunogenic properties, and it is interesting that this phenomenon is conserved in mice. However, the reasons for this across-species immunogenicity remain unclear at this point, but may, at least in part, be explained by the structure and conformation of hPLA2R1 (26, 52).

The disease initially develops slowly during the first weeks but accelerates around the midpoint of the observation period. Notably, 60% of affected mice experienced a more rapid progression, requiring their sacrifice after three-quarters of the observation period. Compared to the rapid disease progression in the spontaneous model this eaMN model exhibits a much slower disease progression though. While still faster than in humans, the progression resembles the situations in patients more accurately than previous PLA2R1 associated mouse models, like the spontaneous and the passive model. One aspect not observed in this eaMN model is spontaneous remission, which may be due to the fact that disease induction occurs through immunisation and not through the development of a classical autoimmune condition. However, neither the precise pathomechanisms in MN is known, nor the phenomenon of spontaneous remission is solved, so we can only speculate that our mice did not show spontaneous remission, due to the active immunisation and the resulting purposeful onset of the disease.

Besides, a close reflection of the clinical symptoms in patients the eaMN model also resembled the histomorphological aspects of the disease: thickening of the GBM, IgG deposition, electron dense deposits and podocyte effacement (**Figure 9**) (11) in hPLA2R1-immunised mice. The eaMN model also showed the translocation of PLA2R1 from cytoplasm to the membrane (**Figure 9**). Accumulation of PLA2R1 at the membrane could probably be the result of a fixation process by anti-PLA2R1 antibodies. Binding of these antibodies could slow down or even prevent internalization and degradation of PLA2R, resulting in an accumulation of PLA2R1 at the membrane. Consequently, newly synthesised PLA2R1 is continuously inserted into the membrane as part of the normal turnover process, further contributing to its buildup (53, 54). Another interesting aspect is the generation of a predominant mIgG1 response in hPLA2R1-immunised mice. Murine IgG1 does not activate complement and can, in this regard, be considered the murine equivalent of non-complement activating human IgG4, which is the dominant IgG subclass in patients with PLA2R1- and THSD7A-associated MN (10, 20). Nonetheless, complement depositions are found in patient biopsies (11) and also in the PLA2R1-associated eaMN model. However, mice also generated complement-activating IgG subclasses, which, similar to the complement-activating IgG subclasses in sera and biopsies (13) of MN patients, were found to be deposited along the glomerular filtration barrier. Recently, Seifert *et al*. (20) demonstrated C1q deposition in the THSD7A associated eaMN model, and we could also detect C1q in co-localisation with mIgG and PLA2R1 (Figure 11), indicating that complement is activated via the classical pathway in this model as well. Which seems logical in regard of the similarities between the THSD7A and PLA2R1 eaMN model. Even though IgG1 is described to be unable to activate the classical pathway (29), we

also found PLA2R1 antibodies from other subclasses and the content of these might be enough to trigger the initiation of the complement system (20).

Besides C1q and C4d, CFB was also detected in our model, which is a part of the alternative pathway. Although the presence of CFB does not necessarily mean that the alternative pathway plays a role in the initiation of the complement system, it is more likely that CFB is activated in an amplification loop. Once C3b is formed it can bind to CFB, allowing its cleavage by factor D, which is a constitutively active serum protease, resulting in the formation of the alternative C3 convertase, C3bBb (31, 55, 56).

4.3 Generation and characterisation of chPLA2R1-positive, C3-knockout mice

The role of the complement system for disease initiation has been discussed controversially. On the one hand there clearly is complement deposition in human biopsies, on the other hand prMN is an autoantibody driven disease with a mainly IgG4 subtype, which is considered to be unable to activate the complement system (29, 57). In attempts to resolve the question, whether the complement system plays a role in the initiation and progression of the disease several rodent models were used.

For several years Heymann nephritis in rats was the leading animal model to study different aspects of MN. Consequently, most studies investigating the impact of the complement system have been conducted in Heymann nephritis. In this model binding of antibodies to the target antigens leads to complement activation and ultimately to the insertion of the membrane attack complex (MAC) into the podocyte membrane (29, 39, 41). Different studies investigating the impact of the complement system showed controversial results. Some studies found an essential role of the complement system in mediation of glomerular injury (58-60). In contrast, two other studies could not demonstrate an impact on proteinuria in complement deficient rats, (61, 62). Importantly, the model of Heymann nephritis in rats has a very profound limitation, since the major autoantigen in this model is megalin, which is not expressed in human podocytes, limiting the specificity of the findings in this model (63). More recently, two antigen-specific mouse models have been developed using the passive transfer of rabbit IgG against PLA2R1 and THSD7A to induce MN. In mice that received anti-PLA2R1 IgG some glomerular C3 deposition was detected (64). Interestingly, in mice that received the anti-THSD7A IgG C3 was barely detectable, even though they had nephrotic-range proteinuria suggesting that complement-independent mechanisms may contribute to the pathogenesis of MN in this model (26). However, these models also have certain limitations. The heterologous IgG may have limited effector functions in mice, like binding to the host C1q, thus leading to in effective of no complement activation at all. Further, the mice develop antibodies against the rabbit IgG, which binding to deposited IgG and exacerbating the disease. The huge amount of antibodies induces a rapid disease onset, which does not reflect the slow buildup of immune complexes in patients. In 2023, Seifert *et al*. established an inducible THSD7A-

associated MN model, that overcome the issues from the passive transfer model. Moreover, they investigated the role of complements system in this model using C3-KO mice (20). Following this approach, the present study utilised a chPLA2R1-positve/C3$^{-/-}$ mouse line to examine the pathogenic role of the complement system as well.

The chPLA2R1-positve/C3$^{-/-}$ mice compared to chPLA2R1-positve/C3^{WT} had a delayed and milder course of disease. Proteinuria and nephrotic syndrome were substantially reduced in mice lacking a functional complement system, hinting at an important role of complement also in PLA2R1-associated MN. Moreover, the survival of chPLA2R1-positve/C3$^{-/-}$ was significantly better than in C3-WT mice, which further supports the assumption that the complement system plays a role in disease initiation and progression. These results are very similar to the findings of Seifert *et al*. (20). Furthermore, chPLA2R1-positve/C3$^{-/-}$ mice had no loss of serum albumin or increase in cholesterol, which would be typical signs of MN in patients. In addition, the electron microscopy revealed that effacement and electron dense deposits do occur in chPLA2R1-positve/C3$^{-/-}$ mice, but to a lower extent as in chPLA2R1-positve/C3^{WT} mice. Of note the effacement was assessed by optical analysis of electron microscopy pictures and not quantified, for a more valid evidence effacement could be quantified by measuring the slit diaphragm density, as it was done in Seifert *et al*. (20). The hPLA2R1 antibody titers and glomerular IgG deposition were the only parameters that remained unaffected in chPLA2R1-positve/C3$^{-/-}$ mice. Which was expected, as C3 is not involved in antibody production or the formation of antibody-secreting cells. Consequently, the deposition of IgG remained unaffected by the absence of C3. Although the mIgG signal was not quantified in this study, Seifert *et al*. performed IgG subclasss quantification, which revealed no significant differences compared to wild-type mice (20). Further, a study against angiotensin II receptor type 1a associated systemic sclerosis also found no significant decrease of IgG deposition in C3-KO mice (65). In immunofluorescence staining the upstream regulators of C3 could be detected in all groups, but C3 and all downstream effectors could not be detected in chPLA2R1-positve/C3$^{-/-}$, demonstrating the successful knock-out of C3 and the absence of the downstream effectors like C5 that are responsible for the formation of the MAC. Absence of C5 might explain the milder course of disease, since the MAC is considered to play an important role in podocyte damage and development of proteinuria in MN (57, 66). The insertion of the MAC leading to disruption of the actin cytoskeleton by initiation of various downstream pathways including protein kinases, lipid metabolism, cytokine production, ROS generation, growth factor signal transduction, endoplasmic reticulum stress, and the ubiquitin-proteasome system (67, 68). However, mice lacking a functional complement system also developed proteinuria, suggesting that complement-independent mechanisms also play a role in the pathogenesis of MN. Such mechanisms are largely unclear to date, but could involve induction of cellular signaling programs or interference with important biological functions of the target antigen (37, 69).

4.4 Deep characterisation of molecular mechanisms

To evaluate potential pathomechanisms, an early and a late time point of the disease were selected. The early time point was defined as initiation phase of the disease, when immune complexes start to build up. Whereas in the late time point defined as a stage with manifested disease but mild podocyte impairment.

For the evaluation of disease progression, a ten-week interval was chosen based on prior experiments indicated reduced survival beyond nine to ten weeks. Interestingly, proteinuria in these cohorts were a bit different from the previous cohorts, where the onset of proteinuria was a bit earlier and higher/stronger. Further, we observed that not all mice got sick. This can be explained by the activity of the Cre-recombinase, some mice might have a weaker Cre-recombinase activity, resulting in low or no expression of chPLA2R1. A recent study found that, Cre-recombinase efficiency is dependent on various factors. One of these is the age of the breeding pair, Cre-recombinase efficiency is usually lower in breeding pairs older than 20 to 25 weeks of age (70). Another point, that this study mentioned is that the efficiency is also dependent on the zygosity of the floxed alleles, where heterozygosity was associated with a higher Cre recombination efficiency than homozygosity (70). Moreover, efficiency is influenced by the Inter-loxp distance (70). Even though we tried to circumvent variations in Cre-recombinase activity, by changing breeding pairs regularly to avoid a decreasing Cre-recombinase activity and using mostly heterozygous mice. Nevertheless, a variation in the activity could not be completely avoided. Unpublished fluorescence-activated cell sorting (FACS) data from podocytes of chPLA2R1-positive mice showed that 85 % of all podocytes express PLA2R1. In contrast to a study from Balkawade, the Cre-recombinase expression per se did not lead to the thickening of the GBM in our mouse model (71).

Following immunisation the chPLA2R1-positive mice developed titers against hPLA2R1 four weeks after basic immunisation. The sudden drop of titers in week five after immunisation hinting at beginning of the disease, when the antibodies bind the chPLA2R1 in the kidneys, matching with immunofluorescence analyses showing slight IgG deposition starting between week four and five in most mice. The increase of antibody titers in week seven is most likely an effect of the boost in week three. After week seven the titers continuously dropped, which is explained by loss of antibodies when the mice get proteinuric. Titers against hPLA2R1 in the urine inversely correlated with titers in the blood (unpublished data). In accordance with our previous definition of an early and a late time point of the disease we decided for week five and nine, based on the combination of the proteinuria and the immunofluorescence staining. In week five, most mice had no proteinuria and incomplete shift of PLA2R1 to the membrane and thin IgG deposition. In week nine, most mice exhibited a moderate proteinuria together with complete shift of PLA2R1 to the membrane and profound IgG deposition, but no severe glomerular damage.

In a first attempt to shed some light on the potential pathomechanisms in the newly established PLA2R1-associtated eaMN model, snRNA sequencing analysis was performed in chPLA2R1-positive mice.

Initial quality analysis revealed a similar quality of all four datasets. Following the removal of low-quality nuclei and those with high mitochondrial or ribosomal RNA contamination, the overall quality remained consistent among the groups. However, group c5 had a slightly lower quality compared to the others, as it has a slightly higher fraction of ribosomal RNA content and contains the lowest number of analysed nuclei. The potential reason for the higher amount of ribosomal RNA might be that the cells got a bit more damaged during the dissociation of the glomeruli into single nuclei (72). Even though c5 and m5 were processed at the same day from the same person, the dissociation steps needed to be performed separately in each group, which can account to the differences. Unsupervised clustering revealed 16 distinct clusters from different glomerular and tubular cells. Even though the glomeruli were isolated and enriched prior to dissociation to single nuclei, the presence of some tubular cell clusters was anticipated, as glomerular isolation cannot completely exclude tubular fragments. However, the majority (65%) of all nuclei originated from the three major glomerular cell types - mesangial cells, glomerular endothelial cells and podocytes, demonstrating a successful glomerular enrichment. Cell clusters were manually annotated using an adapted marker gene set from Liu et al. (73). The identified cell clusters were similar to the ones identified by Liu et al. but were not distinguished between different glomerular or proximal tubule cell types. Further, the distribution of cell types was very different from the distribution of Lui *et al*., but this is probably due to different methods of glomeruli isolation. In contrast to glomeruli isolation using differential adhesion method, Lui *et al*. used Percoll density gradient centrifugation after collagenase V digestion to enrich the glomeruli (73). Using this method, Lui *et al*. could only obtain ~15% glomerular cells (e.g. glomerular endothelial cells: 8.6%, mesangial cells: 5% and podocytes: 1%) (73), while the other cell types belong to the tubular system. In general the distribution of the groups amongst the cell types can hinting at changes in response to the disease but is also dependant on the isolation process. Especially cells from non-glomerular origin are heavily dependent on the quality of the glomerular enrichment. The cleaner the enrichment the less non-glomerular cell types can be detected. As the main focus of this analysis lies on glomerular cells, changes in non-glomerular cell types cannot be drawn in this approach. However, no changes in the distribution of the cell types in the groups does not mean, that there is no change going on. It only reveals that a certain cell type is more or less abundant in one group. For podocytes we cannot see changes in the distribution between the groups which is expected, since we chose a time point where the podocytes are damaged but there was no podocyte loss. Further, it is also not very surprising that there are no big differences in the immune cells between the different groups since the influx of immune cells into patient kidneys is not observed (11). Since immune cells do not play a big role in MN, the immune cell cluster was not further investigated. The markers are mostly from monocytes, and since they exhibit some glomerular endothelial cell (GEC)

markers, these might be tissue resident immune cells. One population that showed a much higher abundance in the m9 group are the proliferating cells. Since in this group the most damage is expected, it seems logic that there are more cells trying to cope with this damage.

Primary MN mainly affects the podocytes, consequently the further analysis focused on chPLA2R1-positive podocytes, as they are the only cells susceptible to targeting by disease-causing anti-PLA2R1 antibodies. When looking at the proportion of podocytes positive for chPLA2R1 it was a bit surprising that only half of them express the chPLA2R1. Previous FACS analysis of chPLA2R1 positive Podocytes showed that approximately 85% of all podocytes express chPL2R1, further immunofluorescence analysis indicates that most of the glomeruli express it. The rather low percentage of podocytes positive for chPLA2R1 might be due to incomplete mRNA transcription during the process of reverse transcription, where only approximately 30 % of the whole mRNA in each cell can be captured. Moreover, the detection of a transcript is a stochastic event and the transcriptome is built as a result of sequencing multiple cells from the same population (74), probably not all of the chPLA2R1 mRNA was captured.

The similar distribution of the groups in chPLA2R1 positive podocytes, show again that we do not have any significant podocyte loss. Further, a similar distribution of the groups is desirable for appropriate differential gene expression analysis. DEG analysis revealed similar upregulated genes in the early and late timepoint, indicating that the changes occurring in the early timepoint will persist over the progression of the disease. Most of these genes are associated with pathways involving the organization of the cytoskeleton. In the late time point some pathways are associated with the axon guidance and development which is not surprising since podocytes and neurons share structural and molecular similarities. Both cell types are terminally differentiated cells, with specialised actin-based projections that are essential for their specialised functions. Further, they share a lot of common proteins like synaptopodin, nephrin and nestin that are crucial for the maintenance of the cellular processes (75, 76).Moreover, both cell types share a common molecular machinery (76).

Ephrin Type-A Receptor (Epha6) belongs to the tyrosin kinases and is the most upregulated gene at both timepoints. In neurons the Ephrin receptor family is essential for regulation of neuronal morphology (77). There is not much research about the Ephrin receptor family in podocytes but a study from 2020 found epha6 to be upregulated in mouse models of focal segmental glomerulus sclerosis (78). Ehprin receptors can bind to the cytoskeletal adapter proteins Nck and Scr, thereby regulating the polymerisation of f-actin (79). A study from 2020 stated that ephrin-B1 play a crucial role in maintaining the slit diaphragm (SD) integrity, but overexpression of ephrin-B1 will lead to a disruption of the SD (80). Possibly the same can be true for Epha6, where overexpression will lead to the disruption of the SD. The staining of Epha6 in our model showed an increase of the Epha6 expression. Nonetheless, there is not much known about the role of ephrin receptors in the kidney.

In our staining the receptor tyrosine kinase Mer (MerTK) and its phosphorylated variant (p-MerTK) had increased signals in the model mice compared to the controls, indication a higher expression and activity of the kinase. The most likely reason why the nephrin signal in the MerTK staining seems a bit faint, is probably due to the close proximity between MerTK and neprin, since both proteins are components of the SD (81). The merge showed a lot of regions where MerTK and nephrin overlap, as indicated by the yellow color. When separately looking at the nephrin signal, the intensity is comparable to the intensity in the Epha6 and p- MerTK staining (**Figure S1**). As already mentioned, MerTK was found to be a component of the SD in podocytes (81). The SD is composed of multiple different proteins that build a complex network, with Nephrin as the central component. The authors suggested that the protein network will on one hand serve as anchoring sites for Nephrin and on the other it is important for the signaling transduction between the extracellular space and the foot process (FP). Further, the authors mentioned that MerTK is known to initiate signaling cascades, like the phosphoinositid-3-kinase (PI3K) pathway, that contribute, among other effects, to the reorganization of the actin cytoskeleton (82). These rearrangements may alter the anchoring of the FP at the GBM, leading to possible modifications regarding the FP morphology and permeation properties of the GBM. A study with cultured podocytes, showed that Nephrin dependent PI3K activation lead retraction of these podocytes resulting in morphological and functional damage (83). Further, Kocylowski *et al*. demonstrated that changes or removal of MerTK signaling results in defective filtration and proteinuria (81). However, the authors only investigated the knockdown of MerTK in *Drosophila*, but not how enhanced MerTK signaling affects the system. Given that MerTK is a kinase in close proximity to nephrin (81) it possibly can phosphorylate nephrin. Phosphorylation of nephrin can lead to various effects including signals for cell survival, cytoskeletal organization and nephrin trafficking (84). MerTK induced phosphorylation of nephrin is not described in the literature so far, but might be a possible mechanism of how overactivation of MerTK can damage podocytes.

Besides the PI3K signaling pathway it is also described that MerTK signaling can activate the MAPK pathway and signal transducers and activators of transcription (STAT) proteins. In line with this, we also found STAT1 to be upregulated. A study from 2019 demonstrated that silencing STAT1 in high glucose-induced podocyte injury can reverse the effects of low cell viability, cell apoptosis and production of reactive oxygen species (ROS), indicating a harmful role of Stat1 activation by promoting apoptosis (85). Furthermore, STAT3, another member of the STAT family, is known to play crucial roles in the pathology of several kidney diseases like diabetic kidney disease, focal segmental sclerosis (FSGS), and lupus nephritis (86).

Although there is variation between the individual mice regarding the signal intensities of Epha6, MerTK and p- MerTK there is a weak positive correlation (not shown data) between proteinuria and signal intensity for both proteins. MerTK and Epha6 were already upregulated in the early time point, where the mice had no proteinuria, leading to the assumption that the upregulations of these proteins contribute to the increase in

proteinuria. However, to further verify a potential pathological role of MerTK and Epha6 in the disease progression further analysis need to be performed.

5. Conclusion and Outlook

To sum up the findings of this research, we successfully developed an experimental and inducible model for PLA2R1-associated MN model in mice. The knock in of the chPLA2R1 does not interfere with a healthy podocyte morphology and behavior. Upon immunisation with the recombinant ectodomain of hPLA2R1 the mice develop an antigen-specific and immune-mediated disease, resembling the key features of the typical clinical pattern in morphology regarding to mIgG and complement deposition. Thus, resembling all key features of MN in patients, which can be considered as the major strength of this new model. Moreover, in contrast to the spontaneously developing disease with exacerbating albuminuria, severe glomerular and tubulointerstitial damage, and deteriorating kidney function, which we observed in hPLA2R1-expressing mice (51) disease developed more slowly and was more stable in the hPLA2R1-immunised chPLA2R1-positive mice presented in this study.

To better understand the role of complement in disease progression, we generated a mouse line expressing the chPLA2R1 with a simultaneous, global knock-out of C3. After immunisation chPLA2R1-positive/$C3^{-/-}$ showed an attenuated course of disease. Onset of proteinuria was delayed and less severe, furthermore the survival of chPLA2R1-positive/$C3^{-/-}$ mice was better. These experiments showed that the complement system plays a role in the pathogenesis in this model of experimental PLA2R1 associated MN. However, the mice got sick, demonstrating also complement independent mechanisms playing a role in disease initiation and progression. To further dissect the role of the complement system more detailed analysis are necessary. Bulk RNA sequencing from sorted podocytes of our model mice can give insight to specific changes on mRNA levels. Further proteome and phospho-proteome analysis will be crucial to see if the changes in the mRNA will translate into increased or decreased protein production, as well as if there is any alteration in the activity of certain proteins. Differences in the regulation of mRNA and proteins will give more insight to complement independent disease mechanisms.

More detailed analysis of the time course in our newly established chPLA2R1 eaMN model let us define an early time point at the initiation phase of the disease, when immune complexes start to build up and mice were not proteinuric. Further, we identified a late time point with manifested disease but mild podocyte-impairment. In a first step to gain insight of potential pathomechanisms, single nucleus RNA sequencing analysis revealed Epha6 as the most upregulated gene in early and late timepoint. Another upregulated gene with is present in both time points is MerTK, which was recently demonstrated to be an essential part of the SD protein network (81). Moreover, we could show an increase in both Epha6 and MerTK signal in immunofluorescence analysis. To verify the role of these two proteins in disease progression and potentially find more important proteins and pathways further analysis are necessary. For

instance, an assay for Transposase-Accessible Chromatin using Sequencing (ATAC-Seq) can verify open chromatin regions, showing potential translational active sites. Further, proteome and phospho-proteome analysis will be crucial to see if the upregulation of these genes will translate into increased protein production and if there is an increase or decrease of their activity. When comparing the results of all these methods, genes and proteins showing up in two or more analyses are good candidates for a more targeted analysis. For their validation, human biopsies from MN patients can be stained for several of these candidates, revealing if there are changes in protein levels. Moreover, specific inhibitor approaches, targeting the identified candidates can be tested in our mouse model, to see the effects under disease conditions.

With more research we are confident to identify complement dependent and independent mechanisms driving the disease progression. A better understanding of these pathomechanims will help to further develop better and more targeted therapeutical options for patients.

6. Annex

6.1 Supplementary data

Figure S1 shows the immunofluorescence analysis of MerTK, Epha6 and p-MerTK. In the MerTK staining for the m9 group it is clearly visible, that the nephrin signal is not reduced, but completely overlaps with the MerTK signal, resulting in a yellow color in the merged picture and is therefore less distinguishable from the green MerTK signal.

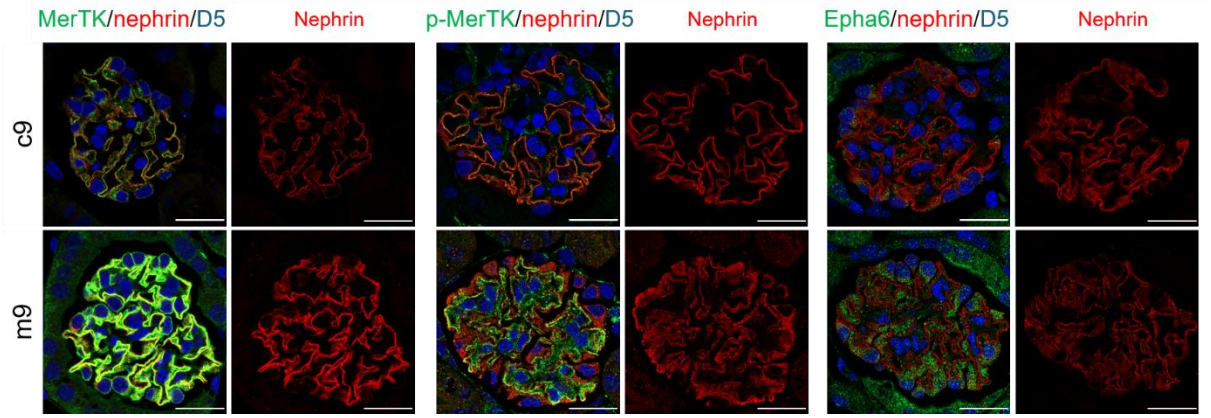

***Figure S1: Immunofluorescence staining of Epha6, MerTK and p-MerTK**. Immunofluorescence staining of MerTK, Epha6, and p-MerTK (all in green) in co-staining with nephrin (red) in control and hPLA2R1-immunised mice (n = 5 analysed per group). Bar = 20 µm*

7. References

1. Erwin-Josef Speckmann JH, Rüdiger Köhling Physiologie Urban & Fischer in Elsevier (Verlag); 2013.
2. Butt L, Unnersjo-Jess D, Hohne M, Edwards A, Binz-Lotter J, Reilly D, et al. A molecular mechanism explaining albuminuria in kidney disease. Nat Metab. 2020;2(5):461-74.
3. Deegens JK, Wetzels JF. Membranous nephropathy in the older adult: epidemiology, diagnosis and management. Drugs Aging. 2007;24(9):717-32.
4. Cattran DC. Idiopathic membranous glomerulonephritis. Kidney Int. 2001;59(5):1983-94.
5. Fervenza FC, Sethi S, Specks U. Idiopathic membranous nephropathy: diagnosis and treatment. Clin J Am Soc Nephrol. 2008;3(3):905-19.
6. Alsharhan L, Beck LH, Jr. Membranous Nephropathy: Core Curriculum 2021. Am J Kidney Dis. 2021;77(3):440-53.
7. Couser WG. Primary Membranous Nephropathy. Clin J Am Soc Nephrol. 2017;12(6):983-97.
8. Ronco P, Beck L, Debiec H, Fervenza FC, Hou FF, Jha V, et al. Membranous nephropathy. Nat Rev Dis Primers. 2021;7(1):69.
9. Keri KC, Blumenthal S, Kulkarni V, Beck L, Chongkrairatanakul T. Primary membranous nephropathy: comprehensive review and historical perspective. Postgraduate Medical Journal. 2019;95(1119):23-31.
10. Laurence H. Beck J, M.D., Ph.D., Ramon G.B. Bonegio, M.D., Gérard Lambeau, Ph.D., David M. Beck, B.A., David W. Powell, Ph.D., Timothy D. Cummins, M.S., Jon B. Klein, M.D., Ph.D., and David J. Salant, M.D. M-Type Phospholipase A2 Receptor as Target Antigen in Idiopathic Membranous Nephropathy. The new england journal of medicine. 2009;361.
11. Fogo AB, Lusco MA, Najafian B, Alpers CE. AJKD Atlas of Renal Pathology: Membranous Nephropathy. Am J Kidney Dis. 2015;66(3):e15-7.
12. Aliza Thompson DCC, Melanie Blank, Patrick H Nachman. Complete and Partial Remission as Surrogate End Points in Membranous Nephropathy. J Am Soc Nephrol. 2015.

13. Cattran DC. Management of membranous nephropathy. Minerva Urol Nefrol. 2002;54(1):19-27.
14. Polanco N, Gutiérrez E, Covarsí A, Ariza F, Carreño A, Vigil A, et al. Spontaneous remission of nephrotic syndrome in idiopathic membranous nephropathy. J Am Soc Nephrol. 2010;21(4):697-704.
15. Tomas NM, Beck LH, Jr., Meyer-Schwesinger C, Seitz-Polski B, Ma H, Zahner G, et al. Thrombospondin type-1 domain-containing 7A in idiopathic membranous nephropathy. N Engl J Med. 2014;371(24):2277-87.
16. Hanasaki K, Arita H. Phospholipase A2 receptor: a regulator of biological functions of secretory phospholipase A2. Prostaglandins Other Lipid Mediat. 2002;68-69:71-82.
17. Augert A, Payre C, de Launoit Y, Gil J, Lambeau G, Bernard D. The M-type receptor PLA2R regulates senescence through the p53 pathway. EMBO Rep. 2009;10(3):271-7.
18. Pan Y, Wan J, Liu Y, Yang Q, Liang W, Singhal PC, et al. sPLA2 IB induces human podocyte apoptosis via the M-type phospholipase A2 receptor. Sci Rep. 2014;4:6660.
19. Ancian P, Lambeau G, Lazdunski M. Multifunctional activity of the extracellular domain of the M-type (180 kDa) membrane receptor for secretory phospholipases A2. Biochemistry. 1995;34(40):13146-51.
20. Seifert L, Zahner G, Meyer-Schwesinger C, Hickstein N, Dehde S, Wulf S, et al. The classical pathway triggers pathogenic complement activation in membranous nephropathy. Nat Commun. 2023;14(1):473.
21. Fresquet M, Jowitt TA, Gummadova J, Collins R, O'Cualain R, McKenzie EA, et al. Identification of a major epitope recognized by PLA2R autoantibodies in primary membranous nephropathy. J Am Soc Nephrol. 2015;26(2):302-13.
22. Kao L, Lam V, Waldman M, Glassock RJ, Zhu Q. Identification of the immunodominant epitope region in phospholipase A2 receptor-mediating autoantibody binding in idiopathic membranous nephropathy. J Am Soc Nephrol. 2015;26(2):291-301.
23. Seitz-Polski B, Debiec H, Rousseau A, Dahan K, Zaghrini C, Payre C, et al. Phospholipase A2 Receptor 1 Epitope

Spreading at Baseline Predicts Reduced Likelihood of Remission of Membranous Nephropathy. J Am Soc Nephrol. 2018;29(2):401-8.
24. Seitz-Polski B, Dolla G, Payre C, Girard CA, Polidori J, Zorzi K, et al. Epitope Spreading of Autoantibody Response to PLA2R Associates with Poor Prognosis in Membranous Nephropathy. J Am Soc Nephrol. 2016;27(5):1517-33.
25. Reinhard L, Zahner G, Menzel S, Koch-Nolte F, Stahl RAK, Hoxha E. Clinical Relevance of Domain-Specific Phospholipase A(2) Receptor 1 Antibody Levels in Patients with Membranous Nephropathy. J Am Soc Nephrol. 2020;31(1):197-207.
26. Fresquet M, Lockhart-Cairns MP, Rhoden SJ, Jowitt TA, Briggs DC, Baldock C, et al. Structure of PLA2R reveals presentation of the dominant membranous nephropathy epitope and an immunogenic patch. Proc Natl Acad Sci U S A. 2022;119(29):e2202209119.
27. van de Logt AE, Fresquet M, Wetzels JF, Brenchley P. The anti-PLA2R antibody in membranous nephropathy: what we know and what remains a decade after its discovery. Kidney Int. 2019;96(6):1292-302.
28. Hoxha E, Reinhard L, Stahl RAK. Membranous nephropathy: new pathogenic mechanisms and their clinical implications. Nat Rev Nephrol. 2022;18(7):466-78.
29. Ronco P, Debiec H. Molecular Pathogenesis of Membranous Nephropathy. Annu Rev Pathol. 2020;15:287-313.
30. Xu X, Wang G, Chen N, Lu T, Nie S, Xu G, et al. Long-Term Exposure to Air Pollution and Increased Risk of Membranous Nephropathy in China. J Am Soc Nephrol. 2016;27(12):3739-46.
31. Christine Schütt BB. Grundwissen Immunologie: Spektrum Akademischer Verlag; 2011. 2 p.
32. Tomas NM. Therapeutic targets in membranous nephropathy: plasma cells and complement. Clin Kidney J. 2024;17(9):sfae243.
33. Haddad G, Lorenzen JM, Ma H, de Haan N, Seeger H, Zaghrini C, et al. Altered glycosylation of IgG4 promotes lectin complement pathway activation in anti-PLA2R1-associated membranous nephropathy. J Clin Invest. 2021;131(5).

34. Bally S, Debiec H, Ponard D, Dijoud F, Rendu J, Faure J, et al. Phospholipase A2 Receptor-Related Membranous Nephropathy and Mannan-Binding Lectin Deficiency. J Am Soc Nephrol. 2016;27(12):3539-44.
35. Tomas NM, Huber TB, Hoxha E. Perspectives in membranous nephropathy. Cell Tissue Res. 2021;385(2):405-22.
36. Fresquet M, Jowitt TA, McKenzie EA, Ball MD, Randles MJ, Lennon R, et al. PLA(2)R binds to the annexin A2-S100A10 complex in human podocytes. Sci Rep. 2017;7(1):6876.
37. Skoberne A, Behnert A, Teng B, Fritzler MJ, Schiffer L, Pajek J, et al. Serum with phospholipase A2 receptor autoantibodies interferes with podocyte adhesion to collagen. Eur J Clin Invest. 2014;44(8):753-65.
38. Heymann W, Hackel DB, Harwood S, Wilson SG, Hunter JL. Production of nephrotic syndrome in rats by Freund's adjuvants and rat kidney suspensions. Proc Soc Exp Biol Med. 1959;100(4):660-4.
39. Kerjaschki D, Farquhar MG. Immunocytochemical localization of the Heymann nephritis antigen (GP330) in glomerular epithelial cells of normal Lewis rats. J Exp Med. 1983;157(2):667-86.
40. Farquhar MG, Saito A, Kerjaschki D, Orlando RA. The Heymann nephritis antigenic complex: megalin (gp330) and RAP. J Am Soc Nephrol. 1995;6(1):35-47.
41. Kerjaschki D, Neale TJ. Molecular mechanisms of glomerular injury in rat experimental membranous nephropathy (Heymann nephritis). J Am Soc Nephrol. 1996;7(12):2518-26.
42. Cybulsky AV, Quigg RJ, Salant DJ. Experimental membranous nephropathy redux. Am J Physiol Renal Physiol. 2005;289(4):F660-71.
43. Perez-Gomez MV, Sanchez-Nino MD, Ortiz A. Megalin/lipoprotein receptor-related protein 2 autoimmunity and kidney disease. Clin Kidney J. 2020;13(3):281-6.
44. Borza DB, Zhang JJ, Beck LH, Jr., Meyer-Schwesinger C, Luo W. Mouse models of membranous nephropathy: the road less travelled by. Am J Clin Exp Immunol. 2013;2(2):135-45.

45. Tomas NM, Hoxha E, Reinicke AT, Fester L, Helmchen U, Gerth J, et al. Autoantibodies against thrombospondin type 1 domain-containing 7A induce membranous nephropathy. J Clin Invest. 2016;126(7):2519-32.
46. Tomas NM, Meyer-Schwesinger C, von Spiegel H, Kotb AM, Zahner G, Hoxha E, et al. A Heterologous Model of Thrombospondin Type 1 Domain-Containing 7A-Associated Membranous Nephropathy. J Am Soc Nephrol. 2017;28(11):3262-77.
47. Meyer-Schwesinger C, Tomas NM, Dehde S, Seifert L, Hermans-Borgmeyer I, Wiech T, et al. A novel mouse model of phospholipase A2 receptor 1-associated membranous nephropathy mimics podocyte injury in patients. Kidney Int. 2020;97(5):913-9.
48. Tomas NM, Schnarre A, Dehde S, Lucas R, Hermans-Borgmeyer I, Kretz O, et al. Introduction of a novel chimeric active immunization mouse model of PLA2R1-associated membranous nephropathy. Kidney Int. 2023;104(5):916-28.
49. Young MD, Behjati S. SoupX removes ambient RNA contamination from droplet-based single-cell RNA sequencing data. GigaScience. 2020;9(12).
50. Korotkevich G, Sukhov V, Budin N, Shpak B, Artyomov MN, Sergushichev A. Fast gene set enrichment analysis. bioRxiv. 2021:060012.
51. Tomas NM, Dehde S, Meyer-Schwesinger C, Huang M, Hermans-Borgmeyer I, Maybaum J, et al. Podocyte expression of human phospholipase A2 receptor 1 causes immune-mediated membranous nephropathy in mice. Kidney Int. 2023;103(2):297-303.
52. Dong Y, Cao L, Tang H, Shi X, He Y. Structure of Human M-type Phospholipase A2 Receptor Revealed by Cryo-Electron Microscopy. J Mol Biol. 2017;429(24):3825-35.
53. Zhang P, Huang W, Zheng Q, Tang J, Dong Z, Jiang Y, et al. A Novel Insight into the Role of PLA2R and THSD7A in Membranous Nephropathy. J Immunol Res. 2021;2021:8163298.
54. Seifert L. Characterization of THSD7A- and PLA2R1-specific antibodies and their role in the pathogenesis of

membranous nephropathy. In: Fakultät für Mathematik IuNFBdUH, editor. https://ediss.sub.uni-hamburg.de/bitstream/ediss/8459/1/Dissertation.pdf2020.
55. Harboe M, Ulvund G, Vien L, Fung M, Mollnes TE. The quantitative role of alternative pathway amplification in classical pathway induced terminal complement activation. Clin Exp Immunol. 2004;138(3):439-46.
56. Thurman JM, Holers VM. The Central Role of the Alternative Complement Pathway in Human Disease1. The Journal of Immunology. 2006;176(3):1305-10.
57. Ma H, Sandor DG, Beck LH, Jr. The role of complement in membranous nephropathy. Semin Nephrol. 2013;33(6):531-42.
58. Baker PJ, Ochi RF, Schulze M, Johnson RJ, Campbell C, Couser WG. Depletion of C6 prevents development of proteinuria in experimental membranous nephropathy in rats. Am J Pathol. 1989;135(1):185-94.
59. Salant DJ, Belok S, Madaio MP, Couser WG. A new role for complement in experimental membranous nephropathy in rats. J Clin Invest. 1980;66(6):1339-50.
60. Perkinson DT, Baker PJ, Couser WG, Johnson RJ, Adler S. Membrane attack complex deposition in experimental glomerular injury. Am J Pathol. 1985;120(1):121-8.
61. Leenaerts PL, Hall BM, Van Damme BJ, Daha MR, Vanrenterghem YF. Active Heymann nephritis in complement component C6 deficient rats. Kidney Int. 1995;47(6):1604-14.
62. Spicer ST, Tran GT, Killingsworth MC, Carter N, Power DA, Paizis K, et al. Induction of passive Heymann nephritis in complement component 6-deficient PVG rats. J Immunol. 2007;179(1):172-8.
63. Lundgren S, Carling T, Hjalm G, Juhlin C, Rastad J, Pihlgren U, et al. Tissue distribution of human gp330/megalin, a putative Ca(2+)-sensing protein. J Histochem Cytochem. 1997;45(3):383-92.
64. Catherine Meyer-Schwesinger NMT, Silke Dehde, Larissa Seifert, Irm Hermans-Borgmeyer, Thorsten Wiech, Friedrich Koch-Nolte, Tobias B. Huber, Gunther Zahner. A novel mouse model of phospholipase A2 receptor 1-associated membranous

nephropathy mimics podocyte injury in patients. Kidney Int. 2020;97(5):913-9.
65. Yin J, Verschoor A, Yue X, Goldmann T, Heidecke H, Riemekasten G, et al. C3 deficiency promotes pulmonary inflammation in AT1R-induced mouse model for systemic sclerosis. Front Immunol. 2024;15:1491324.
66. Borza DB. Alternative Pathway Dysregulation and the Conundrum of Complement Activation by IgG4 Immune Complexes in Membranous Nephropathy. Front Immunol. 2016;7:157.
67. Nagata M. Podocyte injury and its consequences. Kidney Int. 2016;89(6):1221-30.
68. Bruno V, Muhlig AK, Oh J, Licht C. New insights into the immune functions of podocytes: the role of complement. Mol Cell Pediatr. 2023;10(1):3.
69. Köllner SMS, Seifert L, Zahner G, Tomas NM. Strategies Towards Antigen-Specific Treatments for Membranous Nephropathy. Frontiers in Immunology. 2022;13.
70. Hosur V, Erhardt V, Hartig E, Lorenzo K, Megathlin H, Tarchini B. Large-Scale Genome-Wide Optimization and Prediction of the Cre Recombinase System for Precise Genome Manipulation in Mice. Res Sq. 2024.
71. Balkawade RS, Chen C, Crowley MR, Crossman DK, Clapp WL, Verlander JW, et al. Podocyte-specific expression of Cre recombinase promotes glomerular basement membrane thickening. Am J Physiol Renal Physiol. 2019;316(5):F1026-F40.
72. 10XGenomics. Introduction to Ambient RNA Correction https://www.10xgenomics.com/analysis-guides/introduction-to-ambient-rna-correction2023 [Available from: https://www.10xgenomics.com/analysis-guides/introduction-to-ambient-rna-correction.
73. Liu S, Zhao Y, Lu S, Zhang T, Lindenmeyer MT, Nair V, et al. Single-cell transcriptomics reveals a mechanosensitive injury signaling pathway in early diabetic nephropathy. Genome Med. 2023;15(1):2.
74. 10XGenomics. What fraction of mRNA transcripts are captured per cell? [Available from:

https://kb.10xgenomics.com/hc/en-us/articles/360001539051-What-fraction-of-mRNA-transcripts-are-captured-per-cell.
75. Kobayashi N. Mechanism of the process formation; podocytes vs. neurons. Microscopy Research and Technique. 2002;57(4):217-23.
76. Kobayashi N, Gao SY, Chen J, Saito K, Miyawaki K, Li CY, et al. Process formation of the renal glomerular podocyte: is there common molecular machinery for processes of podocytes and neurons? Anat Sci Int. 2004;79(1):1-10.
77. Das G, Yu Q, Hui R, Reuhl K, Gale NW, Zhou R. EphA5 and EphA6: regulation of neuronal and spine morphology. Cell Biosci. 2016;6:48.
78. Bukosza EN, Kratochwill K, Kornauth C, Schachner H, Aufricht C, Gebeshuber CA. Podocyte RNA sequencing reveals Wnt- and ECM-associated genes as central in FSGS. PLoS One. 2020;15(4):e0231898.
79. Hu T, Shi G, Larose L, Rivera GM, Mayer BJ, Zhou R. Regulation of process retraction and cell migration by EphA3 is mediated by the adaptor protein Nck1. Biochemistry. 2009;48(27):6369-78.
80. Takamura S, Fukusumi Y, Zhang Y, Narita I, Kawachi H. Partitioning-Defective-6-Ephrin-B1 Interaction Is Regulated by Nephrin-Mediated Signal and Is Crucial in Maintaining Slit Diaphragm of Podocyte. Am J Pathol. 2020;190(2):333-46.
81. Kocylowski MK, Aypek H, Bildl W, Helmstadter M, Trachte P, Dumoulin B, et al. A slit-diaphragm-associated protein network for dynamic control of renal filtration. Nat Commun. 2022;13(1):6446.
82. Zhang Y, Earp HS, Liu P. Beyond growth signaling: apoptotic sensor MERTK activates AKT by a novel mechanism. Mol Cell Oncol. 2019;6(4):1611161.
83. Nosadini R, Tonolo G. Role of oxidized low density lipoproteins and free fatty acids in the pathogenesis of glomerulopathy and tubulointerstitial lesions in type 2 diabetes. Nutr Metab Cardiovasc Dis. 2011;21(2):79-85.
84. Martin CE, Jones N. Nephrin Signaling in the Podocyte: An Updated View of Signal Regulation at the Slit Diaphragm and Beyond. Front Endocrinol (Lausanne). 2018;9:302.

85. Wang H, Zhang Y, Xia F, Zhang W, Chen P, Yang G. Protective effect of silencing Stat1 on high glucose-induced podocytes injury via Forkhead transcription factor O1-regulated the oxidative stress response. BMC Mol Cell Biol. 2019;20(1):27.
86. Pace J, Paladugu P, Das B, He JC, Mallipattu SK. Targeting STAT3 signaling in kidney disease. Am J Physiol Renal Physiol. 2019;316(6):F1151-F61.